Title
Exploring the neural basis of chemosensory behaviors in Caenorhabditis elegans: How context and experience shape sensory perception

Author
Guillermin, Manon

Publication Date
2018

Peer reviewed|Thesis/dissertation

UNIVERSITY OF CALIFORNIA

Los Angeles

Exploring the neural basis of chemosensory behaviors in *Caenorhabditis elegans:*

How context and experience shape sensory perception

A dissertation submitted in partial satisfaction of the requirements for the degree

Doctor of Philosophy in Microbiology, Immunology and Molecular Genetics

by

Manon Guillermin

2018

ABSTRACT OF THE DISSERTATION

Exploring the neural basis of chemosensory behaviors in *Caenorhabditis elegans:*

How context and experience shape sensory perception

by

Manon Guillermin

Doctor of Philosophy in Microbiology, Immunology and Molecular Genetics

University of California, Los Angeles, 2018

Professor Elissa A. Hallem, Chair

Adaptability is essential to organisms' fitness and survival. Evolutionary success depends on access to an array of behavioral choices in the face of changing environmental conditions. To navigate complex landscapes, organisms can interpret the significance of sensory stimuli, and assign context-appropriate valence, by integrating factors such as cues from their internal and external environments, and memories of previously experienced conditions, to dynamically shape neural circuits and generate ethologically relevant behaviors. In this thesis, I explore the cellular and molecular mechanisms that shape the carbon dioxide (CO_2) circuit in the free-living nematode, *Caenorhabditis elegans*. CO_2 is a complex sensory cue that can signify the presence of fruitful or dangerous surroundings. As a result, *C. elegans* can display a variety of different behaviors in response to CO_2, from robust attraction to robust avoidance. Although sensory signaling of the CO_2-responsive BAG neurons has been extensively characterized, how BAG communicates with postsynaptic interneurons, and how the

CO_2 signal is propagated through the nervous system to generate a context-appropriate behavior is unknown. First, we have found that neuromodulatory state and environmental oxygen (O_2) levels converge on the CO_2 circuit via the URX sensory neurons. The lab-derived N2 *C. elegans* strain expresses high levels of NPR-1 neuropeptide receptor, which inhibits URX and results in CO_2 avoidance, regardless of environmental O_2. In the *C. elegans* wild isolate "Hawaii", loss of *npr-1* leads to modulation of URX by environmental O_2, and results in CO_2 avoidance at low O_2, and loss of CO_2-evoked behavior at high O_2. Second, we present a new circuit motif that demonstrates how divergent responses to a single sensory input, CO_2, can arise from an identical set of sensory and interneuron connections. We show that *C. elegans* exhibit an experience-dependent behavioral valence switch in response to CO_2. While animals raised at ambient CO_2 are repelled by CO_2, animals raised in a high CO_2 environment are attracted to CO_2. Whether CO_2 is attractive or repulsive is determined by the coordinated activity of specialized valence-encoding interneurons, AIY, RIG, and RIA, whose responses are subject to context-dependent modulation. An additional interneuron pair, AIZ, regulates behavioral sensitivity regardless of valence. Glutamatergic and neuropeptidergic signaling mediate both CO_2 avoidance and attraction, and different neuropeptides play distinct roles in regulating valence and sensitivity. Our results elucidate a microcircuit motif whereby a fixed set of neurons are leveraged to generate alternative outputs in response to a single chemosensory input.

The dissertation of Manon Guillermin is approved.

Mark Arthur Frye

Beth Ann Lazazzera

Elissa A. Hallem, Committee Chair

University of California, Los Angeles

2018

Pour Papa, Geraldine, Marie-Aimee, Nils, et Matteo.

Sans votre encouragement et votre soutien, ce travail n'aurait pas été possible.

Je vous remercie du fond de mon cœur.

TABLE OF CONTENTS

LIST OF FIGURES

Chapter 2

Chapter 3

ACKNOWLEDGEMENTS

First, it has been a unique and absolute privilege to be mentored by my professor, Elissa Hallem. Elissa is an incredible scientist and I am honored to have had the opportunity to learn from her. Beyond my graduate experience, I will continue to aspire to be as ambitious and pioneering a scientist as she is, and follow the example she has set. Thank you, Elissa, for your guidance and endless motivation. Thank you for building my confidence by placing your trust in me and encouraging me to follow my scientific instincts. Your unwavering dedication to every member of your lab, and to the integrity of the science performed under your supervision is inspiring.

I would like to thank the wonderful members of my committee: Professors Mark Frye, Beth Lazazzera, and Doug Black. Thank you for your thoughtful advice and feedback, and your constant support over the years. I am so grateful to have had the support of such incredible scientists to guide me during my training.

I also want to acknowledge the members of the lab that made valuable contributions to the work presented in this thesis: Mayra Carrillo, Sophie Rengarajan and Ryo Okubo. And thank you to all the members of the Hallem lab for creating such an enjoyable work environment. It has been a pleasure to work with such lovely and interesting people.

I would like to thank the department of Microbiology, Immunology and Molecular Genetics, especially Bridget Wells, Juana Escobar, and Hillary Trudgeon for their support and commitment to graduate students.

I am incredibly grateful to the NIH for supporting my graduate work through the Cellular and Molecular Biology Training Program. In addition to providing financial support, this grant gave me access to many mentorship opportunities and learning opportunities within the realm of cellular and molecular biology. I am especially grateful to the director, Dr. Steven Clarke. It has also been a privilege to be supported by the National Science Foundation through their Graduate Research Fellowship Program.

Chapter 2 is a version of: Carrillo M.A., Guillermin M.L., Rengarajan S., Okubo R.P., and Hallem E.A. (2013) O_2-sensing neurons control CO_2 response in *C. elegans*. *J Neurosci* 33, 9675-9683. Following initial findings from Sophie Rengarajan and Elissa Hallem, which suggested the neuropeptide receptor NPR-1 acts in the CO_2 circuit, I contributed to this project by demonstrating that NPR-1 acts in the oxygen-sensing URX neurons to regulate CO_2 avoidance. In addition, I showed that regulation of CO_2 avoidance by the URX neurons depends on their ability to sense O_2. Mayra Carrillo and Ryo Okubo followed up on these results and furthered investigated the role of oxygen in modulating CO_2 response behavior.

Chapter 3 is a version of: Guillermin M.L, Carrillo M.A., Hallem E.A. (2017) A single set of interneurons drives opposite behaviors in *C. elegans*. *Curr Biol* 27(17):2630-2639. Along with my professor, Elissa Hallem, I designed this study, executed the experiments, interpreted the data and wrote the manuscript. Mayra Carrillo provided valuable feedback and ideas in the initial stages of this work, and helped to obtain and test several neuropeptide mutant strains. Permission was granted by publisher for use in this thesis.

VITA

Education

B.S. in Biology

McGill University, Montreal, Canada (2005-2009)

Academic Awards

2013 Ruth L. Kirschstein National Research Service Award GM007185

2014 National Science Foundation Graduate Research Fellowship

2005 Williams College Book Award

Publications

Guillermin, M., Carrillo, M., Hallem, E. (2017) A Single Set of Interneurons Drives Opposite Behaviors in *C. elegans*, *Current Biology* 27(17):2630-2639.

Carrillo, M., Guillermin, M., Rengarajan, S., Okubo, R., and Hallem, E. (2013) O_2-Sensing Neurons Control CO_2 Response in *C. elegans. J Neurosci* 33: 9675-9683.

Dillman AR, Guillermin M, Ha Lee J, Kim B, Sternberg PW, Hallem E. (2012) Olfaction shapes host-parasite interactions in parasitic nematodes *PNAS* 109(35):E2324-33.

Guillermin M, Castelletto M, Hallem E. (2011) Differentiation of carbon dioxide-sensing neurons in *Caenorhabditis elegans* requires the ETS-5 transcription factor. *Genetics* 189(4):1327-1339

Selected Presentations

Guillermin M., Carrillo M., Hallem E. A single set of interneurons drives opposite behaviors in *C. elegans***.** Presented at 21th International *C. elegans* Meeting. Los Angeles, CA. June 2017.

Guillermin M. A microcircuit for controlling sensory valence in *Caenorhabditis elegans*. Presented at Association for Chemoreception Sciences (AChemS) Annual Meeting. Bonita Springs, FL. April 2017.

Guillermin, M**.** Dissecting Host-Parasite Interactions in Entomopathogenic Nematodes. UCLA Worm Seminar Series. Los Angeles, CA. April 2011.

Guillermin M. Differentiation of carbon dioxide-sensing neurons in *Caenorhabditis elegans* requires the ETS-5 transcription factor. UCLA Worm Seminar Series. Los Angeles, CA. December 2011.

Chapter 1: Introduction

Investigating the neural basis of behavioral plasticity in *Caenorhabditis elegans*

For all animals, the capacity to keep pace with fluctuating environmental conditions, over long and short timescales, and shape appropriate behaviors determines reproductive success and survival. An important challenge in neuroscience is investigating how adaptive behavioral responses are generated from fixed neural circuits. Rapid behavioral switching provides a unique opportunity to examine how the computational capacity of a fixed neuroanatomy is increased to engender behavioral plasticity. This type of circuit flexibility, and the corresponding ability to extract relevant sensory information from the environment to regulate behaviors accordingly, is essential for human cognitive function. Deficits in set-shifting – the ability to alter a behavioral response in order to adapt to changing contingencies (Monchi et al., 2004) – has been well documented in many psychiatric disorders, most notably schizophrenia and Parkinson's disease (Dirnberger and Jahanshahi, 2013; Gold et al., 2008; Pantelis et al., 1999; Strauss et al., 2011). However, the underlying molecular, cellular, and network level mechanisms that translate sensory signals and modulate downstream processing programs to generate context-appropriate behaviors remain poorly understood.

The free-living nematode, *Caenorhabditis elegans*, is a powerful model for studying the molecular and neural circuit mechanisms that drive behavioral plasticity. The complete reconstruction of the *C. elegans* connectome (Varshney et al., 2011; White et al., 1986) provides a framework to examine the flow of information originating at the sensory neurons and descending through extensively interconnected interneurons to motor neurons that direct appropriate behaviors. However, current research has demonstrated

that the anatomical wiring map is only a starting point for understanding how sensory information evokes context-dependent behaviors. Neuromodulators act on this framework to rapidly alter microcircuit function and generate context-dependent responses to many sensory stimuli (Bargmann, 2012; Bentley et al., 2016; Hobert, 2003; Rengarajan and Hallem, 2016). An extensive set of genetic and molecular tools enable analysis of circuit function at single neuron resolution. Recent technical advances in calcium imaging (Ben Arous et al., 2010; Chronis et al., 2007; Kerr and Schafer, 2006; Nguyen et al., 2015; Schrödel et al., 2013; Zheng et al., 2012), cell-specific silencing/ablation (Pokala et al., 2014; Qi et al., 2012; Schiavo et al., 1992), as well as optogenetics (Leifer et al., 2011; Nagel et al., 2005; Stirman et al., 2011) offer novel ways to probe neural circuit function, namely, neuronal activity can be observed and manipulated in neuron populations, as well as in single neurons, in stationary and freely moving *C. elegans*. Since similar microcircuit motifs are found in *C. elegans* and mammals (Milo et al., 2002; Song et al., 2005; Zhang et al., 2008), mechanisms that drive microcircuit flexibility in *C. elegans* may also operate in higher-order nervous systems.

Despite its simple nervous system, *C. elegans* perceive a number of environmental stimuli - light, temperature, touch, and chemicals - and display a complex behavioral repertoire ranging from motor and sensory behaviors, termed “escape” and “habitat and resource localization” behaviors, to the so-called “housekeeping” behaviors including mating, social, and sleep behaviors (Faumont et al., 2012). Like many organisms, *C. elegans* modulate behavioral responses based on experience as well as internal and external contexts (Hobert, 2003). *C. elegans* generate learned associations between

food cues and environmental conditions, including salt concentration (Bargmann and Horvitz, 1991; Kunitomo et al., 2013; Saeki et al., 2001), oxygen (O_2) concentration (Cheung et al., 2005), and temperature (Hedgecock and Russell, 1975; Kimata et al., 2012; Kuhara et al., 2008; Mori and Ohshima, 1995) and adjusts its behavioral responses to these conditions accordingly. For example, *C. elegans* cultivated at a certain temperature for 3 hours, in the presence of food, will record and store temperature information, and subsequently migrate to their memorized temperature when placed on a temperature gradient (Kimata et al., 2012). Similarly, *C. elegans* in a salt gradient will migrate towards the salt concentration recorded and stored during cultivation (Kunitomo et al., 2013). However, starvation produces the opposite effect. If cultivated without bacteria, *C. elegans* avoid cultivation temperature and salt concentration (Mohri et al., 2005; Saeki et al., 2001). For these reasons, I used *C. elegans* to examine the circuit mechanisms that encode behavioral variability, by investigating how a single sensory input propagates through the nervous system and transforms into different patterns of output activity.

Carbon Dioxide: an ethologically complex sensory cue

The response of *C. elegans* to carbon dioxide (CO_2) can be used as a model for investigating how microcircuits generate alternative behavioral outputs. As a byproduct of respiration, CO_2 is fundamentally involved in metabolism, and is monitored internally and externally by organisms that rely on aerobic respiration. In addition, changes in CO_2 concentration can signal both favorable conditions such as food quality, food availability, and the presence of conspecifics, as well as unfavorable conditions such as the presence of predators or pathogens (Brandt and Ringstad, 2015; Carrillo and Hallem,

2015; Scott, 2011). Therefore, the ability to rapidly alter CO_2 response valence may be essential for survival. Although atmospheric CO_2 is only 0.038%, higher levels have been recorded in environments with higher respiration rates (Lahiri and Forster, 2003). In bee hives, CO_2 concentrations can reach 4% (Seeley, 1974), and in termite nests, CO_2 concentrations ranging from 0.3% to 15% have been recorded (Ziesmann, 1996). In the wild, *C. elegans* primarily inhabit soil environments rich in rotting organic matter, where they feed on bacteria and other microorganisms (Félix and Duveau, 2012; Hodgkin and Doniach, 1997; Kiontke et al., 2011). In this niche, O_2 and CO_2 levels can fluctuate significantly, with O_2 levels falling far below 21% and CO_2 levels rising above 10% (Anderson and Ultsch, 1987; Barrière and Félix, 2005; Burg and Burg, 1965; Félix and Braendle, 2010; Félix and Duveau, 2012).

CO_2-sensing across species

Humans have developed sophisticated mechanisms to monitor internal O_2 levels. O_2 is detected by chemoreceptors in the carotid body, which triggers an increase in respiration rate (Ma and Ringstad, 2012). In contrast, CO_2 is undetectable and odorless in humans at concentrations below 30%. Higher CO_2 concentrations elicit a painful reaction triggered by the trigeminal, rather than olfactory, system (Bensafi et al., 2008; Shusterman and Avila, 2003). Nevertheless, defective response to changes in O_2 and CO_2 concentrations are involved in a number of blood diseases, behavioral disorders, neurodegeneration and cancer (Quaegebeur and Carmeliet, 2010; Semenza et al., 2011). In contrast to humans, studies show that many species of vertebrates and invertebrates are extremely sensitive to their CO_2 environment (Jones, 2013). In rats and bullfrogs, 0.5% CO_2 elicits responses in olfactory epithelium cells (Coates and

Ballam, 1990; Youngentob et al., 1991), and the hawkmoth *Manduca sexta* uses increasing CO_2 as a factor in flower selection. In addition, several blood-feeding insects follow CO_2 gradients as part of host-seeking behavior. Tsetse flies (Voskamp et al., 1999) (sleeping sickness) and sandflies (Pinto et al., 2001) (leishmaniasis), as well as the malaria-carrying mosquito *Anopheles gambiae* (Healy and Copland, 1995), the dengue/yellow fever-causing mosquito *Aedes aegypti* (Eiras and Jepson, 1991), ticks (Steullet and Guerin, 1992) and fleas (Benton and Lee, 1965) are all attracted to CO_2, which can be exhaled at concentrations reaching 4-5% during respiration in mammals (Pleil and Lindstrom, 1995). In the honeybee, *Apis mellifera*, rising CO_2 levels elicit a recruitment of worker bees and increased wing-fanning behavior to ventilate the hive (Seeley, 1974). And in mice, levels of CO_2 above 10% elicit a fear/avoidance response (Ziemann et al., 2009).

Mice detect near-atmospheric concentrations of CO_2 (0.066% CO_2) using a specialized subset of olfactory sensory neurons (OSNs) enriched in carbonic anhydrase-2 (CAII), an enzyme that catalyzes the hydration of CO_2 to generate H^+ and HCO_3^- (Hu et al., 2007). Bicarbonate ions activate OSNs by stimulating a guanylate cyclase, GC-D, opening CNGA3 channels and leading to cell depolarization (Guo et al., 2009; Han and Luo, 2010; Sun et al., 2009). These CO_2-sensing OSNs are unique in the way they project their axons to a series of caudal glomeruli termed necklace glomeruli, instead of a single glomerulus, as is usually seen with olfactory neurons expressing the same receptor (Luo, 2008; Walz et al., 2007). In humans, the GC-D homolog is a pseudogene, which offers some insight into their lack of CO_2 detection capability (Torrents et al., 2003; Young et al., 2007).

In *Drosophila melanogaster,* CO_2 concentrations 0.02% above atmospheric levels elicit an innate avoidance response (Bräcker et al., 2013). However, changes in locomotory state can trigger a context-dependent behavioral switch. CO_2 is aversive in walking flies, but elicits an attractive response in flight. CO_2 triggers avoidance in walking flies at concentrations as low as 0.1% CO_2 (Suh et al., 2004), but attraction when presented with a plume of 100% CO_2 while in flight (Wasserman et al., 2013). As seen in mammals, CO_2 avoidance in *D. melanogaster* is mediated by a set of dedicated CO_2-sensing olfactory neurons: the ab1c sensilla neurons on the antennae that project to the V glomerulus. These CO_2-sensing neurons express two gustatory receptors, *Gr21a* and *Gr63a*, which are required for CO_2 detection (Jones et al., 2007; Kwon et al., 2007). However, avoidance and attraction are thought to be mediated by independent pathways. CO_2 attraction does not require output from *Gr21a* and *Gr63a*-expressiong OSNs, and instead relies on signaling through the acid sensor *Ir64a*, as well as the olfactory co-receptor *Orco* and octopamine signaling (Wasserman et al., 2013). Thus, in *D. melanogaster*, attractive and aversive CO_2 response behaviors arise from segregated circuits.

CO_2-sensing in *Caenorhabditis elegans*

Nematodes like *C. elegans* do not have specialized circulatory or respiratory systems, but instead rely on passive diffusion to exchange respiratory gases (Lee and Atkinson, 1977). Therefore, they can only control internal O_2/CO_2 concentrations by migrating to environments with optimal O_2/CO_2 concentrations. This highlights the importance of a sensitive O_2/CO_2-sensing mechanism to increase its chances of survival. In *C. elegans*, CO_2 detection requires the receptor-type guanylate cyclase GCY-9, expressed in the

pair of sensory BAG neurons (Hallem et al., 2011b; Hallem and Sternberg, 2008; Smith et al., 2013), as well as the cGMP-gated ion channel subunits TAX-2 and TAX-4 (Bretscher et al., 2008; Hallem et al., 2011b; Hallem and Sternberg, 2008). As mentioned above, CO_2-sensitive neurons in the rodent olfactory system also express a guanylate cyclase, GC-D, (Hu et al., 2007), which acts as a receptor for the CO_2 metabolite bicarbonate (Guo et al., 2009; Sun et al., 2009). In contrast, the guanylate cyclase GCY-9 in *C. elegans* has been shown to bind molecular CO_2 (Smith et al., 2013). However, the parallel use of guanylate cyclases suggests that CO_2-sensing mechanisms may be conserved in nematodes and mammals. In addition, the BAG neurons also express a carbonic anhydrase, CAH-2 (Bretscher et al., 2011), also found in the rodent CO_2 detection pathway.

Circuit mechanisms of attractive and aversive olfactory responses

Research into the neuronal basis of innate sensory preferences has revealed - in mammals, insects, and nematodes - the existence of dedicated neuronal populations, or individual neurons, preferentially coded for attraction or aversion to specific stimuli (Marella et al., 2006; Mueller et al., 2005; Root et al., 2014; Tobin et al., 2002; Troemel et al., 1997; Yarmolinsky et al., 2009; Zhao et al., 2003). In mice, projections from the olfactory bulb to the cortical amygdala are spatially stereotyped, suggesting that encoding of attractive and aversive odors is topographically distinct. Indeed, it has been demonstrated that 2,3,5-trimethyl-3-thiazoline (TMT), which elicits an aversive response, and 2-phenylethanol, which elicits an attractive response, activate anatomically segregated neuronal population in the cortical amygdala (Root et al., 2014). Furthermore, it has been demonstrated that this organization is conserved in

cases where a single stimulus can elicit both attractive and aversive responses. In rats, infant-directed aggression is prevalent in males and virgin females, in contrast to active parental care displayed by postpartum and “sensitized” females, *i.e.* virgin females that have had continuous exposure to pups. The control of pup-elicited behavior appears to be mediated by two competing pathways: an aversive circuit seen in males and virgin females is primarily innervated by vomeronasal inputs, is dominant, and suppresses a facilitative circuit. In sensitized females and female rats that have experienced pregnancy, hormonal and neuromodulatory factors activate the facilitative circuit, which silences the aversive circuit (Dulac et al., 2014).

In *C. elegans*, specific sensory neurons have also been linked to particular behavioral outputs: AWA and AWC olfactory neurons mediate responses to attractive odorants, while the AWB, ASH and ADL sensory neurons mediate avoidance of noxious stimuli (Bargmann et al., 1993; Chao et al., 2004; Troemel et al., 1997). The intrinsic property of these neurons was demonstrated by an experiment in which the G-protein coupled olfactory receptor ODR-10, which is endogenously expressed in AWA and mediates attraction to diacetyl, was expressed in AWB, leading to diacetyl avoidance (Sengupta et al., 1996; Troemel et al., 1997). The revelation of odor-concentration dependent functional segregation of these sensory neurons further illustrates the application of the labelled-line theory to *C. elegans* sensory behaviors. Isoamyl alcohol is a chemical cue that elicits both attraction and avoidance in *C. elegans*. At low concentrations, AWC mediates attraction to isoamyl alcohol, and at high concentrations ASH mediates avoidance (Yoshida et al., 2012). Similarly, sensing of high salt vs low salt also requires two different circuits. In animals raised at high salt, the sensory neuron ASE and the

interneuron AIB respond to decreases in salt concentration to redirect animals towards areas of high salt concentration. In contrast, in animals raised in low salt environments, only ASE responds to changes in salt concentration (Kunitomo et al., 2013).

Investigation into the *C. elegans* pheromone-sensing circuit has demonstrated a mechanism whereby more nuanced behaviors can arise. In the RMG “hub-and-spoke’ circuit, a spectrum of behaviors is determined by the antagonistic relationship between ADL, the sensory neuron that promotes pheromone avoidance, and the downstream interneuron RMG’s gap junction circuit which promotes pheromone attraction by potentiating signaling from the sensory neuron ASK (Jang et al., 2012; Macosko et al., 2009). The combination of activity between attraction and avoidance neurons creates a push-pull circuit motif that enables a single sensory input to give rise to multiple behavioral outputs.

Still, the flexibility and breadth of animal behaviors suggests that innate sensory pathways must be subject to context-dependent modification, and that neuronal mechanisms facilitating multifunctionality must exist. Closer examination of the ASH sensory neuron has provided one such example. Although classically known as an avoidance neuron, ASH has been shown to mediate attraction at low concentrations of 1-octanol as well as avoidance at high concentrations of 1-octanol. This is due to the expression of two functionally diverse receptors, one which inhibits aversive responses at low 1-octanol levels, and another which antagonizes this inhibition at high 1-octanol levels (Mills et al., 2011; Wragg et al., 2007). It remains to be seen how these responses are shaped at the interneuron and motorneuron level.

In this thesis, I explore how context can alter the perception of sensory cues, leading to behavioral shifts, and how behavioral flexibility is encoded in the nervous system. We asked what neuronal mechanisms transform sensory experience into coding which determines attractive or repulsive behavioral states. I have examined the cellular and molecular mechanisms that shape a CO_2 circuit in *C. elegans* capable of integrating environmental cues to elicit context-appropriate behavioral CO_2 responses. The CO_2 circuit design I present in the following chapters offers new insights into potential configurations for circuits mediating divergent behaviors, and represents a previously unrecognized microcircuit motif for generating rapid changes in innate chemosensory valence. Although extensive evidence has shown the ways in which specialized neurons direct discrete behaviors, the CO_2-sensing circuit reveals built-in mechanisms of efficiency within the nervous system. We observe through these studies, that a single circuit capable of generating a spectrum of possible behaviors in response to the same chemosensory stimulus bolsters plasticity against the limitations of the labelled line theory, and suggests a novel neuronal paradigm for the generation of context-dependent behaviors.

Chapter 2: O_2-sensing neurons control CO_2 response in *C. elegans*

O_2-Sensing Neurons Control CO_2 Response in *C. elegans*

Mayra A. Carrillo,* Manon L. Guillermin,* Sophie Rengarajan, Ryo P. Okubo, and Elissa A. Hallem
Department of Microbiology, Immunology, and Molecular Genetics, University of California, Los Angeles, Los Angeles, California 90095

Sensory behaviors are often flexible, allowing animals to generate context-appropriate responses to changing environmental conditions. To investigate the neural basis of behavioral flexibility, we examined the regulation of carbon dioxide (CO_2) response in the nematode *Caenorhabditis elegans*. CO_2 is a critical sensory cue for many animals, mediating responses to food, conspecifics, predators, and hosts (Scott, 2011; Buehlmann et al., 2012; Chaisson and Hallem, 2012). In *C. elegans*, CO_2 response is regulated by the polymorphic neuropeptide receptor NPR-1: animals with the N2 allele of *npr-1* avoid CO_2, whereas animals with the Hawaiian (HW) allele or an *npr-1* loss-of-function (*lf*) mutation appear virtually insensitive to CO_2 (Hallem and Sternberg, 2008; McGrath et al., 2009). Here we show that ablating the oxygen (O_2)-sensing URX neurons in *npr-1*(*lf*) mutants restores CO_2 avoidance, suggesting that NPR-1 enables CO_2 avoidance by inhibiting URX neurons. URX was previously shown to be activated by increases in ambient O_2 (Persson et al., 2009; Zimmer et al., 2009; Busch et al., 2012). We find that, in *npr-1*(*lf*) mutants, O_2-induced activation of URX inhibits CO_2 avoidance. Moreover, both HW and *npr-1*(*lf*) animals avoid CO_2 under low O_2 conditions, when URX is inactive. Our results demonstrate that CO_2 response is determined by the activity of O_2-sensing neurons and suggest that O_2-dependent regulation of CO_2 avoidance is likely to be an ecologically relevant mechanism by which nematodes navigate gas gradients.

Introduction

Animals from nematodes to humans respond to environmental gases, such as CO_2 and O_2. CO_2 is aversive for many free-living animals but attractive for many parasitic animals, which rely on CO_2 for host location (Luo et al., 2009; Chaisson and Hallem, 2012). O_2 increases or decreases can evoke avoidance responses in flies and nematodes (Chang et al., 2006; Morton, 2011) and alter foraging and feeding behaviors (Wingrove and O'Farrell, 1999; Cheung et al., 2005; Rogers et al., 2006; Vigne and Frelin, 2010). These responses are critical for survival: exposure to hypercapnia, hyperoxia, or hypoxia can result in reduced neural activity, cell cycle arrest, tumor formation, or death (Wingrove and O'Farrell, 1999; Harris, 2002; West, 2004; Langford, 2005).

The nematode *Caenorhabditis elegans* detects and responds to changes in environmental CO_2 and O_2 (Scott, 2011). *C. elegans* adults migrate away from a CO_2 source and toward ~10% O_2 (Gray et al., 2004; Bretscher et al., 2008; Hallem and Sternberg, 2008). However, CO_2 response can vary with developmental stage and environmental context. For example, CO_2 is repulsive for adults but attractive for dauer larvae (Hallem et al., 2011a), and the behavioral response to simultaneous changes in CO_2 and O_2 levels is indicative of an interaction between the responses to the two gases (Bretscher et al., 2008; McGrath et al., 2009).

The response of *C. elegans* to CO_2 and many other stimuli is regulated by NPR-1, a polymorphic neuropeptide receptor homologous to mammalian neuropeptide Y receptors (de Bono and Bargmann, 1998; Gray et al., 2004; Rogers et al., 2006; Bretscher et al., 2008; Hallem and Sternberg, 2008; Macosko et al., 2009; McGrath et al., 2009; Reddy et al., 2009). The N2 strain of *C. elegans* contains an *npr-1* allele that confers solitary feeding behavior, whereas the CB4856 Hawaiian (HW) strain contains an *npr-1* allele that confers social feeding behavior (de Bono and Bargmann, 1998). N2 animals respond strongly to CO_2 but weakly to O_2 on food, whereas HW animals appear relatively indifferent to CO_2 but respond strongly to O_2 on food (Gray et al., 2004; Bretscher et al., 2008; Hallem and Sternberg, 2008). NPR-1 is thought to act by repressing neural activity (Chang et al., 2006; Macosko et al., 2009).

To investigate the mechanisms of CO_2 response plasticity, we examined the regulation of CO_2 response by NPR-1. We show that HW and *npr-1*(*lf*) animals do not avoid CO_2 despite showing normal CO_2-evoked activity in BAG neurons. However, ablation of URX neurons in *npr-1*(*lf*) animals restores CO_2 avoidance, suggesting that NPR-1 enables CO_2 avoidance by decreasing URX activity. URX is activated by increases in ambient O_2 (Persson et al., 2009; Zimmer et al., 2009; Busch et al., 2012), and we show that its O_2-sensing ability is required to inhibit CO_2 avoidance. We also show that HW and *npr-1*(*lf*) animals avoid CO_2 under low O_2 conditions, when URX is inactive. Our results

Received Sept. 24, 2012; revised April 21, 2013; accepted April 27, 2013.

Author contributions: M.A.C., M.L.G., S.R., and E.A.H. designed research; M.A.C., M.L.G., S.R., R.P.O., and E.A.H. performed research; M.A.C., M.L.G., S.R., and E.A.H. analyzed data; M.A.C., M.L.G., and E.A.H. wrote the paper.

M.A.C. was supported by a National Science Foundation Graduate Research Fellowship (Grant No. DGE-0707424) and a Eugene V. Cota-Robles Fellowship. S.R. was supported by the National Institutes of Health National Institute of General Medical Sciences training Grant GM08042 and the UCLA-Cal Tech Medical Scientist Training Program. E.A.H. is a MacArthur Fellow, an Alfred P. Sloan Research Fellow, a Rita Allen Foundation Scholar, and a Searle Scholar. This work was supported by a National Institutes of Health R00 Grant to E.A.H (Grant No. R00-AI085107). We thank Cori Bargmann, Alon Zaslaver, Paul Sternberg, Jo Anne Powell-Coffman, Miriam Goodman, Maureen Barr, Ikue Mori, Mario de Bono, Shawn Lockery, Shohei Mitani, and the Caenorhabditis Genetics Center for *C. elegans* strains; Cori Bargmann, Alon Zaslaver, and Paul Sternberg for plasmids; Lars Dreier, Michelle Castelletto, Alvaro Sagasti, Doug Black, and Keely Chaisson for critical reading of this manuscript; and Joe Vanderwaart for insightful discussion of this manuscript.

The authors declare no competing financial interests.

*M.A.C. and M.L.G. contributed equally to this work.

Correspondence should be addressed to Dr. Elissa A. Hallem, University of California, Los Angeles, MIMG 237 BSRB, 615 Charles E. Young Drive East, Los Angeles, CA 90095. E-mail: ehallem@microbio.ucla.edu.

DOI:10.1523/JNEUROSCI.4541-12.2013

 0270-6474/13/339675-09$15.00/0

suggest that CO_2 avoidance is regulated by ambient O_2 via a pair of O_2-sensing neurons, allowing flexible responses to fluctuating levels of environmental gases.

Materials and Methods

Strains. *C. elegans* strains are listed in the order in which they appear in the figures. The following strains were used: N2 (Bristol); DA609 *npr-1(ad609);* CB4856 (Hawaiian); CX11697 *kyIs536[flp-17::p17 SL2 GFP, elt-2::mCherry]; kyIs538[glb-5::p12 SL2 GFP, elt-2::mCherry]*; EAH2 *gcy-9(tm2816)*; PS6416 *pha-1(e2123); syEx1206[gcy-33::G-CaMP3.0, pha-1(+)]*; EAH117 *npr-1(ad609); syEx1206[gcy-33::G-CaMP3.0, pha-1(+)]*; EAH119 *bruEx89[gcy-33::G-CaMP-3.0, ets-8::GFP]*; MT17148 *flp-21(ok889); flp-18(n4766)*; PR767 *ttx-1(p767)*; GN112 *pgIs2[gcy-8::caspase, unc-122::GFP]*; PR679 *che-1(p679)*; MT18636 *nIs326[gcy-33::YC3.60]; lin-15AB(n765)*; AX2047 *gcy-8::YC3.60, unc-122::dsRed*; XL115 *flp-6::YC3.60*; CX9592 *npr-1(ad609); kyEx2016[npr-1::npr-1 SL2 GFP, ofm-1::dsRed]*; CX9395 *npr-1(ad609); kyEx1965[gcy-32::npr-1 SL2 GFP, ofm-1::dsRed]*; CX9633 *npr-1(ad609); kyEx2096[flp-8::npr-1 SL2 GFP, ofm-1::dsRed]*; CX9396 *npr-1(ad609); kyEx1966[flp-21::npr-1 SL2 GFP, ofm-1::dsRed]*; CX9644 *npr-1(ad609); kyEx2107[ncs-1::npr-1 SL2 GFP, ofm-1::dsRed]*; CX7102 *lin-15(n765) qaIs2241[gcy-36::egl-1, gcy-35::GFP, lin-15(+)]*; CX7158 *npr-1(ad609) qaIs2241[gcy-36::egl-1, gcy-35::GFP, lin-15(+)]*; ZG629 *iaIs22[gcy-36::GFP, unc-119(+)]*; EAH80 *iaIs22[gcy-36::GFP, unc-119(+)]; npr-1(ad609)*; EAH106 *bruEx86[gcy-36::G-CAMP3.0, coel::RFP]*; EAH114 *npr-1(ad609)*; *bruEx86[gcy-36::G-CaMP3.0, coel::RFP]*; ZG24 *ahr-1(ia3)*; ZG624 *ahr-1(ia3); npr-1(ad609)*; CX6448 *gcy-35(ok769)*; CX7157 *gcy-35(ok769); npr-1(ad609)*; RB1902 *flp-19(ok2460)*; PT501 *flp-8(pk360)*; PT502 *flp-10(pk367)*; EAH123 *npr-1(ad609) flp-19(ok2460)*; EAH141 *npr-1(ad609) flp-8(pk360);* EAH140 *flp-10(pk367); npr-1(ad609);* PS5892 *gcy-33(ok232); gcy-31(ok296)*; EAH127 *gcy-33(ok232); gcy-31(ok296) lon-2(e678) npr-1(ad609).* In addition, CX7376 *kyIs511[gcy-36::G-CaMP, coel::GFP]* and EAH115 *kyIs511[gcy-36::G-CaMP, coel::GFP]; npr-1(ad609)* were used to confirm the results shown in Figure 5*A* with independent transgenes, and RB1903 *flp-19(ok2461)* and EAH139 *npr-1(ad609) flp-19(ok2461)* were used to confirm the results shown in Figure 5*C* with an independent deletion allele of *flp-19*. All transgenes were injected into N2, except *bruEx89*, which was injected into CB4856 to generate EAH119. EAH2 was derived from FX2816 by outcrossing to N2 for five generations. Nematodes were cultured on NGM plates containing *Escherichia coli* OP50 according to standard methods (Brenner, 1974). *C. elegans* dauer larvae were collected from the lids of plates from which the OP50 food source had been depleted ("starved plates") and stored in dH_2O at 15°C before use. All nematodes tested were hermaphrodites.

Generation of reporter transgenes and transgenic animals. To generate EAH119, the *gcy-33::G-CaMP3.0* construct from PS6416 was injected into CB4856 at 50 ng/μl along with *ets-8::GFP* at 50 ng/μl as a coinjection marker. To generate EAH106, a *gcy-36::G-CaMP3.0* transcriptional fusion construct was generated by amplifying a 1.0 kb region upstream of the start codon of the *gcy-36* gene from N2 genomic DNA using primers that included the following sequences: 5′-gatgttggtagatggggtttgga-3′ and 5′-aaattcaaacaagggctacccaaca-3′. The promoter fragment was then cloned into a modified Fire vector containing the G-CaMP3.0 coding region (Tian et al., 2009). The *gcy-36::G-CaMP3.0* construct was injected into N2 animals at a concentration of 25 ng/μl along with 50 ng/μl of *coel::RFP* as a coinjection marker.

Acute CO_2 avoidance assays. Acute CO_2 avoidance assays were performed as previously described (Hallem and Sternberg, 2008; Guillermin et al., 2011; Hallem et al., 2011b). Briefly, ~10–15 young adults were tested on 5 cm assay plates consisting of NGM agar seeded with a thin lawn of *E. coli* OP50 bacteria. Gas stimuli consisted of certified industrial mixes (Airgas or Air Liquide). CO_2 stimuli consisted of 10% CO_2, 10% O_2 (unless otherwise indicated), and the rest N_2. Control stimuli consisted of 10% O_2 (unless otherwise indicated) and the rest N_2. Two 50 ml gas-tight syringes were filled with gas: one with CO_2 and one without CO_2. The mouths of the syringes were connected to flexible PVC tubing attached to Pasteur pipettes, and gases were pumped through the Pasteur pipettes using a syringe pump at a rate of 1.5 ml/min. Worms were exposed to gases by placing the tip of the Pasteur pipette near the head of a forward-moving worm, and a response was scored if the worm reversed within 4 s. Gases were delivered blindly, and worms were scored blindly. An avoidance index was calculated by subtracting the fraction of animals that reversed to the air control from the fraction that reversed to the CO_2. Single-worm acute CO_2 avoidance assays were performed on L4 or young adult laser-ablated animals (see Fig. 3*C*) as described above, except that each animal was tested 12 times with >2 min between trials. For each animal, an avoidance index was calculated by subtracting the fraction of trials in which it reversed to the air control from the fraction of trials in which it reversed to the CO_2 stimulus. The avoidance index for each genotype or treatment was calculated as the mean avoidance index for each animal of the same genotype or treatment.

CO_2 chemotaxis assays. CO_2 chemotaxis assays were performed on young adults essentially as previously described (Bretscher et al., 2008). Briefly, animals were washed off plates and into a 65 mm Syracuse watch glass using M9 buffer. Animals were washed 3× with M9 and transferred from the watch glass to a 1 cm × 1 cm square of Whatman paper. Animals were then transferred from the filter paper to the center of a 9 cm NGM or chemotaxis plate (Bargmann et al., 1993). Gas stimuli were delivered to the plate though holes in the plate lids as previously described (Hallem et al., 2011a; Dillman et al., 2012), except at a flow rate of 2 ml/min. Assay plates were placed on a vibration-reducing platform for 20 min. The number of worms in a 2-cm-diameter circle centered under each gas inlet was then counted, except for Figures 1*B* and 2*A*, *B*, where the number of worms in an area comprising ~3/10 of the plate under each gas inlet was counted. The chemotaxis index was calculated as follows: (no. of worms at CO_2 − no. of worms at control)/(no. of worms at CO_2 + control). Two identical assays were always performed simultaneously with the CO_2 gradient in opposite directions on the two plates to control for directional bias resulting from room vibration; assays were discarded if the difference in the chemotaxis index for the two plates was ≥0.9 or if <7 worms moved into the scoring regions on one or both of the plates.

For CO_2 chemotaxis assays under different O_2 conditions, assays were performed as described above inside airtight canisters (OGGI; 13.3 cm × 10.1 cm) with four holes drilled into the lids to insert tubing for gas flow. One hole was used to establish the ambient O_2 level, two were used to establish the CO_2 gradient, and one was used as an exhaust. A gas mixture consisting of either 7% O_2 and the balance N_2, or 21% O_2 and the balance N_2, was pumped into the chamber at a rate of 2.5 L/min for 1 min and then 0.5 L/min for the duration of the assay. The CO_2 stimulus (10% CO_2, either 7% O_2 or 21% O_2, balance N_2) and control stimulus (7% O_2 or 21% O_2, balance N_2) were pumped into the chamber at a rate of 2 ml/min using a syringe pump, as described above. The assay duration was 25 min.

Dauer CO_2 chemotaxis assays were performed as previously described (Hallem et al., 2011a; Dillman et al., 2012). Briefly, assays were performed on chemotaxis plates (Bargmann et al., 1993). For each assay, ~50–150 dauers were placed in the center of the assay plate. Gas stimuli and gas delivery to the assay plate were as described above, and a chemotaxis index was calculated as described above.

Calcium imaging. Imaging was performed using the genetically encoded calcium indicators G-CaMP (Zimmer et al., 2009), G-CaMP3.0 (Tian et al., 2009), or yellow cameleon YC3.60 (Nagai et al., 2004). Young adult or L4 animals were immobilized onto a cover glass containing a 2% agarose pad made with 10 mM HEPES using Surgi-Lock 2oc instant tissue adhesive (Meridian). A custom-made gas delivery chamber was placed over the cover glass. Gases were delivered at a rate of 0.8–1 L/min. Gas delivery was controlled by a ValveBank4 controller (AutoMate Scientific). Imaging was performed on an AxioObserver A1 inverted microscope (Carl Zeiss) using a 40× EC Plan-NEOFLUAR lens, a Hamamatsu C9100 EM-CCD camera, and AxioVision software (Carl Zeiss). For YC3.60 imaging, the emission image was passed through a DV2 beam splitter (Photometrics) as previously described (Hallem et al., 2011b). Image analysis was performed using AxioVision software (Carl Zeiss) and Microsoft Excel. The mean pixel value of a background region of interest was subtracted from the mean pixel value of a region of interest containing the neuron soma. Fluorescence values were normalized to the average values obtained in the 4 s before CO_2 delivery. For YC3.60 im-

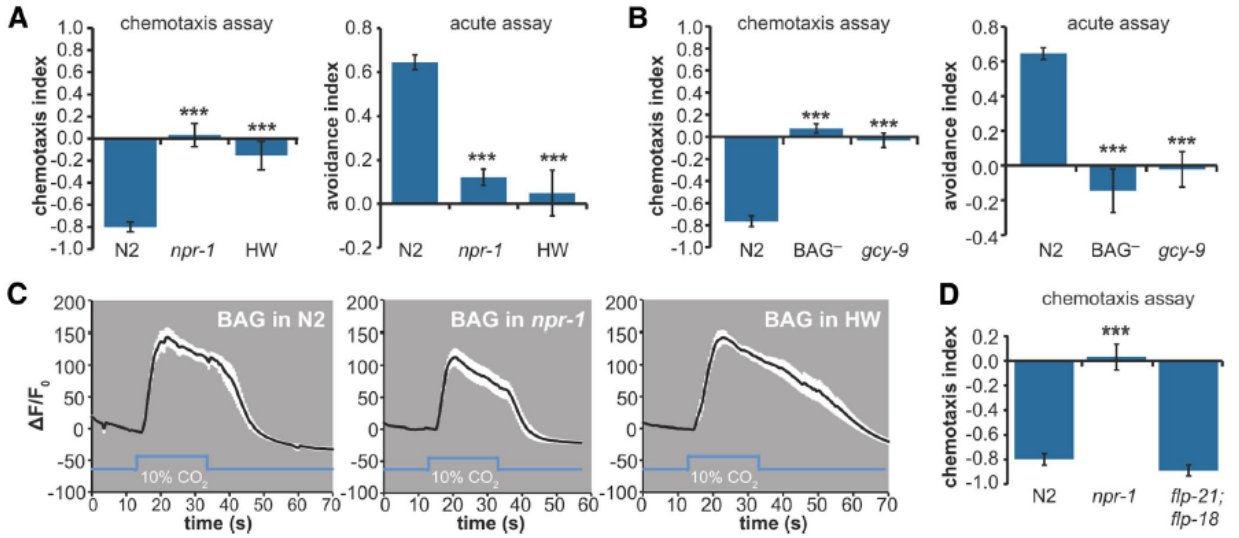

Figure 1. *npr-1* is required for CO_2 avoidance behavior but not CO_2 detection. ***A***, *npr-1* is required for CO_2 avoidance by adults. Left, CO_2 chemotaxis assay. Right, Acute CO_2 avoidance assay. *npr-1(lf)* and HW animals do not respond to CO_2 in either assay. ***$p < 0.001$, one-way ANOVA with Bonferroni post-test. $n = 6–9$ trials (chemotaxis assay) or 10–27 trials (acute assay) for each genotype. Error bars represent SEM. ***B***, Animals that lack BAG neurons and *gcy-9(tm2816)* mutant animals do not respond to CO_2. BAG-ablated animals express a transgene that specifically kills the BAG neurons (Zimmer et al., 2009; Hallem et al., 2011b). Left, CO_2 chemotaxis assay. Right, Acute CO_2 avoidance assay. The CO_2 stimulus was delivered in an airstream containing 10% O_2, which approximates the preferred O_2 concentration for *C. elegans* (Gray et al., 2004); the control airstream also contained 10% O_2. $n = 18$ or 19 trials (chemotaxis assay) or 4–27 trials (acute assay). ***$p < 0.001$, Kruskal–Wallis test with Dunn's post-test (chemotaxis assay) or one-way ANOVA with Bonferroni post-test (acute assay). Error bars represent SEM. ***C***, *npr-1* is not required for CO_2 detection by BAG neurons. BAG neuron cell bodies of N2 (left), *npr-1(lf)* (middle), and HW (right) animals respond to CO_2. Calcium increases were measured using the calcium indicator G-CaMP3.0. Black lines indicate average calcium responses; white shading represents SEM. Blue lines below the traces indicate the timing of the CO_2 pulse. The peak response amplitudes of all three genotypes were not significantly different (one-way ANOVA with Bonferroni post-test). The decay kinetics of all three genotypes were significantly different ($p < 0.001$ using a polynomial curve fit). However, these differences are not likely to be a result of differences at the *npr-1* locus because recordings from BAG neurons of N2 animals using G-CaMP3.0 showed different decay kinetics from BAG neurons of N2 animals using YC3.60 (Fig. 2*C*,*D*). ***D***, The NPR-1 ligands FLP-21 and FLP-18 are not required for CO_2 response. ***$p < 0.001$, one-way ANOVA with Bonferroni post-test. $n = 6–9$ animals for each genotype. Error bars represent SEM.

aging, the YFP/CFP ratio was calculated as previously described (Hallem et al., 2011b). Images were baseline corrected using a linear baseline correction. Traces with unstable baselines before the onset of the CO_2 stimulus were discarded.

Laser ablation. Ablations were performed on L2 and L3 animals as previously described (Hallem and Sternberg, 2008). Briefly, animals were mounted on glass slides for DIC microscopy on a pad consisting of 5% Noble agar in dH_2O with 5% sodium azide as anesthetic. Ablations were performed on a Zeiss AxioImager A2 microscope with an attached MicroPoint laser (Carl Zeiss). Neurons were ablated by focusing a laser microbeam on the cell. Mock-ablated animals were mounted similarly but were not subjected to a laser microbeam. Neurons were identified by both cell position and GFP expression. Loss of the ablated cell was confirmed by observing loss of fluorescence in the adult animal.

Fluorescence microscopy. Nematodes were anesthetized with 3 mM levamisole and mounted on a pad consisting of 5% Noble agar in dH_2O. Epifluorescence images were captured using a Zeiss AxioImager A2 microscope with an attached Zeiss AxioCam camera and Zeiss AxioVision software (Carl Zeiss). To quantify epifluorescence in Figure 4*D*, all images were taken with the same exposure time. Average pixel intensities in the region of interest were quantified using AxioVision software (Carl Zeiss). Relative intensities were normalized by setting the highest mean intensity value to 1.

Statistical analysis. Statistical analysis was performed using GraphPad Instat and Prism. All significance values reported are relative to the N2 control, unless otherwise indicated.

Results

NPR-1 regulates CO_2 avoidance behavior

To investigate the role of *npr-1* in mediating CO_2 response, we examined the CO_2-evoked behavior of N2, HW, and *npr-1(lf)* animals in both a chemotaxis assay and an acute avoidance assay. We found that N2 animals displayed robust CO_2 avoidance in both assays, whereas HW and *npr-1(lf)* animals were essentially unresponsive to CO_2 in both assays (Fig. 1*A*). Thus, the N2 allele of *npr-1* is required for the behavioral response to CO_2. CO_2 avoidance behavior also requires the CO_2-detecting BAG neurons and the receptor guanylate cyclase gene *gcy-9*, which encodes a putative receptor for CO_2 or a CO_2 metabolite (Fig. 1*B*) (Hallem and Sternberg, 2008; Hallem et al., 2011b; Brandt et al., 2012). To test whether *npr-1* is required for CO_2 detection, we imaged from BAG neurons using the genetically encoded calcium indicator G-CaMP3.0 (Tian et al., 2009). We found that the BAG neurons of N2, *npr-1(lf)*, and HW animals all showed CO_2-evoked activity (Fig. 1*C*), suggesting that *npr-1* regulates the behavioral response to CO_2 downstream of the calcium response of BAG neurons. The *flp-21* and *flp-18* genes, which encode NPR-1 ligands, are not required for CO_2 avoidance, suggesting that other ligands are required for the regulation of CO_2 response by *npr-1* (Fig. 1*D*).

In addition to the BAG neurons, the salt-sensing ASE neurons and the temperature-sensing AFD neurons have been implicated in CO_2 detection and avoidance (Bretscher et al., 2011). However, we found that *che-1* mutant animals, which lack functional ASE neurons (Uchida et al., 2003), displayed normal CO_2 avoidance in both a chemotaxis assay and an acute assay (Fig. 2*A*) (Hallem and Sternberg, 2008). Both AFD-ablated animals and *ttx-1* mutant animals, which lack functional AFD neurons (Satterlee et al., 2001), showed defective CO_2 avoidance in a chemotaxis assay but not an acute assay (Fig. 2*A*) (Hallem and Sternberg, 2008). These results suggest that ASE neurons are not required for CO_2 avoidance under our assay conditions and that AFD neurons are required for some but not all CO_2-evoked be-

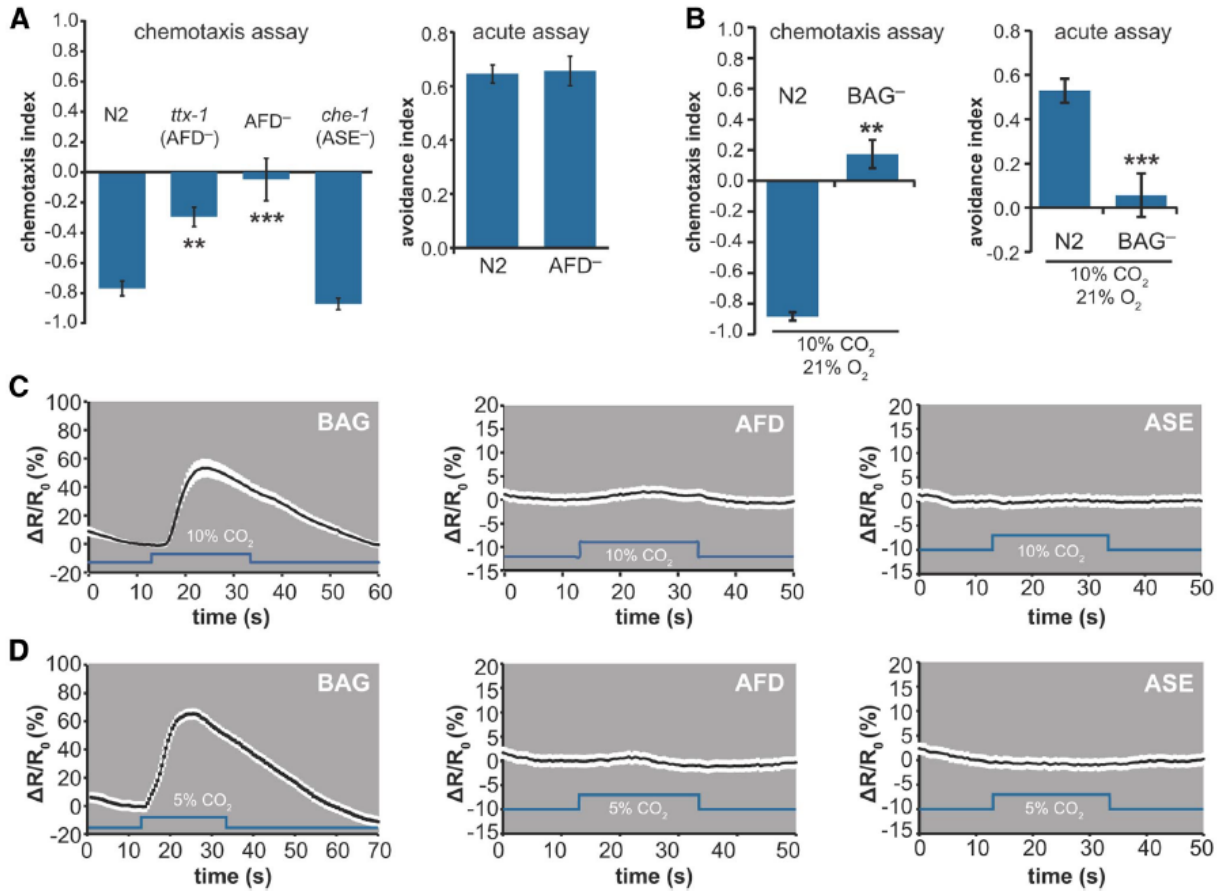

Figure 2. The role of AFD, ASE, and BAG neurons in CO_2 response. ***A***, Animals that lack functional ASE neurons respond normally to CO_2 in both a chemotaxis assay (left graph) and an acute avoidance assay (Hallem and Sternberg, 2008). Animals that lack functional AFD neurons respond normally to CO_2 in an acute avoidance assay (right) but not a chemotaxis assay (left). AFD-ablated animals (AFD^-) express a transgene that specifically kills the AFD neurons (Glauser et al., 2011). The *ttx-1* and *che-1* genes encode transcription factors that are required for normal development of the AFD and ASE neurons, respectively (Satterlee et al., 2001; Uchida et al., 2003; Hobert, 2010). $^{**}p < 0.01$, Kruskal–Wallis test with Dunn's post-test. $^{***}p < 0.001$, Kruskal–Wallis test with Dunn's post-test. $n = 10–18$ trials (chemotaxis assay) or $n = 9–27$ trials (acute assay) for each genotype. Error bars represent SEM. ***B***, Animals that lack BAG neurons do not respond to CO_2 when the CO_2 stimulus is delivered in an airstream containing 21% O_2, which approximates the atmospheric O_2 concentration. The control airstream also contained 21% O_2. $^{**}p < 0.01$, Mann–Whitney test. $^{***}p < 0.001$, one-way ANOVA with Bonferroni post-test. $n = 4–11$ trials (chemotaxis assay) or $n = 10–27$ trials (acute assay). Error bars represent SEM. ***C***, ***D***, Calcium responses of BAG, AFD, and ASE neurons to 10% CO_2 (***C***) and 5% CO_2 (***D***), measured using the ratiometric calcium indicator yellow cameleon YC3.60. Black lines indicate average calcium responses; white shading represents SEM. Blue lines below the traces indicate the timing of the CO_2 pulse. Calcium increases were observed in BAG neuron cell bodies but not AFD and ASE neuron cell bodies. $n = 5–13$ animals for each genotype.

haviors. By contrast, animals lacking BAG neurons showed a complete loss of CO_2 response in both assays, regardless of whether CO_2 was delivered in combination with 10% O_2, which approximates the preferred O_2 concentration of *C. elegans* (Gray et al., 2004), or 21% O_2, which approximates atmospheric O_2 concentration (Figs. 1*B* and 2*B*). We then imaged from BAG, ASE, and AFD neurons using the calcium indicator yellow cameleon YC3.60 (Nagai et al., 2004). We observed CO_2-evoked activity in BAG neurons but not AFD and ASE neurons in response to a 20 s pulse of either 5% or 10% CO_2 (Fig. 2*C*,*D*). Thus, BAG neurons are the primary sensory neurons that contribute to CO_2 response under our assay conditions.

NPR-1 regulates URX neuron activity to control CO_2 avoidance behavior

NPR-1 is not expressed in BAG neurons but is expressed in a number of other sensory neurons as well as some interneurons (Macosko et al., 2009). To identify the site of action for the regulation of CO_2 response by *npr-1*, we introduced the N2 allele of *npr-1* into *npr-1*(*lf*) mutants in different subsets of neurons and assayed CO_2 response. We found that expressing *npr-1* in neuronal subsets that included the O_2-sensing URX neurons (Cheung et al., 2004; Gray et al., 2004) restored CO_2 response (Fig. 3*A*). These results suggest that NPR-1 activity in URX neurons is sufficient to enable CO_2 avoidance. However, we cannot exclude the possibility that NPR-1 function in other neurons also contributes to CO_2 avoidance.

To further investigate the role of the URX neurons in regulating CO_2 response, we ablated URX neurons in both the N2 and *npr-1*(*lf*) backgrounds and assayed CO_2 avoidance behavior. We found that either genetic ablation of a neuronal subset that includes URX or specific laser ablation of URX in the N2 background had no effect on CO_2 avoidance (Fig. 3*B*,*C*). However, both genetic and laser ablation of URX in *npr-1*(*lf*) mutants restored CO_2 avoidance (Fig. 3*B*,*C*). Moreover, the response of URX-ablated *npr-1*(*lf*) animals was not significantly different from the response of URX-ablated N2 animals in our laser ablation experiment (Fig. 3*C*). Thus, in *npr-1*(*lf*) mutants, URX neu-

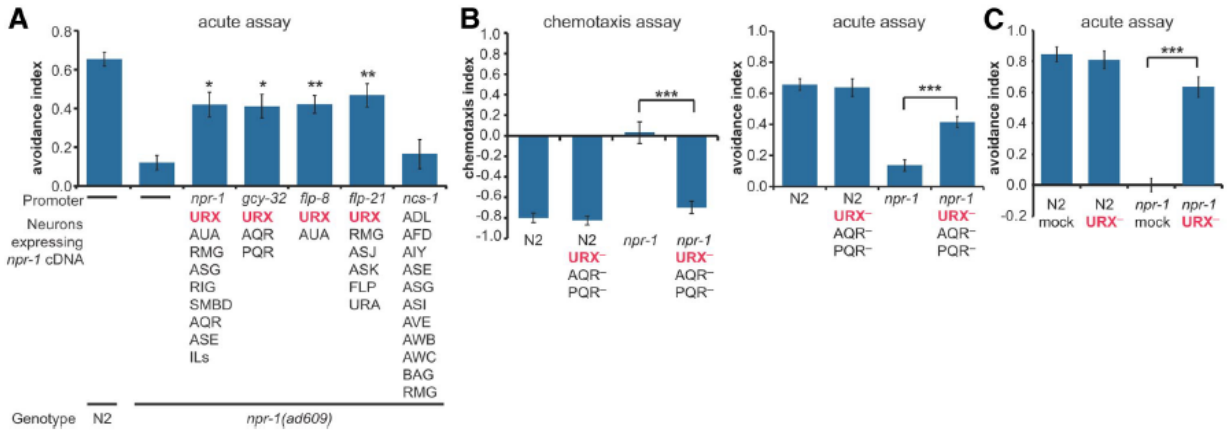

Figure 3. *npr-1* appears to act in URX neurons to regulate CO_2 avoidance. ***A***, Expression of *npr-1* cDNA from N2 animals in subsets of neurons that include URX restores CO_2 avoidance to *npr-1(lf)* mutants in an acute CO_2 avoidance assay. *$p < 0.05$, relative to the *npr-1(lf)* mutant (one-way ANOVA with Bonferroni post-test). **$p < 0.01$, relative to the *npr-1(lf)* mutant (one-way ANOVA with Bonferroni post-test). $n = 16–27$ trials for each genotype. Full expression patterns for each transgene were previously described (Macosko et al., 2009). ***B***, Genetic ablation of a subset of neurons that includes URX in *npr-1(lf)* mutants restores CO_2 avoidance. Left, CO_2 chemotaxis assay. Right, Acute CO_2 avoidance assay. ***$p < 0.001$, relative to the *npr-1(lf)* mutant (one-way ANOVA with Bonferroni post-test). $n = 7$ or 8 trials (chemotaxis assay) or 8–27 trials (acute assay) for each genotype. ***C***, Specific laser ablation of URX neurons in *npr-1(lf)* mutants restores CO_2 avoidance in an acute CO_2 avoidance assay. Ablations were performed on animals expressing a *gcy-36::GFP* transgene to verify the identity of the URX neurons. ***$p < 0.001$ (one-way ANOVA with Bonferroni post-test). The responses of mock-ablated N2 animals, URX-ablated N2 animals, and URX-ablated *npr-1* animals were not significantly different ($p > 0.05$). $n = 7–10$ trials for each treatment. For all graphs, error bars represent SEM.

rons inhibit CO_2 avoidance and removal of URX neurons is sufficient to restore CO_2 avoidance. Our results suggest a model in which CO_2 avoidance behavior is regulated by URX neuron activity. In N2 animals, NPR-1 reduces URX neuron activity, thereby enabling CO_2 avoidance. In *npr-1(lf)* animals, increased activity of URX neurons inhibits the CO_2 circuit, resulting in a loss of CO_2 avoidance.

URX neurons are not required for CO_2 attraction by dauers

In contrast to *C. elegans* adults and developing larvae, *C. elegans* dauer larvae are attracted to CO_2 (Fig. 4*A*) (Guillermin et al., 2011; Hallem et al., 2011a). The dauer is a developmentally arrested, alternative third larval stage that is thought to be analogous to the infective juvenile stage of parasitic nematodes (Hotez et al., 1993). The mechanism responsible for the change in CO_2 response valence that occurs at the dauer stage is not yet known. BAG neurons and the putative CO_2 receptor GCY-9 are required for CO_2 attraction by dauers (Fig. 4*A*) (Hallem et al., 2011a), suggesting that the same mechanism of CO_2 detection operates at the dauer and adult stages. However, *npr-1(lf)* and HW dauers are also attracted to CO_2, indicating that *npr-1* is not required for CO_2 attraction (Fig. 4*B*). The lack of requirement for *npr-1* at the dauer stage is not the result of altered *npr-1* expression in URX neurons because *npr-1* is expressed at comparable levels in N2 dauers and developing third-stage larvae (L3s) (Fig. 4*C*,*D*). To test whether URX neuron activity is required for CO_2 attraction by dauers, we tested whether dauers that lack URX neurons are still attracted to CO_2. We found that URX-ablated N2 and *npr-1(lf)* dauers display normal CO_2 attraction (Fig. 4*E*), indicating that URX neurons are not required to promote CO_2 attraction by dauers. Thus, URX neurons control whether CO_2 is a repulsive or neutral stimulus in adults, but other mechanisms are required to promote CO_2 attraction by dauers.

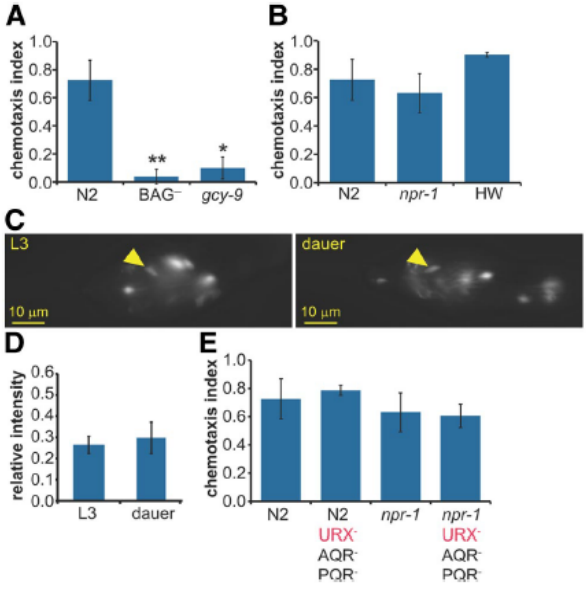

Figure 4. Mechanisms of CO_2 attraction by dauers. ***A***, BAG neurons and the receptor guanylate cyclase gene *gcy-9* are required for CO_2 attraction by dauers. *$p < 0.05$ (Kruskal–Wallis test with Dunn's post-test). **$p < 0.01$ (Kruskal–Wallis test with Dunn's post-test). $n = 4–12$ trials. ***B***, *npr-1* is not required for CO_2 attraction by dauers. $n = 4–8$ trials. ***C***, Epifluorescence images of *npr-1* expression in the URX neurons of L3 (left) and dauer (right) larvae in the N2 background. *npr-1* expression was assayed in *npr-1* animals containing an *npr-1::npr-1 SL2 GFP* transgene (Macosko et al., 2009). Arrowheads indicate the location of the URX neuron cell body. Anterior is to the left. ***D***, *npr-1* expression in the URX neurons of L3 and dauer larvae is not significantly different (unpaired *t* test). $n = 17–20$ animals. ***E***, URX neurons are not required for CO_2 attraction by dauers. Both N2 and *npr-1(lf)* dauers containing a genetic ablation of the URX, AQR, and PQR neurons display normal CO_2 attraction. $n = 4–8$ trials for each genotype. For all graphs, error bars represent SEM.

O_2 sensing by URX neurons is required for regulation of CO_2 avoidance

The URX neurons are O_2-sensing neurons that express O_2 receptors of the soluble guanylate cyclase (sGC) family (Cheung et al., 2004; Gray et al., 2004). Whether the URX neurons are also activated by CO_2 is unclear (Bretscher et al., 2011; Brandt et al., 2012). To test whether URX neurons regulate CO_2 response by directly responding to CO_2, we imaged

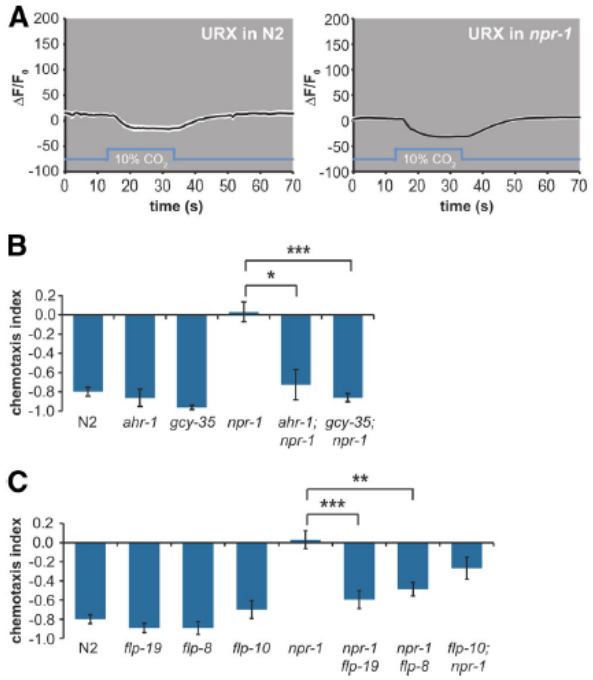

Figure 5. URX neurons mediate O_2-dependent regulation of CO_2 avoidance. ***A***, URX neurons do not respond to CO_2 in either N2 or *npr-1(lf)* animals under our imaging conditions. Calcium transients in URX neuron cell bodies were measured using G-CaMP3.0. Black lines indicate average calcium responses; white shading represents SEM. Blue lines below the traces indicate the timing of the CO_2 pulse. $n = 8$ or 9 animals for each genotype. To verify the lack of CO_2 response in URX neurons, we also imaged from N2 and *npr-1(lf)* animals containing an independently generated construct that expressed G-CaMP in URX (McGrath et al., 2009); these animals also did not display CO_2-evoked activity in URX (data not shown). ***B***, O_2 sensing by URX neurons is required for regulation of CO_2 avoidance. Mutation of *ahr-1* or *gcy-35* rescues the CO_2 response defect of *npr-1(lf)* mutants. $^*p < 0.05$ (Kruskal–Wallis test with Dunn's post-test). $^{***}p < 0.001$ (Kruskal–Wallis test with Dunn's post-test). $n = 4$–9 trials for each genotype. Error bars represent SEM. ***C***, Neuropeptide signaling regulates CO_2 avoidance. Mutation of the URX-expressed neuropeptide genes *flp-8* and *flp-19* significantly rescues the CO_2 response defect of *npr-1(lf)* mutants. $^{**}p < 0.01$, relative to the *npr-1(lf)* mutant (one-way ANOVA with Bonferroni post-test). $^{***}p < 0.001$, relative to the *npr-1(lf)* mutant (one-way ANOVA with Bonferroni post-test). $n = 6$–14 trials. Error bars represent SEM.

from the URX neurons of N2 and *npr-1(lf)* animals during CO_2 exposure using the calcium indicator G-CaMP3.0. We found that URX neurons are not activated by CO_2 (Fig. 5*A*). URX neurons did appear to show a slight decrease in calcium levels in response to CO_2, but whether this decrease is biologically relevant is not yet clear. These results indicate that URX neurons do not regulate CO_2 response as a result of CO_2-induced activation.

To test whether URX neurons instead regulate CO_2 response by responding to O_2, we examined the CO_2-evoked behavior of *aryl hydrocarbon receptor-1* (*ahr-1*) mutants. AHR-1 is a transcription factor that regulates aggregation behavior and that is required for normal expression of sGC O_2 receptors in URX neurons (Qin et al., 2006). We found that *ahr-1* mutants respond normally to CO_2 and that the *ahr-1* mutation rescues the CO_2 response defect of *npr-1(lf)* mutants (Fig. 5*B*). Thus, regulation of CO_2 avoidance by URX neurons of *npr-1(lf)* animals depends on their ability to sense O_2. Furthermore, mutation of the sGC gene *gcy-35,* which encodes an O_2 receptor that is expressed in URX and required for its O_2 response (Zimmer et al., 2009), also rescues the CO_2 response defect of *npr-1* mutants (Fig. 5*B*). Thus, GCY-35-mediated activation of URX neurons by ambient O_2 is required for regulation of CO_2 avoidance behavior. Together, these results demonstrate that CO_2 response is regulated by ambient O_2.

To investigate the mechanism by which URX neurons regulate CO_2 response in *npr-1* mutants, we examined the role of neuropeptide signaling in the regulation of CO_2 avoidance behavior. The URX neurons are known to express FMRFamide-related neuropeptide genes, including *flp-8*, *flp-10*, and *flp-19* (Li and Kim, 2008). To test whether these neuropeptide genes are required for the regulation of CO_2 response, we examined the CO_2-evoked behavior of neuropeptide mutants in the *npr-1(lf)* mutant background. We found that mutation of either *flp-8* or *flp-19*, but not *flp-10*, significantly rescued the CO_2 response defect of *npr-1* mutants (Fig. 5*C*). These results are consistent with the hypothesis that URX neurons modulate CO_2 response via a neuropeptide signaling pathway involving *flp-8* and *flp-19*. However, we cannot exclude the possibility that release of *flp-8* and *flp-19* from other neurons also contributes to the O_2-dependent regulation of CO_2 response.

npr-1(lf) and HW animals avoid CO_2 under low O_2 conditions

The URX neurons are activated when the ambient O_2 concentration increases from 10% to 21% (Zimmer et al., 2009; Busch et al., 2012). This response consists of both phasic and tonic components: a large initial increase in calcium transients is followed by a smaller sustained increase that continues until O_2 levels return to 10% (Busch et al., 2012). The fact that URX neurons remain active at high O_2 levels but are inactive at low O_2 levels led us to hypothesize that *npr-1(lf)* and HW animals might avoid CO_2 under low O_2 conditions, when URX neurons are inactive. We therefore examined the responses of *npr-1(lf)* and HW animals to CO_2 under low O_2 conditions by reducing the ambient O_2 concentration to 7% for the duration of the CO_2 chemotaxis assay. We found that, at 7% ambient O_2, both *npr-1(lf)* and HW animals displayed CO_2 avoidance behavior that was comparable with that of N2 animals (Fig. 6*A*). Thus, *npr-1(lf)* and HW animals are indeed capable of responding robustly to CO_2. However, CO_2 response in these animals is regulated by ambient O_2 such that CO_2 is repulsive at low O_2 concentrations and neutral at high O_2 concentrations.

The BAG neurons, which are activated by CO_2, are also activated by decreases in ambient O_2 from 21% to <10% (Zimmer et al., 2009). This raised the possibility that BAG neurons could cell-autonomously integrate responses to O_2 and CO_2, thus contributing to the O_2-dependent regulation of CO_2 response. To test this possibility, we examined the ability of animals that lack the soluble guanylate cyclase genes *gcy-31* and *gcy-33,* which are expressed in BAG neurons and are required for the O_2-evoked activity of BAG neurons (Zimmer et al., 2009), to respond to CO_2 at low ambient O_2. We found that *gcy-33; gcy-31* mutants responded normally to CO_2 at low ambient O_2 in both N2 and *npr-1(lf)* animals (Fig. 6*B*), indicating that the O_2-sensing ability of BAG is not required for the O_2-dependent regulation of CO_2 response. Consistent with these results, the BAG neurons were recently shown to play only a minor role in the chronic response to ambient O_2 (Busch et al., 2012). Thus, regulation of CO_2 response by ambient O_2 is not a result of cell-intrinsic signaling within BAG but instead requires a pair of designated O_2-sensing neurons.

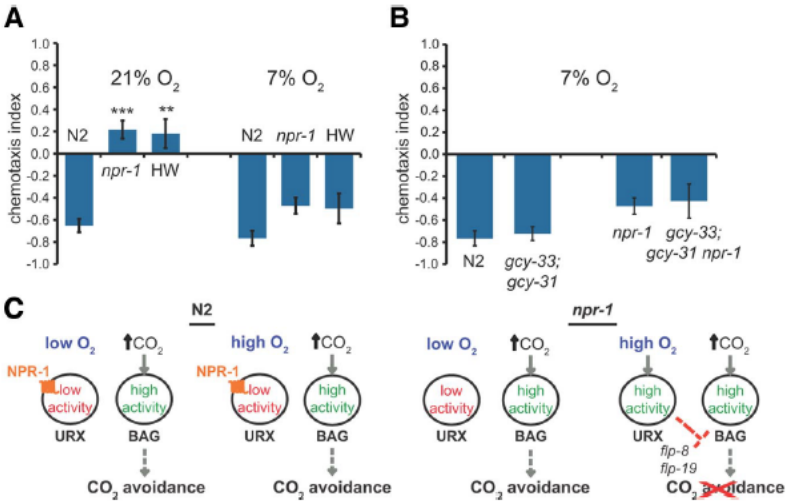

Figure 6. *npr-1(lf)* and HW animals avoid CO_2 under low O_2 conditions. ***A***, *npr-1(lf)* and HW animals do not respond to CO_2 at 21% ambient O_2 but avoid CO_2 at 7% ambient O_2. $^{**}p < 0.01$, relative to N2 control (Kruskal–Wallis test with Dunn's post-test). $^{***}p < 0.001$, relative to N2 control (Kruskal–Wallis test with Dunn's post-test). $n = 7$–26 trials for each genotype and condition. Error bars represent SEM. ***B***, CO_2 response at low ambient O_2 does not require O_2 sensing by BAG neurons. Animals that lack the soluble guanylate cyclase genes *gcy-31* and *gcy-33*, which are required for the O_2 response of BAG neurons (Zimmer et al., 2009), respond normally to CO_2 at 7% ambient O_2 in both the N2 and *npr-1(lf)* mutant backgrounds. The response of N2 animals is not significantly different from the response of *gcy-33; gcy-31* animals, and the response of *npr-1* animals is not significantly different from the response of *gcy-33; gcy-31 npr-1* animals (Kruskal–Wallis test with Dunn's post-test). $n = 8$–26 trials for each genotype. Error bars represent SEM. ***C***, A model for O_2-dependent regulation of CO_2 avoidance. Our results suggest that, in N2 animals, NPR-1 maintains URX in a low activity state, thus enabling CO_2 avoidance even at high ambient O_2. In *npr-1(lf)* mutant animals, reduced activity of URX at low ambient O_2 allows CO_2 avoidance, and increased activity of URX at high ambient O_2 inhibits CO_2 avoidance. Our results also suggest that CO_2 avoidance by URX neurons may be mediated by the URX-expressed neuropeptide genes *flp-8* and *flp-19*.

Discussion

Our results demonstrate that URX neurons control CO_2 response by coordinating the response to CO_2 with the response to ambient O_2. In *npr-1(lf)* animals, O_2-dependent activation of URX neurons determines CO_2 response such that CO_2 is repulsive at low ambient O_2 but neutral at high ambient O_2 (Fig. 6*C*). Moreover, our results are consistent with the hypothesis that URX neurons regulate the activity of the CO_2 circuit via a neuropeptide signaling pathway that involves the FMRFamide-related neuropeptide genes *flp-19* and *flp-8*. By contrast, in N2 animals, the URX neurons do not inhibit CO_2 avoidance at high ambient O_2 as a result of the presence of NPR-1 (Fig. 6*C*). NPR-1 does not constitutively silence the URX neurons of N2 animals because the URX neurons of N2 animals are activated by increases in ambient O_2 and ablation of URX in N2 animals alters O_2 response (Zimmer et al., 2009). However, our results suggest that NPR-1 may reduce URX neuron activity in N2 animals such that URX neurons no longer inhibit the CO_2 avoidance circuit. Alternatively, it is possible that NPR-1 activity is dynamically regulated by its neuropeptide ligands such that it is active under some conditions but not others, or that the URX neurons of N2 animals are sufficiently activated but are incapable of regulating CO_2 avoidance as a result of differences in neural connectivity or signaling between N2 and *npr-1(lf)* animals.

A recent survey of wild *C. elegans* strains revealed that the HW allele of *npr-1* is the natural variant, with the N2 allele having arisen during laboratory culturing (McGrath et al., 2009). HW animals were previously thought to be virtually insensitive to CO_2 (Hallem and Sternberg, 2008; McGrath et al., 2009), raising the question of whether CO_2 avoidance is exclusively a laboratory-derived behavior. Our results demonstrate that HW animals do indeed display robust CO_2 avoidance, but this behavior is restricted to low O_2 conditions. Wild *C. elegans* adults have been found in fallen rotting fruit and in the soil under rotting fruit, where O_2 levels are lower and CO_2 levels are higher than in the atmosphere (Felix and Duveau, 2012). Inside rotting fruit, *C. elegans* occupies microhabitats replete with bacteria, fungi, worms, insects, and other small invertebrates (Felix and Duveau, 2012). In this context, fluctuating levels of CO_2 and O_2 likely serve as important indicators of food availability, population density, and predator proximity (Bendesky et al., 2011; Milward et al., 2011; Scott, 2011). Suppression of CO_2 avoidance at high ambient O_2 may allow worms to migrate toward rotting fruit, which emits CO_2. Once inside the low O_2 environment of rotting fruit, CO_2 avoidance may allow worms to avoid cohabitating predators or overcrowding. Thus, O_2-dependent regulation of CO_2 avoidance is likely to be an ecologically relevant mechanism by which nematodes navigate gas gradients.

In addition to CO_2 response, a number of other chemosensory behaviors in *C. elegans* are subject to context-dependent changes in sensory valence (Sengupta, 2012). For example, olfactory and gustatory behavior exhibits experience-dependent plasticity, in which chemicals that are attractive to naive animals become neutral or repulsive after prolonged or repeated exposure in the absence of food (Sengupta, 2012). Olfactory plasticity occurs as a result of altered signaling in the AWC olfactory neurons (Tsunozaki et al., 2008), and salt plasticity occurs as a result of altered signaling in the ASE gustatory neurons and the downstream AIA and AIB interneurons (Tomioka et al., 2006; Adachi et al., 2010; Oda et al., 2011). Similarly, O_2 preference is modulated by prior O_2 exposure and the presence of bacterial food as a result of altered signaling in a distributed network of chemosensory neurons (Cheung et al., 2005; Chang et al., 2006). Our results suggest that CO_2 response is modulated by ambient O_2 via the activity of a pair of O_2-detecting neurons that interact with the CO_2 circuit downstream of CO_2 detection by BAG neurons (Fig. 6*C*). The neurons that act downstream of BAG and URX to control CO_2 response have not yet been identified. A number of interneurons receive synaptic input from both BAG and URX (White et al., 1986), and it will be interesting to determine whether any of them play a role in CO_2 avoidance.

CO_2-evoked behaviors in insects are also subject to context-dependent modulation. For example, the fruit fly *Drosophila melanogaster* is repelled by CO_2 when walking (Suh et al., 2004) but attracted to CO_2 in flight, a valence change that is modulated by octopamine signaling (Wasserman et al., 2013). In addition, both CO_2 repulsion by walking *D. melanogaster* and CO_2 attraction by mosquitoes can be suppressed by food odorants, which

directly alter the activity of the CO_2 receptor (Turner and Ray, 2009; Turner et al., 2011). Insects as well as many other animals, both free-living and parasitic, occupy microhabitats where environmental levels of O_2 and CO_2 vary greatly as a function of food or host availability, population density, and microorganism composition. Thus, it will be interesting to determine whether the control of CO_2 response by O_2-sensing neurons is a conserved feature of gas-sensing circuits.

References

Adachi T, Kunitomo H, Tomioka M, Ohno H, Okochi Y, Mori I, Iino Y (2010) Reversal of salt preference is directed by the insulin/PI3K and Gq/PKC signaling in *Caenorhabditis elegans*. Genetics 186:1309–1319. CrossRef Medline

Bargmann CI, Hartwieg E, Horvitz HR (1993) Odorant-selective genes and neurons mediate olfaction in *C. elegans*. Cell 74:515–527. CrossRef Medline

Bendesky A, Tsunozaki M, Rockman MV, Kruglyak L, Bargmann CI (2011) Catecholamine receptor polymorphisms affect decision-making in *C. elegans*. Nature 472:313–318. CrossRef Medline

Brandt JP, Aziz-Zaman S, Juozaityte V, Martinez-Velazquez LA, Petersen JG, Pocock R, Ringstad N (2012) A single gene target of an ETS-family transcription factor determines neuronal CO_2-chemosensitivity. PLoS One 7:e34014. CrossRef Medline

Brenner S (1974) The genetics of *Caenorhabditis elegans*. Genetics 77:71–94. Medline

Bretscher AJ, Busch KE, de Bono M (2008) A carbon dioxide avoidance behavior is integrated with responses to ambient oxygen and food in *Caenorhabditis elegans*. Proc Natl Acad Sci U S A 105:8044–8049. CrossRef Medline

Bretscher AJ, Kodama-Namba E, Busch KE, Murphy RJ, Soltesz Z, Laurent P, de Bono M (2011) Temperature, oxygen, and salt-sensing neurons in *C. elegans* are carbon dioxide sensors that control avoidance behavior. Neuron 69:1099–1113. CrossRef Medline

Buehlmann C, Hansson BS, Knaden M (2012) Path integration controls nest-plume following in desert ants. Curr Biol 22:645–649. CrossRef Medline

Busch KE, Laurent P, Soltesz Z, Murphy RJ, Faivre O, Hedwig B, Thomas M, Smith HL, de Bono M (2012) Tonic signaling from O_2 sensors sets neural circuit activity and behavioral state. Nat Neurosci 15:581–591. CrossRef Medline

Chaisson KE, Hallem EA (2012) Chemosensory behaviors of parasites. Trends Parasitol 28:427–436. CrossRef Medline

Chang AJ, Chronis N, Karow DS, Marletta MA, Bargmann CI (2006) A distributed chemosensory circuit for oxygen preference in *C. elegans*. PLoS Biol 4:e274. CrossRef Medline

Cheung BH, Arellano-Carbajal F, Rybicki I, de Bono M (2004) Soluble guanylate cyclases act in neurons exposed to the body fluid to promote *C. elegans* aggregation behavior. Curr Biol 14:1105–1111. CrossRef Medline

Cheung BH, Cohen M, Rogers C, Albayram O, de Bono M (2005) Experience-dependent modulation of *C. elegans* behavior by ambient oxygen. Curr Biol 15:905–917. CrossRef Medline

de Bono M, Bargmann CI (1998) Natural variation in a neuropeptide Y receptor homolog modifies social behavior and food response in *C. elegans*. Cell 94:679–689. CrossRef Medline

Dillman AR, Guillermin ML, Lee JH, Kim B, Sternberg PW, Hallem EA (2012) Olfaction shapes host-parasite interactions in parasitic nematodes. Proc Natl Acad Sci U S A 109:E2324–E2333. CrossRef Medline

Félix MA, Duveau F (2012) Population dynamics and habitat sharing of natural populations of *Caenorhabditis elegans* and *C. briggsae*. BMC Biol 10:59. CrossRef Medline

Glauser DA, Chen WC, Agin R, Macinnis BL, Hellman AB, Garrity PA, Tan MW, Goodman MB (2011) Heat avoidance is regulated by transient receptor potential (TRP) channels and a neuropeptide signaling pathway in *Caenorhabditis elegans*. Genetics 188:91–103. CrossRef Medline

Gray JM, Karow DS, Lu H, Chang AJ, Chang JS, Ellis RE, Marletta MA, Bargmann CI (2004) Oxygen sensation and social feeding mediated by a *C. elegans* guanylate cyclase homologue. Nature 430:317–322. CrossRef Medline

Guillermin ML, Castelletto ML, Hallem EA (2011) Differentiation of carbon dioxide-sensing neurons in *Caenorhabditis elegans* requires the ETS-5 transcription factor. Genetics 189:1327–1339. CrossRef Medline

Hallem EA, Sternberg PW (2008) Acute carbon dioxide avoidance in *Caenorhabditis elegans*. Proc Natl Acad Sci U S A 105:8038–8043. CrossRef Medline

Hallem EA, Dillman AR, Hong AV, Zhang Y, Yano JM, DeMarco SF, Sternberg PW (2011a) A sensory code for host seeking in parasitic nematodes. Curr Biol 21:377–383. CrossRef Medline

Hallem EA, Spencer WC, McWhirter RD, Zeller G, Henz SR, Ratsch G, Miller DM 3rd, Horvitz HR, Sternberg PW, Ringstad N (2011b) Receptor-type guanylate cyclase is required for carbon dioxide sensation by *Caenorhabditis elegans*. Proc Natl Acad Sci U S A 108:254–259. CrossRef Medline

Harris AL (2002) Hypoxia: a key regulatory factor in tumour growth. Nat Rev Cancer 2:38–47. CrossRef Medline

Hobert O. (2010) Neurogenesis in the nematode *Caenorhabditis elegans*. In: WormBook. www.WormBook.org. Accessed May 8th, 2013.

Hotez P, Hawdon J, Schad GA (1993) Hookworm larval infectivity, arrest and amphiparatenesis: the *Caenorhabditis elegans* Daf-c paradigm. Parasitol Today 9:23–26. CrossRef Medline

Langford NJ (2005) Carbon dioxide poisoning. Toxicol Rev 24:229–235. CrossRef Medline

Li C, Kim, K. (2008) Neuropeptides. In: WormBook, www.WormBook.org. Accessed May 8th, 2013.

Luo M, Sun L, Hu J (2009) Neural detection of gases—carbon dioxide, oxygen—in vertebrates and invertebrates. Curr Opin Neurobiol 19:354–361. CrossRef Medline

Macosko EZ, Pokala N, Feinberg EH, Chalasani SH, Butcher RA, Clardy J, Bargmann CI (2009) A hub-and-spoke circuit drives pheromone attraction and social behaviour in *C. elegans*. Nature 458:1171–1175. CrossRef Medline

McGrath PT, Rockman MV, Zimmer M, Jang H, Macosko EZ, Kruglyak L, Bargmann CI (2009) Quantitative mapping of a digenic behavioral trait implicates globin variation in *C. elegans* sensory behaviors. Neuron 61:692–699. CrossRef Medline

Milward K, Busch KE, Murphy RJ, de Bono M, Olofsson B (2011) Neuronal and molecular substrates for optimal foraging in *Caenorhabditis elegans*. Proc Natl Acad Sci U S A 108:20672–20677. CrossRef Medline

Morton DB (2011) Behavioral responses to hypoxia and hyperoxia in *Drosophila* larvae: molecular and neuronal sensors. Fly (Austin) 5:119–125. CrossRef Medline

Nagai T, Yamada S, Tominaga T, Ichikawa M, Miyawaki A (2004) Expanded dynamic range of fluorescent indicators for Ca^{2+} by circularly permuted yellow fluorescent proteins. Proc Natl Acad Sci U S A 101:10554–10559. CrossRef Medline

Oda S, Tomioka M, Iino Y (2011) Neuronal plasticity regulated by the insulin-like signaling pathway underlies salt chemotaxis learning in *Caenorhabditis elegans*. J Neurophysiol 106:301–308. CrossRef Medline

Persson A, Gross E, Laurent P, Busch KE, Bretes H, de Bono M (2009) Natural variation in a neural globin tunes oxygen sensing in wild *Caenorhabditis elegans*. Nature 458:1030–1033. CrossRef Medline

Qin H, Zhai Z, Powell-Coffman JA (2006) The *Caenorhabditis elegans* AHR-1 transcription complex controls expression of soluble guanylate cyclase genes in the URX neurons and regulates aggregation behavior. Dev Biol 298:606–615. CrossRef Medline

Reddy KC, Andersen EC, Kruglyak L, Kim DH (2009) A polymorphism in *npr-1* is a behavioral determinant of pathogen susceptibility in *C. elegans*. Science 323:382–384. CrossRef Medline

Rogers C, Persson A, Cheung B, de Bono M (2006) Behavioral motifs and neural pathways coordinating O_2 responses and aggregation in *C. elegans*. Curr Biol 16:649–659. CrossRef Medline

Satterlee JS, Sasakura H, Kuhara A, Berkeley M, Mori I, Sengupta P (2001) Specification of thermosensory neuron fate in *C. elegans* requires *ttx-1*, a homolog of *otd/Otx*. Neuron 31:943–956. CrossRef Medline

Scott K (2011) Out of thin air: sensory detection of oxygen and carbon dioxide. Neuron 69:194–202. CrossRef Medline

Sengupta P (2013) The belly rules the nose: feeding state-dependent modulation of peripheral chemosensory responses. Curr Opin Neurobiol 23:68–75. CrossRef Medline

Suh GS, Wong AM, Hergarden AC, Wang JW, Simon AF, Benzer S, Axel R, Anderson DJ (2004) A single population of olfactory sensory neurons mediates an innate avoidance behaviour in *Drosophila*. Nature 431:854–859. CrossRef Medline

Tian L, Hires SA, Mao T, Huber D, Chiappe ME, Chalasani SH, Petreanu L, Akerboom J, McKinney SA, Schreiter ER, Bargmann CI, Jayaraman V, Svoboda K, Looger LL (2009) Imaging neural activity in worms, flies and mice with improved GCaMP calcium indicators. Nat Methods 6:875–881. CrossRef Medline

Tomioka M, Adachi T, Suzuki H, Kunitomo H, Schafer WR, Iino Y (2006) The insulin/PI 3-kinase pathway regulates salt chemotaxis learning in *Caenorhabditis elegans*. Neuron 51:613–625. CrossRef Medline

Tsunozaki M, Chalasani SH, Bargmann CI (2008) A behavioral switch: cGMP and PKC signaling in olfactory neurons reverses odor preference in *C. elegans*. Neuron 59:959–971. CrossRef Medline

Turner SL, Ray A (2009) Modification of CO_2 avoidance behaviour in *Drosophila* by inhibitory odorants. Nature 461:277–281. CrossRef Medline

Turner SL, Li N, Guda T, Githure J, Cardé RT, Ray A (2011) Ultra-prolonged activation of CO_2-sensing neurons disorients mosquitoes. Nature 474:87–91. CrossRef Medline

Uchida O, Nakano H, Koga M, Ohshima Y (2003) The *C. elegans che-1* gene encodes a zinc finger transcription factor required for specification of the ASE chemosensory neurons. Development 130:1215–1224. CrossRef Medline

Vigne P, Frelin C (2010) Hypoxia modifies the feeding preferences of *Drosophila*: consequences for diet dependent hypoxic survival. BMC Physiol 10:8. CrossRef Medline

Wasserman S, Salomon A, Frye MA (2013) *Drosophila* tracks carbon dioxide in flight. Curr Biol 23:301–306. CrossRef Medline

West JB (2004) The physiologic basis of high-altitude diseases. Ann Intern Med 141:789–800. CrossRef Medline

White JG, Southgate E, Thomson JN, Brenner S (1986) The structure of the nervous system of the nematode *Caenorhabditis elegans*. Philos Trans R Soc Lond B Biol Sci 314:1–340. CrossRef Medline

Wingrove JA, O'Farrell PH (1999) Nitric oxide contributes to behavioral, cellular, and developmental responses to low oxygen in *Drosophila*. Cell 98:105–114. CrossRef Medline

Zimmer M, Gray JM, Pokala N, Chang AJ, Karow DS, Marletta MA, Hudson ML, Morton DB, Chronis N, Bargmann CI (2009) Neurons detect increases and decreases in oxygen levels using distinct guanylate cyclases. Neuron 61:865–879. CrossRef Medline

Follow-up for Carrillo, Guillermin et al 2013.

The results of this study implicate the URX-expressed neuropeptides FLP-8 and FLP-19 in the O_2-dependent modulation of CO_2 response in *npr-1(lf)* animals. Since both *flp-8* and *flp-19* are expressed in multiple sensory and interneurons (Kim and Li, 2004), we rescued *flp-19* expression in the URX neurons to determine whether *flp-19* regulates CO_2 avoidance specifically via the URX neurons (Figure 7). We found that expression of *flp-19* under the control of the URX-specific promoter, *gcy-36*, in the *npr-1(lf) flp-19* double mutants rescued the inhibition of CO_2 avoidance. Our results demonstrate that O_2-dependent regulation of CO_2 response requires expression of *flp-19* in the URX neurons. The same rescue experiments will have to be done with *flp-8* to determine if *flp-8* also acts directly in the URX neurons. It is important to note, however, that these rescue experiments do not directly confirm the either neuropeptide acts in URX under normal conditions, but may only demonstrate that the expression of these neuropeptides is sufficient to regulate CO_2 response. Alternatively, cell-specific RNAi knock-down of *flp-19* and *flp-8* will show specifically the relevance of URX-derived neuropeptides in regulating CO_2 response. Subsequently, we will have to determine the neuronal targets of *flp-8* and *flp-19*, which may also serve as points of integration for URX signaling within the CO_2 circuit. To that end, we have begun elucidating the cognate receptors for *flp-8* and *flp-19*. We have conducted a screen of GPCR mutants, crossed to *npr-1(lf)* animals, and searched for mutants which phenocopied the *npr-1 flp-8* and *npr-1 flp-19* double mutants (Figure 8). Our screen revealed that a mutation in the neuropeptide receptor *npr-5* rescues CO_2 avoidance in *npr-1(lf)* animals. More extensive work will have to be done to determine whether *npr-5* is a receptor for *flp-8*,

flp-19, or perhaps a neuropeptide we have yet to identify. In parallel, individually ablating cells that express *npr-5* in *npr-1(lf)* animals and subsequently testing CO_2 response in these animals will help to determine where *npr-5* may be acting to regulate CO_2 behavior. Following these experiments, cell-specific rescue of *npr-5* in *npr-5; npr-1(lf)* animals will be required to further confirm where *flp-8* or *flp-19* may be acting to modulate URX-mediated O_2-dependent regulation of CO_2 response behavior. In addition, since the URX neurons have several downstream interneurons in common with the BAG neurons (Figure 9), examining those interneurons may reveal how the URX neurons regulate the CO_2 circuit. URX synapses onto RIG, RIA, and AIZ which we have demonstrated regulate CO_2 response (Guillermin et al., 2017). Measuring CO_2-evoked activity in RIG, RIA and AIZ in *npr-1(lf)* animals under high and low O_2 conditions would indicate whether URX may be regulating CO_2 response through signaling to either of these interneurons. Although not directly connected to the URX neurons, recent evidence has shown that the AIY interneurons regulate O_2-evoked behaviors in *npr-1(lf)* animals (Laurent et al., 2015). In this case, the URX neurons may be regulating AIY through neuromodulatory signaling. Measuring the CO_2-evoked activity of AIY in *npr-1(lf)* animals under high and low O_2 conditions would indicate whether AIY activity reflects O_2 conditions in order to regulate CO_2 response behavior. Together, these experiments will expand on our knowledge of mechanisms that drive multisensory integration, by offering insight into the cellular and molecular signaling pathways which underlie the integration of environmental O_2 levels into the CO_2 circuit.

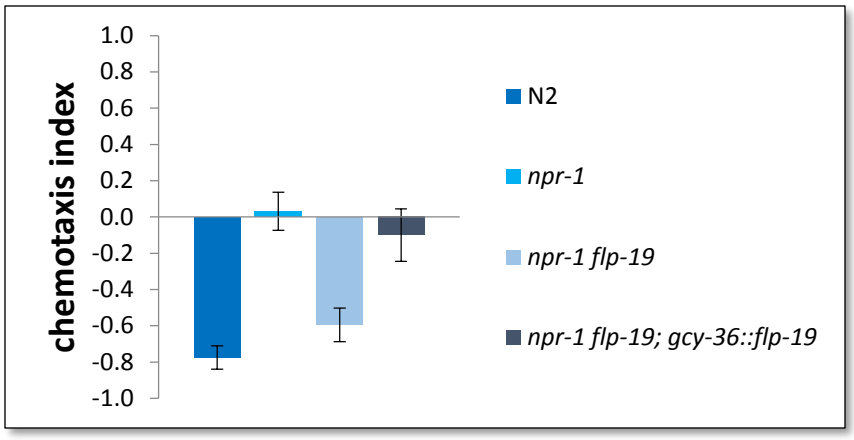

Figure 7. URX-specific expression of *flp-19* rescues *npr-1(lf)* CO_2 response. The URX-specific promoter *gcy-36* was used to express *flp-19* in *npr-1(lf)flp-19* animals. *n*=8-10 trials per genotype. Assays were done using 10% CO_2, 10% O_2, balance N_2 mix. Error bars represent SEM.

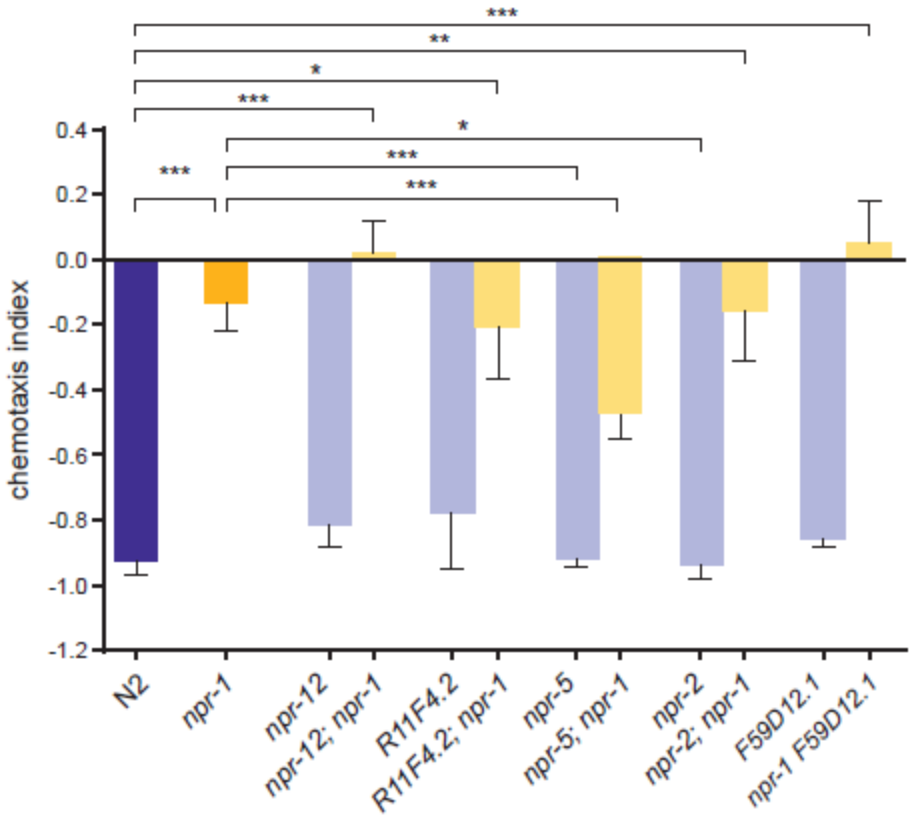

Figure 8. An *npr-5* mutation rescues CO_2 avoidance behavior in *npr-1(lf)* mutants. We screened five GPCR mutants, crossed to *npr-1(lf)*, for double mutants which would phenocopy *npr-1 flp-8* and *npr-1 flp-19* CO_2 responses. The *npr-5; npr-1* double mutant exhibited CO_2 avoidance behavior, in contrast to the neutral response of *npr-1(lf)* animals. Assays were done using 10% CO_2, 10% O_2, balance N_2 mix. n=4-24 trials per genotype. **p*<0.05, ***p*<0.01, ****p*<0.001, Kruskal-Wallis test with Dunn's post-test. Error bars represent SEM.

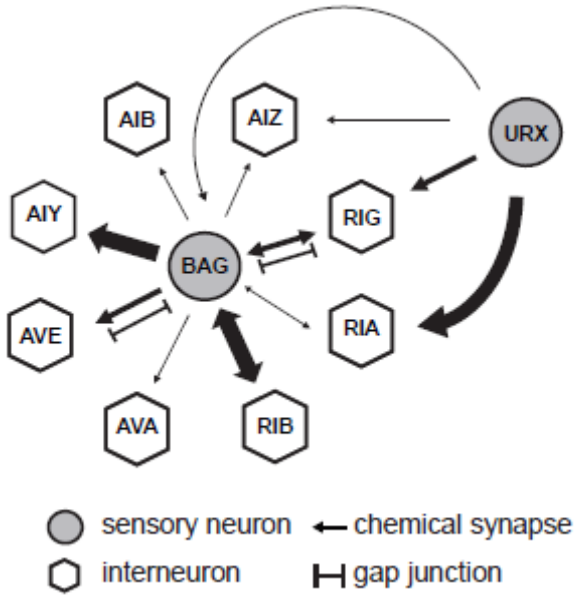

Figure 9. Structural connectivity of the CO_2-detecting BAG neurons and O_2-detecting URX neurons (White et al., 1986; Xu et al., 2013). Arrow thickness reflects the number of synaptic connections (1-2 synapses, 4-7 synapses, or 10+ synapses) from BAG and URX to the downstream interneurons. Both BAG and URX are also presynaptic to interneurons not shown here.

Chapter 3: A single set of interneurons drives opposite behaviors in *C. elegans*

A Single Set of Interneurons Drives Opposite Behaviors in *C. elegans*

Manon L. Guillermin,[1] Mayra A. Carrillo,[1] and Elissa A. Hallem[1,2,*]
[1]Department of Microbiology, Immunology, and Molecular Genetics, University of California, Los Angeles, Los Angeles, CA 90095, USA
[2]Lead Contact
*Correspondence: ehallem@ucla.edu
http://dx.doi.org/10.1016/j.cub.2017.07.023

SUMMARY

Many chemosensory stimuli evoke innate behavioral responses that can be either appetitive or aversive, depending on an animal's age, prior experience, nutritional status, and environment [1–9]. However, the circuit mechanisms that enable these valence changes are poorly understood. Here, we show that *Caenorhabditis elegans* can alternate between attractive or aversive responses to carbon dioxide (CO_2), depending on its recently experienced CO_2 environment. Both responses are mediated by a single pathway of interneurons. The CO_2-evoked activity of these interneurons is subject to extreme experience-dependent modulation, enabling them to drive opposite behavioral responses to CO_2. Other interneurons in the circuit regulate behavioral sensitivity to CO_2 independent of valence. A combinatorial code of neuropeptides acts on the circuit to regulate both valence and sensitivity. Chemosensory valence-encoding interneurons exist across phyla, and valence is typically determined by whether appetitive or aversive interneuron populations are activated. Our results reveal an alternative mechanism of valence determination in which the same interneurons contribute to both attractive and aversive responses through modulation of sensory neuron to interneuron synapses. This circuit design represents a previously unrecognized mechanism for generating rapid changes in innate chemosensory valence.

RESULTS AND DISCUSSION

Here, we investigated the molecular, cellular, and circuit mechanisms that determine CO_2 response in the free-living roundworm *C. elegans*. CO_2 is a byproduct of cellular respiration that can signal the presence of food, mates, predators, or pathogens [10–13]. We found that CO_2 can be attractive or repulsive for *C. elegans* adults, depending on their recently experienced environmental CO_2 levels. We raised animals at either ambient or high (2.5%) CO_2 for one generation and tested their response to CO_2 in a chemotaxis assay (Figure S1A). Although the level of atmospheric CO_2 is only 0.038% [10], wild *C. elegans* inhabit environments rich in rotting organic matter, where CO_2 levels can rise above 10% [14]. As previously reported, animals raised at ambient CO_2 avoided CO_2 (Figure 1A) [15, 16]. In contrast, animals raised at high CO_2 showed robust CO_2 attraction (Figure 1A). In both cases, response valence was consistent across concentrations (Figures S1B and S1C). Thus, *C. elegans* can show attraction or repulsion to CO_2, depending on its prior cultivation conditions.

We then examined the behavior of animals raised at either ambient or 2.5% CO_2 in three different CO_2 gradients: 0%–2.5%, 2.5%–10%, and 2.5%–40%. We found that animals raised at ambient CO_2 avoided the higher concentration of CO_2 under all three conditions (Figure S1D). By contrast, animals raised at 2.5% CO_2 were attracted to the higher CO_2 concentration in both the 0%–2.5% and 2.5%–10% CO_2 gradients (Figure S1D). Thus, cultivating animals at high CO_2 results in a drive toward higher CO_2 levels rather than a preference for their previous cultivation condition. This is in contrast to other sensory behaviors in *C. elegans*, including salt chemotaxis and thermotaxis, where animals are attracted to their prior cultivation condition [17, 18]. Animals raised at high CO_2 were not attracted to 40% CO_2 in the 2.5%–40% CO_2 gradient (Figure S1D), suggesting that they retain the ability to avoid toxic levels of CO_2 [19].

To determine whether CO_2 preferences are flexible, we transferred animals raised at ambient CO_2 to high CO_2, and vice versa, and assayed their responses to 2.5% CO_2 over the course of 9 hr. We found that animals displayed rapid adaptation to their new environment. Animals raised at ambient CO_2 showed CO_2 attraction after 1 hr at high CO_2 and exhibited maximum attraction by 6 hr (Figure 1B). Animals raised at high CO_2 displayed decreased attraction after 3 hr at ambient CO_2 and recovery of CO_2 avoidance by 9 hr (Figure 1B). Thus, CO_2 response valence is experience dependent and flexible.

The Same Pair of Sensory Neurons Is Required for CO_2 Attraction and Repulsion

We next investigated the mechanisms that drive CO_2-evoked behaviors of opposing valence. We previously showed that the BAG sensory neurons detect CO_2 and are required for CO_2 avoidance [12, 15, 20]. We therefore examined the role of BAG in mediating CO_2 attraction. We found that BAG is required for CO_2 attraction as well as repulsion: animals lacking BAG failed to respond to CO_2, regardless of their prior cultivation conditions (Figures 1C and S1E). We tested animals with increased neurotransmission in BAG due to cell-specific expression of a gain-of-function (*gf*) allele of the protein kinase C gene *pkc-1* [21, 22] and found that *BAG::pkc-1(gf)* animals raised at ambient

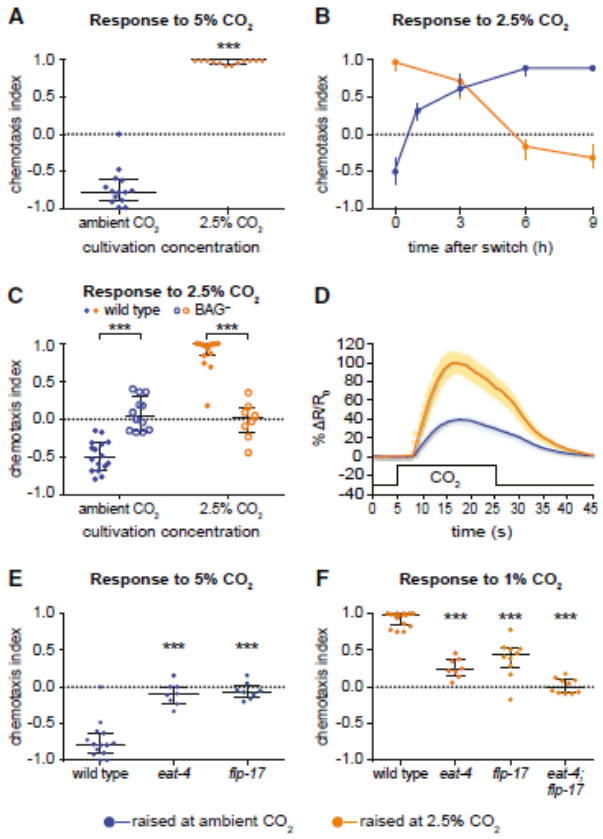

Figure 1. *C. elegans* Shows Both Attractive and Aversive Responses to CO_2

(A) Animals raised at ambient CO_2 (0.038%) avoid 5% CO_2, while animals raised at high (2.5%) CO_2 are attracted to 5% CO_2. ***$p < 0.001$, Mann-Whitney test. n = 12–14 trials per condition.

(B) Adults raised at ambient CO_2 were incubated at high (2.5%) CO_2 for 1, 3, 6, or 9 hr and then assayed for their response to 2.5% CO_2 (blue), while adults raised at high CO_2 were put at ambient CO_2 for 3, 6, or 9 hr and then assayed for their response to 2.5% CO_2 (orange). A switch in CO_2 environment triggers a rapid change in CO_2 response valence. n = 8–24 trials per condition.

(C) BAG sensory neurons are required for CO_2 avoidance and attraction. Wild-type animals raised at ambient CO_2 avoid 2.5% CO_2, while wild-type animals raised at high (2.5%) CO_2 are attracted to 2.5% CO_2. BAG-ablated animals (BAG^-) do not respond to CO_2 under either condition. ***$p < 0.001$, two-way ANOVA with Sidak's post-test. n = 8–16 trials per condition.

(D) BAG neurons of animals raised at high (2.5%) CO_2 respond more robustly to CO_2 than BAG neurons of animals raised at ambient CO_2. Graph shows the calcium responses of BAG to 15% CO_2, for animals raised at ambient CO_2 (blue) or high CO_2 (orange), measured using the ratiometric calcium indicator Yellow Cameleon 3.60 (YC3.60). Solid lines indicate average calcium responses; shading represents SEM. Black line indicates the CO_2 pulse. Animals raised at high CO_2 show an increased BAG response relative to animals raised at ambient CO_2 ($p < 0.001$, unpaired t test). n = 10–15 animals per condition.

(E and F) *eat-4* and *flp-17* are required for normal CO_2 response. (E) Mutation of *eat-4* or *flp-17* abolishes CO_2 avoidance in animals raised at ambient CO_2. Responses shown are to 5% CO_2. ***$p < 0.001$, Kruskal-Wallis test with Dunn's post-test. n = 8–14 trials per genotype and condition. (F) Mutation of either *eat-4* or *flp-17* reduces CO_2 attraction, and mutation of both genes abolishes CO_2 attraction, in animals raised at high (2.5%) CO_2. Responses shown are to 1% CO_2. ***$p < 0.001$, one-way ANOVA with Dunnett's post-test. n = 8–16 trials per genotype and condition.

For (A)–(C), (E), and (F), graphs depict medians with interquartile ranges.

See also Figures S1 and S2.

CO_2 showed enhanced CO_2 avoidance (Figure S1E). Thus, BAG activity modulates the strength of the behavioral response to CO_2.

To test whether recently experienced CO_2 levels affect the response of BAG to CO_2, we compared the CO_2-evoked activity of BAG in animals raised at ambient versus high CO_2 using calcium imaging. In animals raised at ambient CO_2, exposure to CO_2 resulted in a rapid depolarization, consistent with previous reports (Figure 1D) [12, 20, 23]. In animals raised at high CO_2, exposure to CO_2 resulted in a 2.5-fold increase in the magnitude of the depolarization (Figure 1D). In addition, the CO_2-evoked responses of BAG in animals raised at ambient CO_2 were previously shown to be concentration dependent [20], and we observed that the CO_2-evoked responses of BAG in animals raised at high CO_2 are also concentration dependent (Figure S1F). Since CO_2 response valence is consistent across concentrations in animals raised at ambient or high CO_2 (Figures S1B and S1C), yet the CO_2-evoked activity of BAG is concentration dependent in both cases, CO_2 response valence is encoded downstream of the calcium response of BAG.

The increased BAG activity in animals raised at high CO_2 correlated with increased expression of the receptor guanylate cyclase gene *gcy-9*, which encodes a putative CO_2 receptor [20, 23–25] (Figure S2A). These results are consistent with the increased behavioral sensitivity to CO_2 exhibited by animals raised at high CO_2: whereas animals raised at ambient CO_2 are repelled by CO_2 concentrations above 5%, animals raised at high CO_2 are attracted to CO_2 concentrations as low as 0.25% (Figures S1B and S1C). Thus, cultivation at high CO_2 alters both the valence and sensitivity of CO_2-evoked behavior. The increased CO_2 sensitivity following prolonged exposure to high CO_2 is unusual in that prolonged exposure to a chemosensory stimulus generally results in reduced sensitivity as a result of adaptation [26], and in fact prolonged exposure of insects and fish to high CO_2 environments results in reduced sensitivity to CO_2 [27, 28]. *C. elegans* responds differently to prolonged CO_2 exposure, perhaps because it often inhabits high CO_2 environments. That the sensitivity of *C. elegans* to CO_2 may be determined by regulating the level of expression of the CO_2 receptor in BAG rather than by regulating interneuron input to BAG may reflect the fact that *C. elegans* chemosensory neurons respond to multiple chemosensory stimuli due to the compact nature of the *C. elegans* nervous system [29]. In particular, BAG responds to both CO_2 and O_2 [30], and therefore regulating the sensitivity of BAG to CO_2 by regulating CO_2 receptor expression may be a mechanism that adjusts CO_2 sensitivity while leaving O_2 sensitivity unaltered.

CO_2 Avoidance and Attraction Require Neuropeptide and Glutamate Signaling

We then investigated the signaling mechanisms used by BAG in animals raised at ambient versus high CO_2 to generate attractive or repulsive responses to CO_2. The FMRFamide-like neuropeptide FLP-17 is expressed specifically in BAG [31, 32]. We found

that *flp-17* mutants raised at ambient CO_2 did not respond to any concentration of CO_2 (Figures 1E and S2B). By contrast, *flp-17* mutants raised at high CO_2 were still attracted to CO_2, but to a lesser extent than wild-type animals (Figures 1F and S2C). Thus, FLP-17 is required for CO_2 avoidance but acts in combination with other signaling mechanisms to mediate CO_2 attraction. A candidate for such an additional signaling mechanism is glutamate, since BAG expresses the vesicular glutamate transporter EAT-4 [33]. We found that *eat-4* mutants raised at ambient CO_2 failed to respond to CO_2, while *eat-4* mutants raised at high CO_2 showed decreased CO_2 attraction (Figures 1E, 1F, S2B, and S2C). However, *eat-4; flp-17* double mutants raised at high CO_2 did not respond to CO_2, suggesting that FLP-17 and glutamate act partially redundantly to mediate CO_2 attraction (Figures 1F and S2C). Moreover, restoring *eat-4* expression specifically in BAG partially restored CO_2 avoidance and attraction (Figures S2D and S2E). Thus, *eat-4* acts in BAG to mediate CO_2 response, although glutamatergic signaling from other neurons may also contribute. These results indicate that BAG mediates both CO_2 avoidance and attraction via neuropeptide and glutamate signaling.

A Single Pathway of Interneurons Drives CO_2 Avoidance and Attraction

To gain insight into the CO_2 circuit that operates downstream of BAG, we examined the requirement for the 8 interneurons postsynaptic to BAG [34, 35] that have been previously implicated in chemosensory behaviors [36–42] (Figure S3A). We first tested whether these interneurons are required for CO_2 avoidance in animals raised at ambient CO_2, using strains in which individual interneurons or subsets of interneurons were genetically ablated or silenced with tetanus toxin [43, 44]. When tested with 1% CO_2, a concentration that is neutral to wild-type animals, AIB$^-$ AIZ$^-$ and AIY$^-$ animals showed avoidance, and RIA$^-$ animals showed attraction (Figure 2A). AIB$^-$ animals responded normally to CO_2, suggesting that the phenotype of the AIB$^-$ AIZ$^-$ animals resulted from the loss of AIZ activity (Figure 2A). When tested with 10% CO_2, RIG$^-$ animals showed reduced avoidance relative to wild-type animals (Figure 2B). The increased avoidance of AIB$^-$ AIZ$^-$ and AIY$^-$ animals and the reduced avoidance of RIG$^-$ and RIA$^-$ animals were consistent across concentrations (Figures 2C–2F). In contrast, *AIY::pkc-1(gf)* animals showed weaker avoidance, while *RIG::pkc-1(gf)* and *RIA::pkc-1(gf)* animals showed enhanced avoidance relative to wild-type animals (Figures 2C–2E). Transiently silencing AIY and RIA in adult animals using the histamine-gated chloride channel HisCl1 [45, 46] had the same effect on CO_2-evoked behavior as genetic ablation (Figure 2G). Together, these results suggest that CO_2 avoidance is mediated by four pairs of first-order interneurons—AIY, AIZ, RIA, and RIG—whose real-time activity levels determine behavior.

To identify interneurons that regulate CO_2 attraction, we raised interneuron-ablated or -silenced strains at high CO_2 and assayed their responses to 0.1% and 0.25% CO_2. Animals raised at high CO_2 were tested with lower concentrations of CO_2 than animals raised at ambient CO_2 due to their increased CO_2 sensitivity; 0.1% and 0.25% CO_2 were chosen because they elicited non-saturating responses from wild-type animals (Figure S1C). We found that AIB$^-$ AIZ$^-$ and RIA$^-$ animals showed stronger attraction, and that AIY$^-$ animals showed weaker attraction, than wild-type animals (Figures 3A–3E). AIB$^-$ animals showed normal CO_2 attraction, suggesting that the phenotype of AIB$^-$ AIZ$^-$ animals is due to the loss of AIZ activity (Figures 3A and 3B). In contrast, *AIY::pkc-1(gf)* animals raised at high CO_2 showed stronger attraction, while *RIA::pkc-1(gf)* animals showed weaker attraction relative to wild-type animals (Figures 3C and 3D). Transiently silencing AIY and RIA in animals raised at high CO_2 had the same effect on CO_2-evoked behavior as genetic ablation (Figures 3F and 3G). Moreover, we found that RIG$^-$ animals showed a delayed shift from attraction to avoidance following a transition from high to ambient CO_2 (Figures 3H and 3I). Whereas wild-type animals recovered 77% of their maximum avoidance after 6 hr, RIG$^-$ animals recovered only 11%. Conversely, AIY$^-$ animals showed a delayed shift, and RIA$^-$ animals showed an accelerated shift, from repulsion to attraction following a transition from ambient to high CO_2 (Figures 3J and 3K). After 3 hr at high CO_2, wild-type animals reached 81% of their maximum attraction, whereas AIY$^-$ animals reached only 23% and RIA$^-$ animals reached 99%. Taken together, these results suggest that the same set of interneurons regulates CO_2 attraction and repulsion.

AIY expresses the inhibitory glutamate-gated chloride channel subunit GLC-3 [47]. We therefore tested whether GLC-3 plays a role in suppressing AIY activity to promote CO_2 avoidance. We found that *glc-3* mutants grown at ambient CO_2 responded normally to CO_2 but that *glc-3* mutants raised at high CO_2 and transferred to ambient CO_2 showed a delayed shift from attraction to repulsion (Figures S3B and S3C). This phenotype was rescued by cell-specific expression of *glc-3* in AIY (Figure S3C). Thus, inhibition of AIY via *glc-3* is required for animals to adapt normally to a shift from high to ambient CO_2.

We next examined the CO_2-evoked activity of AIY, RIA, and RIG by calcium imaging to determine how CO_2 response valence arises from the activity of these interneurons. We found that AIY showed a CO_2-evoked depolarization in animals raised at high CO_2 and a small but significant hyperpolarization in animals raised at ambient CO_2 (Figure 4A). In contrast, RIA showed a CO_2-evoked depolarization in animals raised at ambient CO_2, consistent with a previous report [48], and a CO_2-evoked hyperpolarization in animals raised at high CO_2 (Figure 4B). RIG also showed a CO_2-evoked depolarization in animals raised at ambient CO_2 but showed no response in animals raised at high CO_2 (Figure 4C). The CO_2-evoked responses of AIY, RIA, and RIG were BAG dependent (Figures 4A–4C). Thus, AIY, RIA, and RIG show qualitative differences in their CO_2-evoked activity in animals raised at ambient versus high CO_2.

Together, our behavioral and calcium imaging data demonstrate that CO_2 repulsion and attraction are mediated by the coordinated activity of the same set of first-order interneurons. The CO_2-evoked activity of these interneurons is contextually modulated to drive opposite responses to CO_2. Inhibition of AIY promotes avoidance, while activation of AIY promotes attraction. In contrast, inhibition of RIA and silencing of RIG promotes attraction, while activation of RIA and RIG promotes avoidance. Thus, CO_2 avoidance arises from the activation of RIA and RIG and inhibition of AIY; CO_2 attraction arises from the activation of AIY, inhibition of RIA, and silencing of RIG.

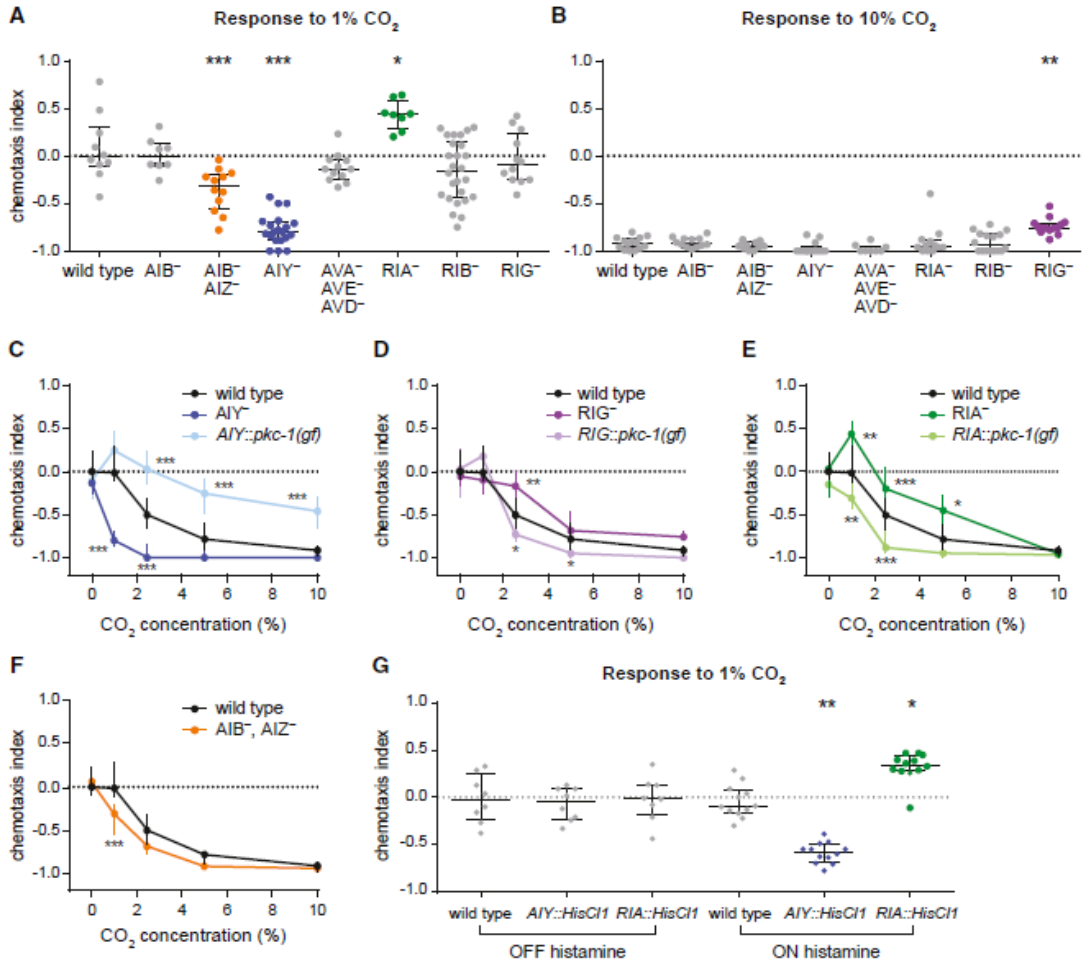

Figure 2. Distinct Interneurons Act in Opposition to Regulate CO_2 Avoidance in Animals Raised at Ambient CO_2

(A and B) In animals raised at ambient CO_2, silencing of AIZ and ablation of AIY enhances CO_2 avoidance, ablation of RIG reduces CO_2 avoidance, and ablation of RIA results in CO_2 attraction. Animals were raised at ambient CO_2 and screened for responses to 1% CO_2 (A) and 10% CO_2 (B). Interneurons were either genetically ablated individually (AIB^-, AIY^-, RIA^-, RIB^-, and RIG^-), genetically ablated simultaneously (AVA^- AVE^- AVD^-); or silenced with tetanus toxin simultaneously (AIB^- AIZ^-). *$p < 0.05$; **$p < 0.01$; ***$p < 0.001$, one-way ANOVA with Dunnett's post-test (A) or Kruskal-Wallis test with Dunn's post-test (B). n = 8–26 trials per genotype and condition.

(C) Ablation of AIY enhances CO_2 avoidance. By contrast, animals with more active AIY neurons due to AIY-specific expression of *pkc-1(gf)* show reduced CO_2 avoidance. Animals were raised at ambient CO_2. ***$p < 0.001$, two-way ANOVA with Dunnett's post-test. n = 8–26 trials per genotype and condition.

(D) Ablation of RIG reduces CO_2 avoidance. By contrast, animals with more active RIG neurons due to RIG-specific expression of *pkc-1(gf)* show enhanced CO_2 avoidance. Animals were raised at ambient CO_2. *$p < 0.05$; **$p < 0.01$, two-way ANOVA with Dunnett's post-test. n = 8–30 trials per genotype and condition.

(E) Ablation of RIA reduces CO_2 avoidance. By contrast, animals with more active RIA neurons due to RIA-specific expression of *pkc-1(gf)* show enhanced CO_2 avoidance. Animals were raised at ambient CO_2. *$p < 0.05$; **$p < 0.01$; ***$p < 0.001$, two-way ANOVA with Dunnett's post-test. n = 8–16 trials per genotype and condition.

(F) Silencing of AIZ enhances CO_2 avoidance. Animals were raised at ambient CO_2. ***$p < 0.001$, two-way ANOVA with Sidak's post-test. n = 8–16 trials per genotype and condition.

(G) Animals with AIY neurons transiently silenced by expression of the histamine-gated chloride channel HisCl1 in AIY show enhanced CO_2 avoidance. By contrast, animals with RIA neurons transiently silenced using the same approach show CO_2 attraction. Responses to 1% CO_2 were tested for wild-type animals and animals expressing HisCl1 in either AIY or RIA without histamine (negative control) and with histamine (neuronal silencing); changes in CO_2 response were observed only in the presence of histamine. Animals were raised at ambient CO_2. *$p < 0.05$; **$p < 0.01$, Kruskal-Wallis test with Dunn's post-test. n = 8–12 trials per genotype and condition.

For (A)–(G), graphs show medians and interquartile ranges.

See also Figure S3.

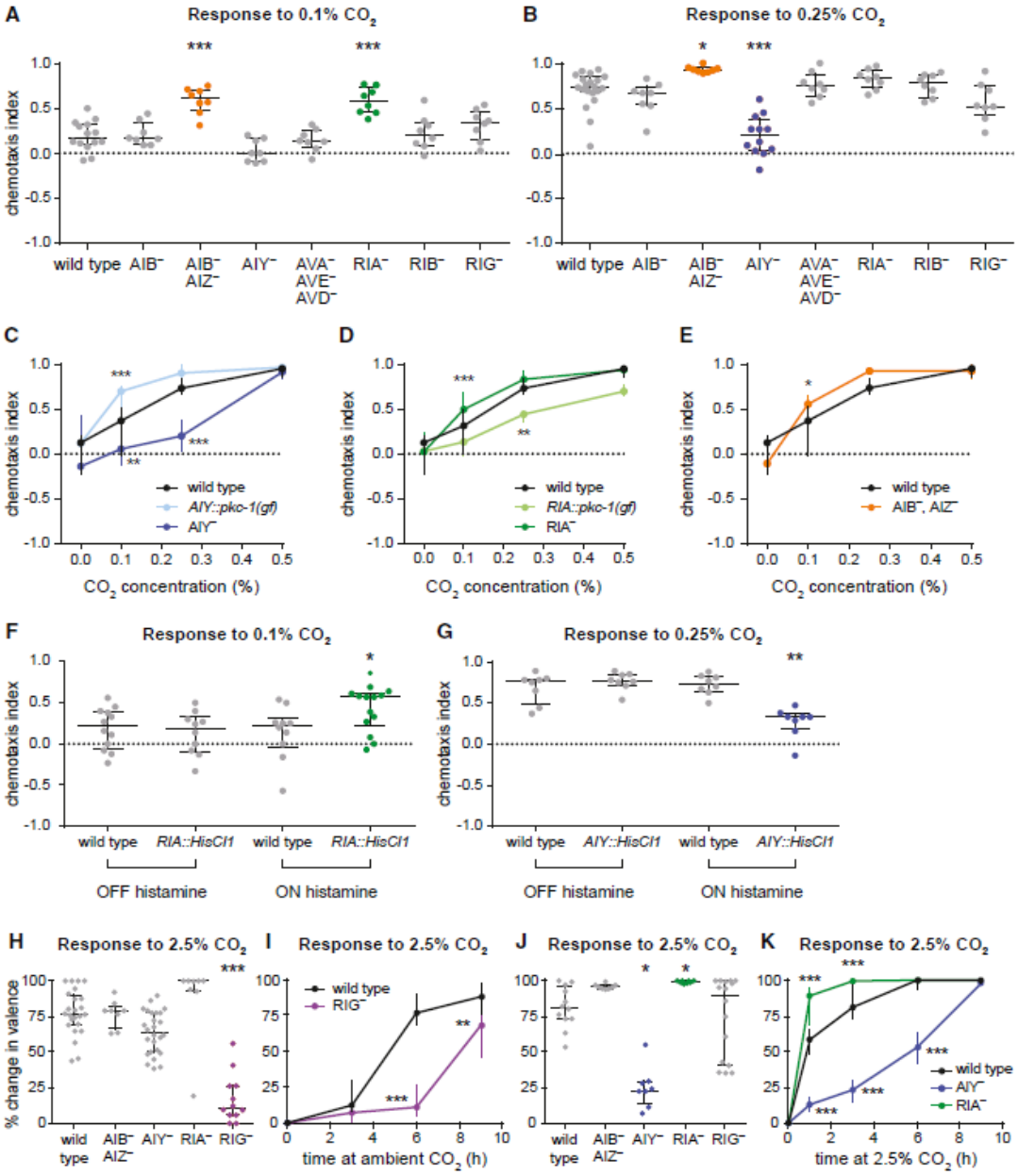

Figure 3. The Same Set of Interneurons Contributes to CO_2 Avoidance and Attraction

(A and B) In animals raised at high (2.5%) CO_2, silencing of AIZ and ablation of RIA enhances CO_2 attraction, while ablation of AIY reduces CO_2 attraction. Graphs show responses to 0.1% CO_2 (A) or 0.25% CO_2 (B). *$p < 0.05$; ***$p < 0.001$, one-way ANOVA with Dunnett's post-test (A) or Kruskal-Wallis test with Dunn's post-test (B). n = 6–20 trials per genotype and condition.

(C) Ablation of AIY reduces CO_2 attraction. By contrast, animals with more active AIY neurons due to AIY-specific expression of *pkc-1(gf)* show enhanced CO_2 attraction. Animals were raised at high (2.5%) CO_2. **$p < 0.01$; ***$p < 0.001$, two-way ANOVA with Dunnett's post-test. n = 6–20 trials per genotype and condition.

(D) Ablation of RIA enhances CO_2 attraction. By contrast, animals with more active RIA neurons due to RIA-specific expression of *pkc-1(gf)* show reduced CO_2 attraction. Animals were raised at high (2.5%) CO_2. **$p < 0.01$; ***$p < 0.001$, two-way ANOVA with Dunnett's post-test. n = 8–24 trials per genotype and condition.

(E) Silencing of AIZ enhances CO_2 attraction. Animals were raised at high (2.5%) CO_2. *$p < 0.05$, two-way ANOVA with Sidak's post-test. n = 8–20 trials per genotype and condition.

(F and G) Animals with RIA neurons transiently silenced by expression of the histamine-gated chloride channel HisCl1 in RIA show enhanced CO_2 attraction (F). By contrast, animals with AIY neurons transiently silenced using the same approach show reduced CO_2 attraction (G). Responses to 0.1% CO_2 (F) and 0.25% CO_2 (G) were tested for wild-type animals and animals expressing HisCl1 in either RIA or AIY without histamine (negative control) and with histamine (neuronal

Distinct Interneurons Regulate Valence and Sensitivity

In contrast to AIY, RIA, and RIG, AIZ showed similar CO_2-evoked activity in animals raised at ambient versus high CO_2 (Figure 4D). This activity was decreased, but not eliminated, in BAG$^-$ animals, suggesting additional CO_2-dependent inputs into AIZ (Figure 4D). The magnitude of the depolarization in AIZ did not differ under ambient versus high CO_2 conditions, despite BAG activity being significantly different (Figures 1D and 4D), suggesting that AIZ activity may be constrained by gain control mechanisms. In addition, the fact that AIZ activity does not differ in animals raised at ambient versus high CO_2 demonstrates that raising animals at high CO_2 does not result in a general physiological change that alters the CO_2-evoked activity of all interneurons in the circuit; rather, it results in cell-specific changes to the CO_2-evoked activity of RIG, RIA, and AIY. Furthermore, we found that AIB does not show CO_2-evoked activity in animals raised at ambient or high CO_2 (Figure S3D), suggesting that the phenotypes of the AIB$^-$ AIZ$^-$ animals are attributable to AIZ. However, we cannot exclude the possibility that AIB contributes indirectly to CO_2 response in combination with AIZ. Together with our behavioral data showing that silencing AIZ enhances both CO_2 attraction and repulsion (Figures 2F and 3E), these results demonstrate that AIZ regulates behavioral sensitivity to CO_2, regardless of valence. Thus, distinct interneurons regulate valence and sensitivity.

A Combinatorial Code of Neuropeptides Regulates Valence and Sensitivity

The rapid shift in CO_2 response valence that occurs following a change in environmental CO_2 levels is consistent with a mechanism of valence encoding that involves neuromodulation rather than synaptic rewiring [49–51]. To gain insight into the neuromodulators that regulate CO_2 response valence, we examined the CO_2-evoked behaviors of animals lacking individual neuropeptides that were previously shown to be enriched in BAG [20]. We first examined the CO_2 response of animals raised at ambient CO_2 and found that animals lacking the FMRFamide-like neuropeptide FLP-27 showed reduced avoidance, while animals lacking the neuropeptide-like protein NLP-1 showed enhanced avoidance (Figures S4A and S4B). We then examined the CO_2 response of animals raised at high CO_2 and found that animals lacking FLP-27 showed reduced attraction, while animals lacking FLP-16 showed enhanced attraction (Figures S4C and S4D). These data suggest that FLP-16 reduces CO_2 attraction, NLP-1 reduces CO_2 repulsion, and FLP-27 enhances CO_2 response regardless of valence. Thus, different neuropeptides play distinct roles in regulating CO_2 response valence and sensitivity. Our results raise the intriguing possibility that BAG secretes different combinations of neuropeptides in animals raised at ambient versus high CO_2 to generate experience-appropriate responses to CO_2. Activity-dependent regulation of neuropeptide expression has been demonstrated in BAG, where *flp-19* expression is greatly reduced in the absence of the CO_2-sensing pathway [52]. However, these neuropeptides may also act in other neurons to regulate the CO_2 circuit. Alternatively, modulation of the CO_2 circuit could be achieved through changes in receptor expression in the postsynaptic AIY, RIA, and RIG interneurons or modulatory input from other neurons.

A Novel Mechanism of Valence Encoding

We have examined the neural basis of CO_2 response and found that both CO_2 attraction and repulsion are mediated by a single microcircuit consisting of the BAG sensory neurons and four postsynaptic interneuron pairs: AIY, AIZ, RIA, and RIG (Figure 4E). CO_2 avoidance results from the activation of RIA and RIG and the inhibition of AIY. CO_2 attraction results from the activation of AIY, inhibition of RIA, and silencing of RIG. The valence associated with activation of each interneuron does not change as a result of experience: activation of AIY is always correlated with CO_2 attraction, and activation of RIA and RIG is always correlated with CO_2 avoidance. However, our data demonstrate that CO_2 response is determined by the combined activity states of AIY, RIA, and RIG and not solely by the interneuron (or interneurons) whose activation is correlated with its valence. The fourth interneuron pair, AIZ, regulates sensitivity, regardless of valence. Furthermore, a combinatorial code of neuropeptides acts on the CO_2 circuit to regulate valence and sensitivity. Thus, the specific behavioral response to CO_2 is determined by the coordinated activity of four interneuron types, two of which are capable of showing both CO_2-evoked excitation and CO_2-evoked inhibition.

CO_2-evoked behaviors are also subject to modulation in other organisms. For example, CO_2 avoidance by the fruit fly *Drosophila melanogaster* and CO_2 attraction by the mosquito *Aedes aegypti* are reduced in the presence of food odorants through direct inhibition of CO_2-detecting sensory neurons [53, 54]. CO_2 avoidance in *D. melanogaster* can also be attenuated by food odors through a mechanism in which the pathway mediating the response to food odors and the

silencing); changes in CO_2 response were observed only in the presence of histamine. Animals were raised at high (2.5%) CO_2. *$p < 0.05$; **$p < 0.01$, one-way ANOVA with Sidak's post-test (F) or Kruskal-Wallis test with Dunn's post-test (G). n = 8–14 trials per genotype and condition.

(H and I) Ablation of RIG delays the shift from CO_2 attraction to repulsion in animals raised at high (2.5%) CO_2 and transferred to ambient CO_2. Animals were tested for their response to 2.5% CO_2 after 3, 6, or 9 hr at ambient CO_2. Responses were compared to those of animals of the same genotype raised at ambient CO_2 and high CO_2 to determine the percent change in valence (see STAR Methods). Graphs show the percent change in valence after 6 hr (H) or as a function of time (I). **$p < 0.01$; ***$p < 0.001$, Kruskal-Wallis test with Dunn's post-test (H) or two-way ANOVA with Sidak's post-test (I). n = 8–26 trials per genotype, time point, and condition.

(J and K) Ablation of AIY delays the shift, and ablation of RIA accelerates the shift, from CO_2 repulsion to attraction in animals raised at ambient CO_2 and transferred to high (2.5%) CO_2. Animals were tested for their response to 2.5% CO_2 after 1, 3, 6, or 9 hr at high CO_2. Responses were compared to those of animals of the same genotype raised at ambient CO_2 and high CO_2 to determine the percent change in valence (see STAR Methods). Graphs show the percent change in valence after 3 hr (J) or as a function of time (K). *$p < 0.05$; ***$p < 0.001$, Kruskal-Wallis test with Dunn's post-test (J) or two-way ANOVA with Dunnett's post-test (K). n = 8–16 trials per genotype, time point, and condition.

For (A)–(K), graphs show medians and interquartile ranges.

See also Figure S3.

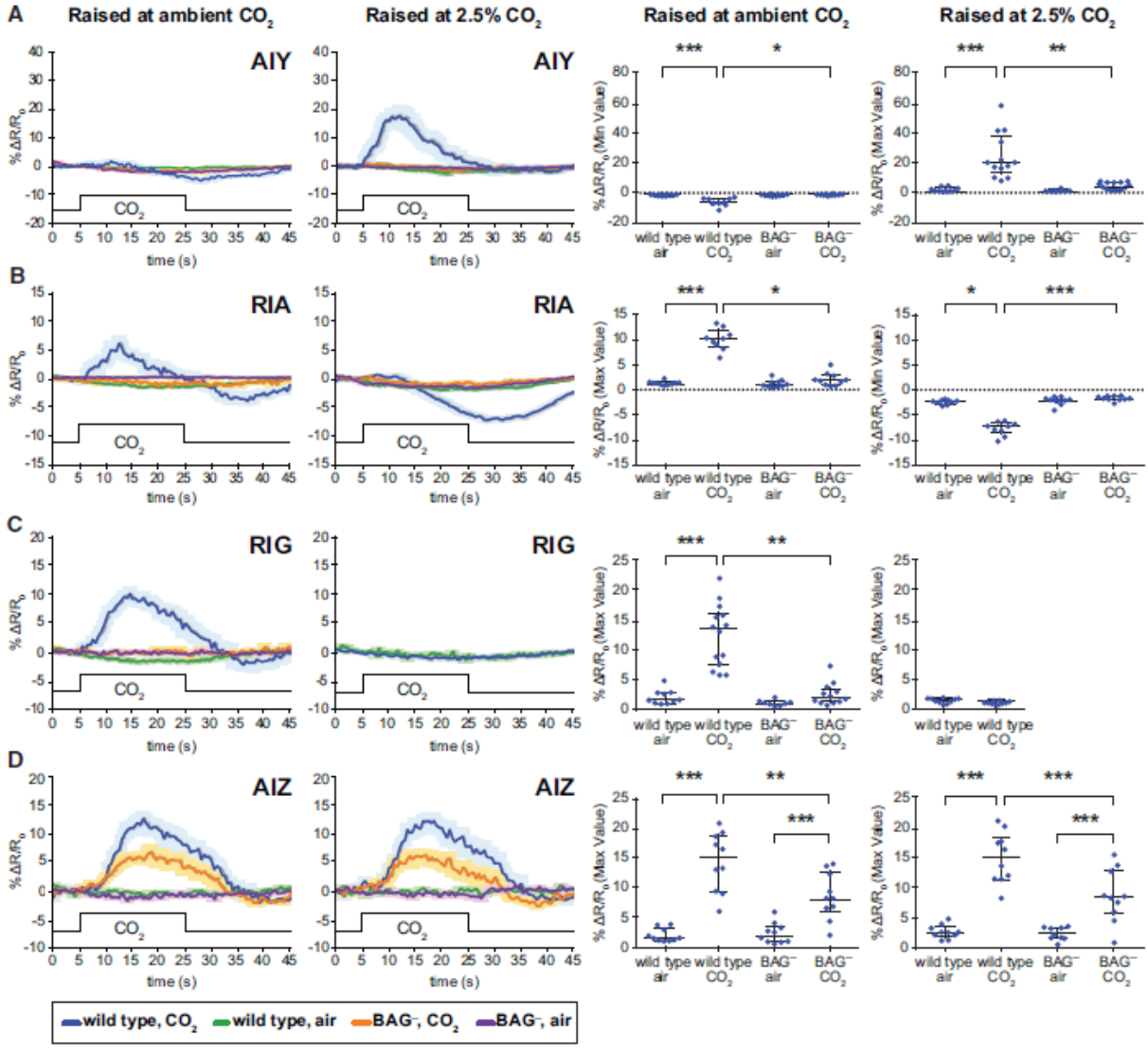
A
Raised at ambient CO2
Raised at 2.5% CO2
Raised at ambient CO2
Raised at 2.5% CO2
AIY
RIA
RIG
AIZ
% ΔR/R0
time (s)
CO2
% ΔR/R0 (Min Value)
% ΔR/R0 (Max Value)
wild type air
wild type CO2
BAG− air
BAG− CO2
wild type, CO2
wild type, air
BAG−, CO2
BAG−, air

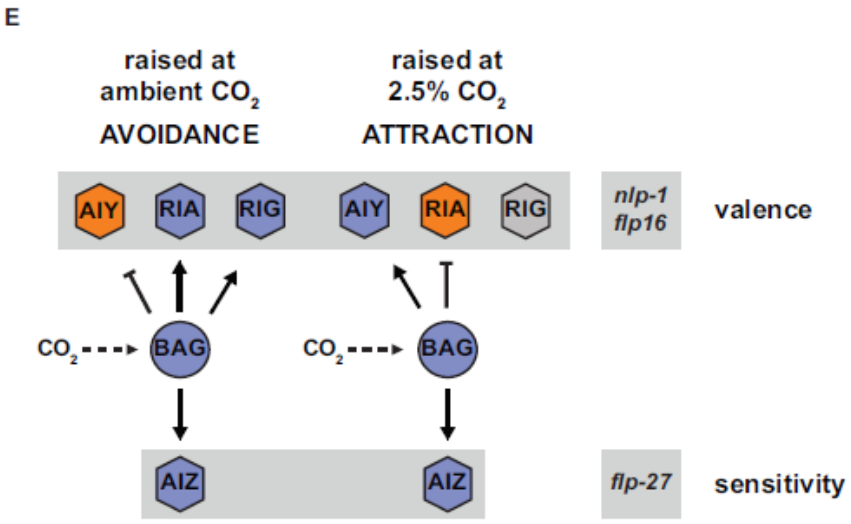
E
raised at ambient CO2
AVOIDANCE
raised at 2.5% CO2
ATTRACTION
AIY
RIA
RIG
nlp-1
flp16
valence
CO2
BAG
AIZ
flp-27
sensitivity

pathway mediating CO_2 response converge in the mushroom body [55, 56]. In addition, CO_2 is aversive to walking flies but attractive to flying flies, and different sets of chemoreceptors are required in the two conditions [57]. Thus, CO_2 response can be modulated by a number of different mechanisms across phyla.

In both invertebrates and vertebrates, a common mechanism for determining chemosensory valence involves two separate pathways, one that promotes attraction and one that promotes repulsion. Valence is then determined by which of these opposing pathways is activated [3, 58]. Here, we describe a novel mechanism of valence determination that instead involves a single pathway of interneurons. The CO_2-evoked activity of these interneurons is subject to extreme experience-dependent modulation based on the animal's recent exposure to CO_2, allowing them to contribute to both attractive and aversive responses to CO_2 (Figure 4E). Thus, the functional connectivity of sensory-neuron-to-interneuron synapses rapidly changes to reflect the current ethological state of the animal. Valence-encoding interneurons have been identified in mammals [3, 59], but whether their activity is modulated to drive changes in innate valence has not yet been investigated. Our finding that *C. elegans* can generate opposite behavioral responses to the same chemosensory input as a result of experience-dependent modulation of sensory-neuron-to-interneuron synapses raises the possibility that similar mechanisms operate in mammals to mediate rapid changes in innate valence.

STAR★METHODS

Detailed methods are provided in the online version of this paper and include the following:

- KEY RESOURCES TABLE
- CONTACT FOR REAGENT AND RESOURCE SHARING
- EXPERIMENTAL MODEL AND SUBJECT DETAILS
- METHOD DETAILS
  - CO_2 chemotaxis assays
  - Calcium imaging
  - Fluorescence microscopy
  - Molecular biology
- QUANTIFICATION AND STATISTICAL ANALYSIS

SUPPLEMENTAL INFORMATION

Supplemental Information includes four figures and can be found with this article online at http://dx.doi.org/10.1016/j.cub.2017.07.023.

AUTHOR CONTRIBUTIONS

Conceptualization, M.L.G., M.A.C., and E.A.H.; methodology, M.L.G., M.A.C., and E.A.H.; investigation, M.L.G. and M.A.C.; writing, M.L.G. and E.A.H.; funding acquisition, E.A.H.

ACKNOWLEDGMENTS

We thank C. Bargmann (Rockefeller University, New York, NY), M. de Bono (MRC Laboratory of Molecular Biology, Cambridge, UK), Y. Iino (University of Tokyo, Tokyo, Japan), S. Chalasani (UCSD, San Diego, CA), D. Biron (University of Chicago, Chicago, IL), A. Maricq (University of Utah, Salt Lake City, UT), D. Colón-Ramos (Yale University, New Haven, CT), I. Mori (Nagoya University, Nagoya, Japan), Y. Jin (UCSD, San Diego, CA), L. Salkoff (Washington University in St. Louis, St. Louis, MO), S. Mitani (Tokyo Women's Medical University, Tokyo, Japan), T. Hirotsu (Kyushu University, Fukuoka, Japan), and the *Caenorhabditis* Genetics Center for *C. elegans* strains and plasmids. We also thank J. Peña for assisting with molecular biology and A. Bryant, S. Rengarajan, K. Yankura, and M. Frye for insightful comments on the manuscript. This work was supported by an NSF Graduate Research Fellowship (DGE-1144087) and an NIH Ruth L. Kirschstein National Research Service Award (GM007185) to M.L.G.; an NSF Graduate Research Fellowship (DGE-0707424) and a Eugene V. Cota-Robles Fellowship to M.A.C.; and an NSF Division of Integrative Organismal Systems grant (IOS-1456064), a McKnight Scholar Award, and an HHMI Faculty Scholar Award to E.A.H.

Received: March 13, 2017
Revised: June 6, 2017
Accepted: July 10, 2017
Published: August 17, 2017

Figure 4. First-Order Interneurons Contribute to CO_2 Avoidance and Attraction through Experience-Dependent Modulation of Their CO_2-Evoked Activity

(A) AIY is inhibited by CO_2 in animals raised at ambient CO_2 and activated by CO_2 in animals raised at high (2.5%) CO_2. Both responses are BAG dependent. $^*p < 0.05$; $^{**}p < 0.01$; $^{***}p < 0.001$, Kruskal-Wallis test with Dunn's post-test. n = 8–14 animals per genotype and condition.

(B) RIA is activated by CO_2 in animals raised at ambient CO_2 and inhibited by CO_2 in animals raised at high (2.5%) CO_2. Both responses are BAG dependent. $^*p < 0.05$; $^{***}p < 0.001$, Kruskal-Wallis test with Dunn's post-test. n = 9–10 animals per genotype and condition.

(C) RIG is activated by CO_2 in animals raised at ambient CO_2 but does not respond to CO_2 in animals raised at high (2.5%) CO_2. The response is BAG dependent. $^{**}p < 0.01$; $^{***}p < 0.001$, Kruskal-Wallis test with Dunn's post-test (raised at ambient CO_2), or $p = 0.1060$, unpaired t test (raised at high CO_2). n = 8–14 animals per genotype and condition.

(D) AIZ is activated by CO_2 in animals raised at both ambient and high (2.5%) CO_2. Both responses show BAG-dependent and BAG-independent components. $^{**}p < 0.01$; $^{***}p < 0.001$, one-way ANOVA with Sidak's post-test. n = 10 animals per genotype and condition.

For (A)–(D), calcium responses were measured using the ratiometric calcium indicators Yellow Cameleon YC3.60 or YC2.12. Left graphs show composite calcium responses to a 20-s pulse of 15% CO_2. Solid lines indicate average calcium responses; shading represents SEM. Blue lines indicate the response of wild-type animals to CO_2; green lines indicate the response of wild-type animals to an air control; orange lines indicate the response of BAG-ablated animals to CO_2; purple lines indicate the response of BAG-ablated animals to an air control. Right graphs show maximum values (for excitatory or neutral responses) or minimum values (for inhibitory responses) of % $\Delta R/R_0$ for each animal. Lines show medians and interquartile ranges.

(E) A model for CO_2 response in *C. elegans*. Animals raised at ambient CO_2 avoid CO_2, while animals raised at high CO_2 (2.5% CO_2) are attracted to CO_2. CO_2 response valence is determined by the coordinated activity of three interneuron pairs postsynaptic to the CO_2-sensing BAG neurons: AIY, RIA, and RIG. In animals raised at ambient CO_2, activation of RIG and RIA combined with inhibition of AIY results in CO_2 avoidance. In animals raised at high CO_2, activation of AIY, inhibition of RIA, and silencing of RIG result in CO_2 attraction. Activation of a fourth interneuron pair, AIZ, dampens behavioral sensitivity to CO_2, regardless of valence. CO_2 response is regulated by a combinatorial code of neuropeptides: NLP-1 reduces CO_2 avoidance in animals raised at ambient CO_2, FLP-16 reduces CO_2 attraction in animals raised at high CO_2, and FLP-27 enhances CO_2 response under both conditions.

See also Figures S3 and S4.

REFERENCES

1. Mennella, J.A., Pepino, M.Y., and Reed, D.R. (2005). Genetic and environmental determinants of bitter perception and sweet preferences. Pediatrics *115*, e216–e222.
2. O'Doherty, J., Rolls, E.T., Francis, S., Bowtell, R., McGlone, F., Kobal, G., Renner, B., and Ahne, G. (2000). Sensory-specific satiety-related olfactory activation of the human orbitofrontal cortex. Neuroreport *11*, 893–897.
3. Li, Q., and Liberles, S.D. (2015). Aversion and attraction through olfaction. Curr. Biol. *25*, R120–R129.
4. Lee, J.H., Dillman, A.R., and Hallem, E.A. (2016). Temperature-dependent changes in the host-seeking behaviors of parasitic nematodes. BMC Biol. *14*, 36.
5. Kimata, T., Sasakura, H., Ohnishi, N., Nishio, N., and Mori, I. (2012). Thermotaxis of *C. elegans* as a model for temperature perception, neural information processing and neural plasticity. Worm *1*, 31–41.
6. Mengoni, S.L., Lorenzo-Figueiras, A.N., and Minoli, S.A. (2017). Experience-dependent modulation of the attraction to faeces in the kissing bug *Triatoma infestans*. J. Insect Physiol. *98*, 23–28.
7. Chao, M.Y., Komatsu, H., Fukuto, H.S., Dionne, H.M., and Hart, A.C. (2004). Feeding status and serotonin rapidly and reversibly modulate a *Caenorhabditis elegans* chemosensory circuit. Proc. Natl. Acad. Sci. USA *101*, 15512–15517.
8. Sengupta, P. (2013). The belly rules the nose: feeding state-dependent modulation of peripheral chemosensory responses. Curr. Opin. Neurobiol. *23*, 68–75.
9. Sakai, N., Iwata, R., Yokoi, S., Butcher, R.A., Clardy, J., Tomioka, M., and Iino, Y. (2013). A sexually conditioned switch of chemosensory behavior in *C. elegans*. PLoS ONE *8*, e68676.
10. Scott, K. (2011). Out of thin air: sensory detection of oxygen and carbon dioxide. Neuron *69*, 194–202.
11. Ma, D.K., and Ringstad, N. (2012). The neurobiology of sensing respiratory gases for the control of animal behavior. Front. Biol. (Beijing) *7*, 246–253.
12. Carrillo, M.A., Guillermin, M.L., Rengarajan, S., Okubo, R.P., and Hallem, E.A. (2013). O_2-sensing neurons control CO_2 response in *C. elegans*. J. Neurosci. *33*, 9675–9683.
13. Brandt, J.P., and Ringstad, N. (2015). Toll-like receptor signaling promotes development and function of sensory neurons required for a *C. elegans* pathogen-avoidance behavior. Curr. Biol. *25*, 2228–2237.
14. Burg, S.P., and Burg, E.A. (1965). Gas exchange in fruits. Physiol. Plant. *18*, 870–884.
15. Hallem, E.A., and Sternberg, P.W. (2008). Acute carbon dioxide avoidance in *Caenorhabditis elegans*. Proc. Natl. Acad. Sci. USA *105*, 8038–8043.
16. Bretscher, A.J., Busch, K.E., and de Bono, M. (2008). A carbon dioxide avoidance behavior is integrated with responses to ambient oxygen and food in *Caenorhabditis elegans*. Proc. Natl. Acad. Sci. USA *105*, 8044–8049.
17. Hedgecock, E.M., and Russell, R.L. (1975). Normal and mutant thermotaxis in the nematode *Caenorhabditis elegans*. Proc. Natl. Acad. Sci. USA *72*, 4061–4065.
18. Kunitomo, H., Sato, H., Iwata, R., Satoh, Y., Ohno, H., Yamada, K., and Iino, Y. (2013). Concentration memory-dependent synaptic plasticity of a taste circuit regulates salt concentration chemotaxis in *Caenorhabditis elegans*. Nat. Commun. *4*, 2210.
19. Sharabi, K., Hurwitz, A., Simon, A.J., Beitel, G.J., Morimoto, R.I., Rechavi, G., Sznajder, J.I., and Gruenbaum, Y. (2009). Elevated CO_2 levels affect development, motility, and fertility and extend life span in *Caenorhabditis elegans*. Proc. Natl. Acad. Sci. USA *106*, 4024–4029.
20. Hallem, E.A., Spencer, W.C., McWhirter, R.D., Zeller, G., Henz, S.R., Rätsch, G., Miller, D.M., 3rd, Horvitz, H.R., Sternberg, P.W., and Ringstad, N. (2011). Receptor-type guanylate cyclase is required for carbon dioxide sensation by *Caenorhabditis elegans*. Proc. Natl. Acad. Sci. USA *108*, 254–259.
21. Sieburth, D., Madison, J.M., and Kaplan, J.M. (2007). PKC-1 regulates secretion of neuropeptides. Nat. Neurosci. *10*, 49–57.
22. Sieburth, D., Ch'ng, Q., Dybbs, M., Tavazoie, M., Kennedy, S., Wang, D., Dupuy, D., Rual, J.F., Hill, D.E., Vidal, M., et al. (2005). Systematic analysis of genes required for synapse structure and function. Nature *436*, 510–517.
23. Brandt, J.P., Aziz-Zaman, S., Juozaityte, V., Martinez-Velazquez, L.A., Petersen, J.G., Pocock, R., and Ringstad, N. (2012). A single gene target of an ETS-family transcription factor determines neuronal CO_2-chemosensitivity. PLoS ONE *7*, e34014.
24. Smith, E.S., Martinez-Velazquez, L., and Ringstad, N. (2013). A chemoreceptor that detects molecular carbon dioxide. J. Biol. Chem. *288*, 37071–37081.
25. Guillermin, M.L., Castelletto, M.L., and Hallem, E.A. (2011). Differentiation of carbon dioxide-sensing neurons in *Caenorhabditis elegans* requires the ETS-5 transcription factor. Genetics *189*, 1327–1339.
26. Dalton, P. (2000). Psychophysical and behavioral characteristics of olfactory adaptation. Chem. Senses *25*, 487–492.
27. Sachse, S., Rueckert, E., Keller, A., Okada, R., Tanaka, N.K., Ito, K., and Vosshall, L.B. (2007). Activity-dependent plasticity in an olfactory circuit. Neuron *56*, 838–850.
28. Dennis, C.E., 3rd, Adhikari, S., Wright, A.W., and Suski, C.D. (2016). Molecular, behavioral, and performance responses of juvenile largemouth bass acclimated to an elevated carbon dioxide environment. J. Comp. Physiol. B *186*, 297–311.
29. Bargmann, C.I. (2006). Chemosensation in *C. elegans*. WormBook, 1–11, http://www.wormbook.org.
30. Zimmer, M., Gray, J.M., Pokala, N., Chang, A.J., Karow, D.S., Marletta, M.A., Hudson, M.L., Morton, D.B., Chronis, N., and Bargmann, C.I. (2009). Neurons detect increases and decreases in oxygen levels using distinct guanylate cyclases. Neuron *61*, 865–879.
31. Ringstad, N., and Horvitz, H.R. (2008). FMRFamide neuropeptides and acetylcholine synergistically inhibit egg-laying by *C. elegans*. Nat. Neurosci. *11*, 1168–1176.
32. Peymen, K., Watteyne, J., Frooninckx, L., Schoofs, L., and Beets, I. (2014). The FMRFamide-like peptide family in nematodes. Front. Endocrinol. (Lausanne) *5*, 90.
33. Serrano-Saiz, E., Poole, R.J., Felton, T., Zhang, F., De La Cruz, E.D., and Hobert, O. (2013). Modular control of glutamatergic neuronal identity in *C. elegans* by distinct homeodomain proteins. Cell *155*, 659–673.
34. White, J.G., Southgate, E., Thomson, J.N., and Brenner, S. (1986). The structure of the nervous system of the nematode *Caenorhabditis elegans*. Philos. Trans. R. Soc. Lond. B Biol. Sci. *314*, 1–340.
35. Xu, M., Jarrell, T.A., Wang, Y., Cook, S.J., Hall, D.H., and Emmons, S.W. (2013). Computer assisted assembly of connectomes from electron micrographs: application to *Caenorhabditis elegans*. PLoS ONE *8*, e54050.
36. Chalasani, S.H., Chronis, N., Tsunozaki, M., Gray, J.M., Ramot, D., Goodman, M.B., and Bargmann, C.I. (2007). Dissecting a circuit for olfactory behaviour in *Caenorhabditis elegans*. Nature *450*, 63–70.
37. Chronis, N., Zimmer, M., and Bargmann, C.I. (2007). Microfluidics for in vivo imaging of neuronal and behavioral activity in *Caenorhabditis elegans*. Nat. Methods *4*, 727–731.
38. Yu, S., Avery, L., Baude, E., and Garbers, D.L. (1997). Guanylyl cyclase expression in specific sensory neurons: a new family of chemosensory receptors. Proc. Natl. Acad. Sci. USA *94*, 3384–3387.
39. Ha, H.I., Hendricks, M., Shen, Y., Gabel, C.V., Fang-Yen, C., Qin, Y., Colón-Ramos, D., Shen, K., Samuel, A.D., and Zhang, Y. (2010). Functional organization of a neural network for aversive olfactory learning in *Caenorhabditis elegans*. Neuron *68*, 1173–1186.
40. Singh, K., Chao, M.Y., Somers, G.A., Komatsu, H., Corkins, M.E., Larkins-Ford, J., Tucey, T., Dionne, H.M., Walsh, M.B., Beaumont, E.K., et al. (2011). *C. elegans* Notch signaling regulates adult chemosensory response and larval molting quiescence. Curr. Biol. *21*, 825–834.

41. Tsalik, E.L., and Hobert, O. (2003). Functional mapping of neurons that control locomotory behavior in *Caenorhabditis elegans*. J. Neurobiol. *56*, 178–197.
42. Zheng, Y., Brockie, P.J., Mellem, J.E., Madsen, D.M., and Maricq, A.V. (1999). Neuronal control of locomotion in *C. elegans* is modified by a dominant mutation in the GLR-1 ionotropic glutamate receptor. Neuron *24*, 347–361.
43. Schiavo, G., Benfenati, F., Poulain, B., Rossetto, O., Polverino de Laureto, P., DasGupta, B.R., and Montecucco, C. (1992). Tetanus and botulinum-B neurotoxins block neurotransmitter release by proteolytic cleavage of synaptobrevin. Nature *359*, 832–835.
44. Macosko, E.Z., Pokala, N., Feinberg, E.H., Chalasani, S.H., Butcher, R.A., Clardy, J., and Bargmann, C.I. (2009). A hub-and-spoke circuit drives pheromone attraction and social behaviour in *C. elegans*. Nature *458*, 1171–1175.
45. Pokala, N., Liu, Q., Gordus, A., and Bargmann, C.I. (2014). Inducible and titratable silencing of *Caenorhabditis elegans* neurons in vivo with histamine-gated chloride channels. Proc. Natl. Acad. Sci. USA *111*, 2770–2775.
46. Jin, X., Pokala, N., and Bargmann, C.I. (2016). Distinct circuits for the formation and retrieval of an imprinted olfactory memory. Cell *164*, 632–643.
47. Ohnishi, N., Kuhara, A., Nakamura, F., Okochi, Y., and Mori, I. (2011). Bidirectional regulation of thermotaxis by glutamate transmissions in *Caenorhabditis elegans*. EMBO J. *30*, 1376–1388.
48. Kodama-Namba, E., Fenk, L.A., Bretscher, A.J., Gross, E., Busch, K.E., and de Bono, M. (2013). Cross-modulation of homeostatic responses to temperature, oxygen and carbon dioxide in *C. elegans*. PLoS Genet. *9*, e1004011.
49. Dickinson, P.S. (2006). Neuromodulation of central pattern generators in invertebrates and vertebrates. Curr. Opin. Neurobiol. *16*, 604–614.
50. Lee, S.H., and Dan, Y. (2012). Neuromodulation of brain states. Neuron *76*, 209–222.
51. Bargmann, C.I. (2012). Beyond the connectome: how neuromodulators shape neural circuits. BioEssays *34*, 458–465.
52. Rojo Romanos, T., Petersen, J.G., and Pocock, R. (2017). Control of neuropeptide expression by parallel activity-dependent pathways in *Caenorhabditis elegans*. Sci. Rep. *7*, 38734.
53. Turner, S.L., and Ray, A. (2009). Modification of CO_2 avoidance behaviour in *Drosophila* by inhibitory odorants. Nature *461*, 277–281.
54. Turner, S.L., Li, N., Guda, T., Githure, J., Cardé, R.T., and Ray, A. (2011). Ultra-prolonged activation of CO_2-sensing neurons disorients mosquitoes. Nature *474*, 87–91.
55. Bräcker, L.B., Siju, K.P., Varela, N., Aso, Y., Zhang, M., Hein, I., Vasconcelos, M.L., and Grunwald Kadow, I.C. (2013). Essential role of the mushroom body in context-dependent CO_2 avoidance in *Drosophila*. Curr. Biol. *23*, 1228–1234.
56. Lewis, L.P., Siju, K.P., Aso, Y., Friedrich, A.B., Bulteel, A.J., Rubin, G.M., and Grunwald Kadow, I.C. (2015). A higher brain circuit for immediate integration of conflicting sensory information in *Drosophila*. Curr. Biol. *25*, 2203–2214.
57. Wasserman, S., Salomon, A., and Frye, M.A. (2013). *Drosophila* tracks carbon dioxide in flight. Curr. Biol. *23*, 301–306.
58. Knaden, M., and Hansson, B.S. (2014). Mapping odor valence in the brain of flies and mice. Curr. Opin. Neurobiol. *24*, 34–38.
59. Root, C.M., Denny, C.A., Hen, R., and Axel, R. (2014). The participation of cortical amygdala in innate, odour-driven behaviour. Nature *515*, 269–273.
60. Calhoun, A.J., Tong, A., Pokala, N., Fitzpatrick, J.A., Sharpee, T.O., and Chalasani, S.H. (2015). Neural mechanisms for evaluating environmental variability in *Caenorhabditis elegans*. Neuron *86*, 428–441.
61. Luo, L., Cook, N., Venkatachalam, V., Martinez-Velazquez, L.A., Zhang, X., Calvo, A.C., Hawk, J., MacInnis, B.L., Frank, M., Ng, J.H., et al. (2014). Bidirectional thermotaxis in *Caenorhabditis elegans* is mediated by distinct sensorimotor strategies driven by the AFD thermosensory neurons. Proc. Natl. Acad. Sci. USA *111*, 2776–2781.
62. Kuhara, A., Ohnishi, N., Shimowada, T., and Mori, I. (2011). Neural coding in a single sensory neuron controlling opposite seeking behaviours in *Caenorhabditis elegans*. Nat. Commun. *2*, 355.
63. Kuhara, A., and Mori, I. (2006). Molecular physiology of the neural circuit for calcineurin-dependent associative learning in *Caenorhabditis elegans*. J. Neurosci. *26*, 9355–9364.
64. Uozumi, T., Hirotsu, T., Yoshida, K., Yamada, R., Suzuki, A., Taniguchi, G., Iino, Y., and Ishihara, T. (2012). Temporally-regulated quick activation and inactivation of Ras is important for olfactory behaviour. Sci. Rep. *2*, 500.
65. Qi, Y.B., Garren, E.J., Shu, X., Tsien, R.Y., and Jin, Y. (2012). Photo-inducible cell ablation in *Caenorhabditis elegans* using the genetically encoded singlet oxygen generating protein miniSOG. Proc. Natl. Acad. Sci. USA *109*, 7499–7504.
66. Stiernagle, T. (2006). Maintenance of *C. elegans*. WormBook, 1–11, http://www.wormbook.org.
67. Bargmann, C.I., Hartwieg, E., and Horvitz, H.R. (1993). Odorant-selective genes and neurons mediate olfaction in *C. elegans*. Cell *74*, 515–527.
68. Nagai, T., Yamada, S., Tominaga, T., Ichikawa, M., and Miyawaki, A. (2004). Expanded dynamic range of fluorescent indicators for $Ca^{(2+)}$ by circularly permuted yellow fluorescent proteins. Proc. Natl. Acad. Sci. USA *101*, 10554–10559.
69. Colón-Ramos, D.A., Margeta, M.A., and Shen, K. (2007). Glia promote local synaptogenesis through UNC-6 (netrin) signaling in *C. elegans*. Science *318*, 103–106.
70. Hendricks, M., Ha, H., Maffey, N., and Zhang, Y. (2012). Compartmentalized calcium dynamics in a *C. elegans* interneuron encode head movement. Nature *487*, 99–103.
71. Fernandes, J.S., and Sternberg, P.W. (2007). The tailless ortholog *nhr-67* regulates patterning of gene expression and morphogenesis in the *C. elegans* vulva. PLoS Genet. *3*, e69.
72. Li, C., and Kim, K. (2008). Neuropeptides. WormBook, 1–36, http://www.wormbook.org.
73. Clark, D.A., Biron, D., Sengupta, P., and Samuel, A.D. (2006). The AFD sensory neurons encode multiple functions underlying thermotactic behavior in *Caenorhabditis elegans*. J. Neurosci. *26*, 7444–7451.
74. Salkoff, L., Butler, A., Fawcett, G., Kunkel, M., McArdle, C., Paz-y-Mino, G., Nonet, M., Walton, N., Wang, Z.W., Yuan, A., and Wei, A. (2001). Evolution tunes the excitability of individual neurons. Neuroscience *103*, 853–859.
75. Chelur, D.S., and Chalfie, M. (2007). Targeted cell killing by reconstituted caspases. Proc. Natl. Acad. Sci. USA *104*, 2283–2288.

STAR★METHODS

KEY RESOURCES TABLE

REAGENT or RESOURCE	SOURCE	IDENTIFIER
Bacterial and Virus Strains		
Escherichia coli: Strain OP50	*Caenorhabditis* Genetics Center	OP50
Chemicals, Peptides, and Recombinant Proteins		
Histamine	Sigma-Aldrich	H7250-10MG
HEPES	Sigma-Aldrich	H0887-20ML
Butler Schein Animal Health Surgi-lock 2-octyl cyanoacrylate instant tissue adhesive	Fisher Scientific	NC9812699
Experimental Models: Organisms/Strains		
C. elegans: Strain N2: Bristol	*Caenorhabditis* Genetics Center	N2
C. elegans: Strain CX11697: *kyIs536[flp-17::p17::SL2::GFP, elt-2::mCherry]; kyIs538[glb-5::p12::SL2::GFP, elt-2::mCherry*	[12, 23, 25]	CX11697
C. elegans: Strain EAH263: *bruEx155[flp-17::pkc-1(gf)::SL2::GFP]*	This paper	EAH263
C. elegans: Strain AX2073: *lin-15(n765ts); dbEx[flp-17::YC3.60, lin-15(+)]*	[48]	AX2073
C. elegans: Strain EAH67: *bruEx49[gcy-9::GFP, pax-2::GFP]*	[25]	EAH67
C. elegans: Strain MT15933: *flp-17(n4894)*	*Caenorhabditis* Genetics Center	MT15933
C. elegans: Strain MT6308: *eat-4(ky5)*	*Caenorhabditis* Genetics Center	MT6308
C. elegans: Strain MT6318: *eat-4(n2474)*	*Caenorhabditis* Genetics Center	MT6318
C. elegans: Strain EAH312: *eat-4(ky5); flp-17(n4894)*	This paper	EAH312
C. elegans: Strain EAH346: *eat-4(ky5); bruEx180 [flp-17::eat-4::SL2::GFP]*	This paper	EAH346
C. elegans: Strain EAH347: *eat-4(ky5); bruEx181 [flp-17::eat-4::SL2::GFP]*	This paper	EAH347
C. elegans: Strain EAH202: *ls[npr-9::casp1 unc122::mCherry]; ls[npr-1::venus]*	[18]	EAH202
C. elegans: Strain IV316: *ueEx194[odr-2b3a::TeTx::GFP, elt-2::SL2::GFP]*	[60]	IV316
C. elegans: Strain EAH284: *bruEx138[ttx-3::casp-3(p17), ttx-3::casp-3(p12), myo-2::dsRed]*	This paper	EAH284
C. elegans: Strain OH8: *ttx-3(mg158)*	*Caenorhabditis* Genetics Center	OH8
C. elegans: Strain OH99: *mgIs18[ttx-3::GFP]*	*Caenorhabditis* Genetics Center	OH99
C. elegans: Strain EAH314: *akIs11[lin-15(+), nmr-1::ICE]*	This paper	EAH314
C. elegans: Strain EAH241: *lin-15(n765ts); njIs11 [glr-3::GFP, ges-1::RFP]; ajEx211[glr-3::GFP, glr-3::ICE, lin-15(+)]*	This paper	EAH241
C. elegans: Strain TV2217: *wyIs93(glr-3::mCherry::rab-3, glr-3::glr-1::GFP); wyEx828(glr-3::caspase, glr-3::mCherry, coel::RFP)*	[61]	TV2217
C. elegans: Strain EAH319: *bruEx171[glr-3::casp-3(p17), glr-3::casp-3(p12), myo-2::dsRed]*	This paper	EAH319
C. elegans: Strain IK716: *njIs11[glr-3::GFP, ges-1::RFP]*	*Caenorhabditis* Genetics Center	IK716
C. elegans: Strain EAH281: *bruEx162[cex-1::casp-3(p17), cex-1::casp-3(p12), myo-2::dsRed]*	This paper	EAH281
C. elegans: Strain EAH242: *bruEx142 [cex-1-tomm-20N::miniSOG::SL2::GFP]*	This paper	EAH242

(*Continued on next page*)

Continued

REAGENT or RESOURCE	SOURCE	IDENTIFIER
C. elegans: Strain EAH268: *bruEx160[twk-3::casp-3(p17), twk-3::casp-3(p12), myo-2::dsRed]*	This paper	EAH268
C. elegans: Strain EAH267: *bruEx159[twk-3::casp-3(p17), twk-3::casp-3(p12), myo-2::dsRed]*	This paper	EAH267
C. elegans: Strain EAH269: *bruEx161 [twk-3-tomm-20N::miniSOG::SL2::GFP]*	This paper	EAH269
C. elegans: Strain EAH266: *bruEx158[ttx-3::pkc-1(gf)::SL2::GFP]*	This paper	EAH266
C. elegans: Strain EAH287: *bruEx163[twk-3::pkc-1(gf)::SL2::GFP]*	This paper	EAH287
C. elegans: Strain EAH342: *bruEx176[glr-3::pkc-1(gf)::SL2::GFP]*	This paper	EAH342
C. elegans: Strain CX16880: *kyEx5847[ttx-3::HisCl1::SL2::GFP, myo-3::mCherry]*	[46]	CX16880
C. elegans: Strain CX15141: *kyEx5063[glr-3::HisCl1::SL2::mCherry, glr-3::TRPV1::SL2::mCherry, elt-2::mCherry]*	[46]	CX15141
C. elegans: Strain RB594: *glc-3(ok321)*	*Caenorhabditis* Genetics Center	RB594
C. elegans: Strain CX6930: *glc-3(ok321); kyEx773 [ttx-3::glc-3, elt-2::GFP]*	[36]	CX6930
C. elegans: Strain IK1405: *njEx568[ttx-3::YC3.60, ges-1::NLS-RFP]*	[62]	IK1405
C. elegans: Strain EAH227: *kyIs536[flp-17::p17::SL2::GFP, elt-2::mCherry]; kyIs538[glb-5::p12::SL2::GFP, elt-2::mCherry]; njEx568[ttx-3::YC3.60, ges-1::NLS-RFP]*	This paper	EAH227
C. elegans: Strain AX2361: *dbEx[glr-3::YC3.60]*	[48]	AX2361
C. elegans: Strain EAH325: *kyIs536[flp-17::p17::SL2::GFP, elt-2::mCherry]; kyIs538[glb-5::p12::SL2::GFP, elt-2::mCherry]; dbEx[glr-3::YC3.60]*	This paper	EAH325
C. elegans: Strain PS6028: *syEx1134[twk-3::YC3.60]*	This paper	PS6028
C. elegans: Strain EAH148: *kyIs536[flp-17::p17::SL2::GFP, elt-2::mCherry]; kyIs538[glb-5::p12::SL2::GFP, elt-2::mCherry]; syEx1134[twk-3::YC3.60]*	This paper	EAH148
C. elegans: Strain IK686: *njEx344[lin-11::YC2.12, ges-1::NLS-GFP]*	[63]	IK686
C. elegans: Strain EAH324: *kyIs536[flp-17::p17::SL2::GFP, elt-2::mCherry]; kyIs538[glb-5::p12::SL2::GFP, elt-2::mCherry]; njEx344[lin-11::YC2.12, ges-1::NLS-GFP]*	This paper	EAH324
C. elegans: Strain EAH259: *ex[odr-2(1b)::YC3.60; lin-44::GFP]*	[64]	EAH259
C. elegans: Strain FX05158: *flp-16(tm5158)*	S. Mitani, National BioResource Project	FX05158
C. elegans: Strain FX04829: *flp-16(tm4829)*	S. Mitani, National BioResource Project	FX04829
C. elegans: Strain RB2275: *flp-16(ok3085)*	*Caenorhabditis* Genetics Center	RB2275
C. elegans: Strain RB1903: *flp-19(ok2461)*	*Caenorhabditis* Genetics Center	RB1903
C. elegans: Strain RB1902: *flp-19(ok2460)*	*Caenorhabditis* Genetics Center	RB1902
C. elegans: Strain VC2012: *flp-27(gk3331) Y17G7B.22(gk1062); gkDf45*	*Caenorhabditis* Genetics Center	VC2012
C. elegans: Strain VC2180: *Y17G7B.22(gk1010)*	*Caenorhabditis* Genetics Center	VC2180
C. elegans: Strain VC2063: *Y17G7B.22(gk1012)*	*Caenorhabditis* Genetics Center	VC2063
C. elegans: Strain FX04612: *flp-27(tm4612)*	S. Mitani, National BioResource Project	FX04612
C. elegans: Strain IK581: *ins-1(nj32)*	*Caenorhabditis* Genetics Center	IK581

(*Continued on next page*)

Continued

REAGENT or RESOURCE	SOURCE	IDENTIFIER
C. elegans: Strain FX02416: *ins-6(tm2416)*	S. Mitani, National BioResource Project	FX02416
C. elegans: Strain FX00790: *ins-17(tm790)*	S. Mitani, National BioResource Project	FX00790
C. elegans: Strain RB1341: *nlp-1(ok1470)*	*Caenorhabditis* Genetics Center	RB1341
C. elegans: Strain RB1340: *nlp-1(ok1469)*	*Caenorhabditis* Genetics Center	RB1340
C. elegans: Strain FX02984: *nlp-7(tm2984)*	S. Mitani, National BioResource Project	FX02984
C. elegans: Strain FX01880: *nlp-14(tm1880)*	S. Mitani, National BioResource Project	FX01880
Oligonucleotides		
flp-17: 5′-gcggccgcaaaattatctggattcaccaac-3′	This paper	flp-17 up
flp-17: 5′-ggatccggaaaatatttccacacagaat-3′	This paper	flp-17 down
ttx-3: 5′-gcggccgcaagctttttgaaacgatctt-3′	This paper	ttx-3 prom UP
ttx-3: 5′-ggatccatttgacaccgaagacaatt-3′	This paper	ttx-3 prom DOWN
cex-1: 5′-gtcgacttttaaatggaaagtaaaacga-3′	This paper	cex-1-up
cex-1: 5′-ggatccttctgaaagtataagatttgactga-3′	This paper	cex-1-down
glr-3: 5′-gcatgcatcactgagccagagatgag-3′	This paper	glr-3 prom UP
glr-3: 5′-ggatccatgttaatagcaaatattgaagattc-3′	This paper	glr-3 prom DOWN
eat-4: 5′-gctagccatgtcgtcatggaacgag-3′	This paper	eat-4 cDNA UP
eat-4: 5′-ggtaccagatggcgatctgatgacag-3′	This paper	eat-4 cDNA DOWN
Recombinant DNA		
flp-17::eat-4::SL2::GFP	This paper	pMLG017
flp-21::pkc-1(gf)::SL2::GFP	[44]	PEM-15
flp-17::pkc-1(gf)::SL2::GFP	This paper	pMLG009
ttx-3::pkc-1(gf)::SL2::GFP	This paper	pMLG010
twk-3::pkc-1(gf)::SL2::GFP	This paper	pMLG012
glr-3:: pkc-1(gf)::SL2::GFP	This paper	pMLG016
ttx-3::casp-3(p17)	[61]	DACR335
ttx-3::casp-3(p12)	[61]	DACR336
glr-3::casp-3(p17)	[61]	DACR77
glr-3::casp-3(p12)	[61]	DACR76
cex-1::casp-3(p17)	This paper	N/A
cex-1::casp-3(p12)	This paper	N/A
twk-3::casp-3(p17)	This paper	N/A
twk-3::casp-3(p12)	This paper	N/A
tomm-20(N'-55AA)::miniSOG in pENTR	[65]	pCZGY#1534
cex-1-tomm-20(N'-55AA)::miniSOG::SL2::GFP	This paper	pMLG014
twk-3-tomm-20(N'-55AA)::miniSOG::SL2::GFP	This paper	pMLG015
Software and Algorithms		
GraphPad Prism 6	GraphPad	http://www.graphpad.com
Zeiss AxioVision 4.8	Carl Zeiss	https://www.zeiss.com/microscopy/us/products/microscope-software/axiovision.html
Other		
DigiTherm CO_2 heating/cooling incubator	Tritech Research	DT2-CO2-47
Certified gas mixes	Airgas	N/A
PHD 22/2000 syringe pump	Harvard Apparatus	70-2003
Zeiss AxioObserver A1 inverted microscope, 40X EC Plan-Neofluar lens	Carl Zeiss	N/A
EM-CCD camera	Hamamatsu	C9100-02
DV2 multichannel imaging system	Photometrics	N/A
100-mm fully stackable vented Petri dishes	Tritech Research	T3371

CONTACT FOR REAGENT AND RESOURCE SHARING

Further information and requests for strains and reagents should be directed to and will be fulfilled by the Lead Contact, Dr. Elissa Hallem (ehallem@ucla.edu).

EXPERIMENTAL MODEL AND SUBJECT DETAILS

The free-living nematode *Caenorhabditis elegans* was used as the experimental model for this study. *C. elegans* has two sexes, hermaphrodites and males. Our experiments were carried out with hermaphrodites; males were used only for crosses. Unless otherwise noted, all experiments were done using *C. elegans* young adults. Strains were maintained at room temperature (RT, ~22°C) and ambient CO_2 (0.038% CO_2) on Nematode Growth Media (NGM) plates containing a thin lawn of *Escherichia coli* OP50 bacteria, according to standard methods [66]. Strains raised at high CO_2 were placed in a Tritech Research DigiTherm CO_2 heating/cooling incubator, at 22°C and 2.5% CO_2, for one generation and subsequently tested. Strains transferred from ambient CO_2 to high CO_2 were maintained at RT and ambient CO_2, and transferred to the CO_2 incubator (22°C; 2.5% CO_2) for the indicated amount of time. Strains transferred from high CO_2 to ambient CO_2 were maintained at RT and ambient CO_2, raised in the CO_2 incubator (22°C; 2.5% CO_2) for one generation, and subsequently transferred to RT and ambient CO_2 for the indicated amount of time. All transgenic strains were made by microinjection of plasmid DNA into N2 hermaphrodites. See Key Resources Table for details.

EAH202 was obtained from Y. Iino (University of Tokyo, Tokyo, Japan) and then given an EAH strain number for identification purposes. EAH284 was generated by microinjecting the following plasmids, obtained from D. Colón-Ramos: DACR335 *ttx-3::casp-3(p17)* and DACR336 *ttx-3::casp-3(p12)*. EAH314 was derived from VM4770 [42] by outcrossing to N2 for 3 generations. The following strains were used to confirm results with independent transgenes: TV2217, EAH319, EAH267, and EAH346. TV2217 was obtained from D. Colón-Ramos [61]. The AIY ablation phenotype was confirmed using strain OH8, which contains a *ttx-3* mutation. EAH319 was generated by microinjecting the following plasmids, obtained from D. Colón-Ramos: DACR77 *glr-3::casp-3(p17)* and DACR76 *glr-3::casp-3(p12)*. The following GFP reporter strains were used to confirm cell ablations: OH99, EAH242, EAH269, IK716. EAH242 and EAH269 were generated using pCZGY#1534, obtained from Y. Jin [65]. The following strains were used to confirm results with independent deletion alleles: FX04829, RB2275, RB1902, FX04612, RB1340. The following strains were tested to rule out the possibility that the phenotypes observed with VC2012 were due to a deletion in *Y17G7B.22* rather than *flp-27*: VC2180 and VC2063. The AIB AIZ-silenced strain IV316 was obtained from S. Chalasani [60]. Calcium imaging of AIY and AIZ was performed using strains IK1405 and IK686, respectively, which were obtained from I. Mori [62, 63]. Calcium imaging of RIA was performed using strain AX2361, which was obtained from M. de Bono [48]. Calcium imaging of AIB was performed using EAH259, which was obtained from T. Hirotsu [64].

METHOD DETAILS

CO_2 chemotaxis assays

Chemotaxis assays were performed as previously described (Figure S1A) [12]. Young adult animals were washed off plates using M9 buffer [66] and collected into a 65-mm Syracuse watch glass. Animals were washed 3x with M9 buffer and transferred to a 1-cm x 1-cm square of Whatman paper. Animals were then transferred from the filter paper to the center of a 100-mm NGM or chemotaxis plate [67]. The actual potential crawling distance of the animals is the diameter of the inside base of the plate, which measures 84.4 mm. A CO_2 gradient was generated by delivering gas stimuli to the plate through holes in the plate lids as previously described [12]. Unless otherwise indicated, a 21% O_2, balance N_2 air control was delivered through one hole, and a certified mixture containing a designated CO_2 concentration with 21% O_2 and the balance N_2 (Airgas) was delivered through the other hole. Gases were pumped through ¼-inch flexible PVC tubing using a syringe pump (PHD 2000, Harvard Apparatus) at a rate of 2 mL/min. The duration of the assay was 20 min. The number of animals in a 20-mm diameter circle centered under each gas inlet was counted and used to determine the chemotaxis index (CI), according to the formula:

$$CI = \frac{\#\ of\ animals\ at\ CO_2 - \#\ of\ animals\ at\ air\ control}{\#\ of\ animals\ at\ CO_2 + air\ control}.$$

To control for directional bias due to subtle room vibrations, two identical assays were always performed simultaneously with the CO_2 gradient in opposite directions. Assays were discarded if the difference in the CI for the two plates was $\geq$ 0.9 or if fewer than 7 worms moved into the scoring regions on either plate. Transgenic strains expressing the histamine-gated chloride channel HisCl1 were incubated on NGM plates containing 10 mM histamine but not *E. coli* OP50 [45] for 20 min prior to the chemotaxis assay.

For assays where animals were raised at ambient CO_2 and transferred to high (2.5%) CO_2, the extent to which the animals had switched valence to attraction was calculated for each trial by comparing the CI for the current trial to the mean CIs for animals of the same genotype cultivated at either ambient or high CO_2 according to the following formula:

$$\%\ change\ in\ valence = \frac{CI\ for\ current\ trial - mean\ CI\ for\ ambient\ CO_2\ trials}{mean\ CI\ for\ high\ CO_2\ trials - mean\ CI\ for\ ambient\ CO_2\ trials} \times 100.$$

For assays where the animals were raised at high CO_2 and transferred to ambient CO_2, the extent to which the animals had switched valence to avoidance was calculated for each trial by comparing the CI for the current trial to the mean CIs for animals of the same genotype cultivated at either ambient or high CO_2 according to the following formula:

$$\%\ change\ in\ valence = \frac{mean\ CI\ for\ high\ CO_2\ trials - CI\ for\ current\ trial}{mean\ CI\ for\ high\ CO_2\ trials - mean\ CI\ for\ ambient\ CO_2\ trials} \times 100.$$

Values below 0 were counted as 0. Values greater than 100 were counted as 100.

Calcium imaging

Imaging was performed as previously described [12] using the genetically encoded calcium indicators yellow cameleon YC2.12 and YC3.60 [68]. Young adults were immobilized onto a cover glass containing a 2% agarose pad made with 10 mM HEPES using Butler Schein Animal Health Surgi-lock 2-octyl cyanoacrylate instant tissue adhesive. A custom-made gas delivery chamber was secured over the cover glass. Gases were delivered at a rate of 0.7-0.8 L/min. During the assay, 20 s of 21% O_2 was followed by a 20-s pulse of 15% CO_2, followed by 20 s of 21% O_2. Imaging was performed on a Zeiss AxioObserver A1 inverted microscope using a 40X EC Plan-NEOFLUAR lens, a Hamamatsu C9100 EM-CCD camera, and AxioVision software. The EM gain was set at 30. The emission image was passed through a DV2 beam splitter (Photometrics) as previously described [12]. Image analysis was performed using Zeiss AxioVision Software and Microsoft Excel.

For each recording, the mean pixel value of a background region of interest was subtracted from the mean pixel value of a region of interest containing the neuron soma (RIG, AIZ, AIB) or neuron process (AIY, RIA). When imaging from AIY, we focused on the synapse-rich segment of the process designated zone 2 [69]. When imaging from RIA, we focused primarily on the "loop" segment of the RIA process, and occasionally on nrV, the ventral segment of the process in the nerve ring [70]. Fluorescence values were normalized to the average values obtained 10 s prior to CO_2 delivery. The YFP/CFP ratio was calculated as previously described [20]. Images were baseline-corrected using a linear baseline correction. Traces with unstable baselines prior to the onset of the CO_2 pulse were discarded. To establish appropriate criteria for including traces as either depolarizations or hyperpolarizations, we recorded control traces for each genotype using a 21% O_2, balance N_2 air control pulse. We then calculated the standard deviation of the set containing the maximum value of each control trace (max set), and the standard deviation of the set containing the minimum value of each control trace (min set). Traces recorded with a CO_2 pulse where the maximum value exceeded 3 standard deviations from the mean of the air control (max set) were designated depolarizations; traces recorded with a CO_2 pulse where the minimum value exceeded 3 standard deviations from the mean of the air control (min set) were designated hyperpolarizations. For cases where we observed CO_2-evoked depolarizations or hyperpolarizations, traces where the maximum or minimum value, respectively, was within 3 standard deviations of the mean of the max or min set for the air control were discarded.

For imaging animals raised at high CO_2, animals were incubated at 2.5% CO_2 for one generation. Prior to imaging, cameleon-expressing animals were placed on individual plates so they could subsequently be removed from the incubator one at a time to minimize time at ambient CO_2. Immediately prior to recording, individual animals were removed from the incubator and then prepared for imaging, spending approximately 5 min at ambient CO_2 before imaging. We note that for all imaging experiments, the CO_2 concentrations used for calcium imaging cannot be directly compared to the CO_2 concentrations used for behavioral assays due to differences in the setup for CO_2 delivery in the two cases.

Fluorescence microscopy

Images of *gcy-9::GFP*-expressing animals were acquired as previously described [12]. Animals were selected at the L4 stage using the co-injection marker *pax-2::GFP*. *pax-2* expression is visible in the vulva at the L4 stage [71]. Selection based on *pax-2* expression was used to limit bias and obtain a representative sample of *gcy-9* expression.

Molecular biology

To achieve BAG-specific expression of *pkc-1(gf)*, a 3-kb sequence upstream of the *flp-17* gene [31, 72] was PCR-amplified from genomic DNA using primers 5′-gcggccgcaaaattatctggattcaccaac-3′ and 5′-ggatccggaaaatatttccacacagaat-3′, and used to drive expression of *pkc-1(gf)* [44]. A plasmid containing the *pkc-1(gf)* sequence was obtained from C. Bargmann (Rockefeller University, NY). AIY-specific expression of *pkc-1(gf)* was achieved using a 4-kb region of the *ttx-3* gene [69, 73] that was PCR-amplified from genomic DNA using primers 5′-gcggccgcaagctttttttgaaacgatctt-3′ and 5′-ggatccatttgacaccgaagacaatt-3′. RIG-specific expression of *pkc-1(gf)* was achieved using a 149-bp region of the *twk-3* promoter [74]. A plasmid containing the *twk-3* promoter sequence was obtained from L. Salkoff (Washington University, MO). RIA-specific expression of *pkc-1(gf)* was achieved using a 1.2-kb region of the *glr-3* gene [70] that was PCR-amplified from genomic DNA using primers 5′-gcatgcatcactgagccagagatgag-3′ and 5′-ggatcc atgttaatagcaaatattgaagattc-3′. To generate a BAG-specific rescue of *eat-4*, we obtained a plasmid from I. Mori (Nagoya University, Japan) containing *eat-4* cDNA. *eat-4* cDNA was PCR-amplified from the plasmid using primers 5′-gctagccatgtcgtcatggaacgag-3′ and 5′-ggtaccagatggcgatctgatgacag-3′. Using our previously generated *flp-17::pkc-1(gf)::SL2::GFP* plasmid, we replaced the *pkc-1(gf)* sequence with the *eat-4* cDNA sequence and injected the resulting *flp-17::eat-4::SL2::GFP* plasmid into the MT6308 *eat-4(ky5)* strain, at 50 ng/μL. Behavioral results were confirmed with two independently derived rescue lines.

Interneuron ablation strains were generated using the two-component reconstituted caspase system previously described [75]. For genetic ablation of AIY, the following plasmids were obtained from D. Colón-Ramos (Yale University): DACR335

ttx-3::casp-3(p17) and DACR336 *ttx-3::casp-3(p12)* [69, 73]. For genetic ablation of RIB, cell-specific expression was achieved using the *cex-1* promoter [69]. A 1-kb sequence upstream of *cex-1* was PCR-amplified from genomic DNA using primers 5′-gtcgacttttta aatggaaagtaaaacga-3′ and 5′-ggatccttctgaaagtataagatttgactga-3′. The *cex-1* sequence, along with DACR335 and DACR336, were used to generate *cex-1::casp-3(p17)* and *cex-1::casp-3(p12)*. For genetic ablation of RIG, cell-specific expression was achieved using the same 149-bp promoter region of *twk-3* used to generate *RIG::pkc-1(gf)* (described above). The *twk-3* sequence, along with DACR335 and DACR336, were used to make *twk-3::casp-3(p17)* and *twk-3::casp-3(p12)*. For genetic ablation of RIA, cell-specific expression was achieved using the promoter region of the *glr-3* gene [70]. The following plasmids were obtained from D. Colón-Ramos (Yale University): DACR77 *glr-3::casp-3(p17)* and DACR76 *glr-3::casp-3(p12)*. Plasmids were injected at 50 ng/μL (AIY), 15 ng/μL (RIB), 35 ng/μL (RIG) or 35 ng/μL (RIA), along with the coinjection marker *myo-2::dsRed* (10 ng/μL), using standard microinjection techniques. Stable transgenic lines expressing *myo-2::dsRed* were crossed to the following GFP reporter strains to confirm loss of the respective interneurons: OH99 (AIY), EAH242 (RIB), EAH269 (RIG), and IK716 (RIA).

QUANTIFICATION AND STATISTICAL ANALYSIS

Statistical analysis was performed using GraphPad Prism 6 using standard significance tests. Significance values were calculated relative to the N2 control, unless otherwise indicated. All statistical details for each experiment can be found in the figure legends. The D'Agostino-Pearson omnibus normality test was used to determine whether values came from a Gaussian distribution; if data were not normally distributed, non-parametric tests were used.

Supplemental Information

A Single Set of Interneurons Drives Opposite Behaviors in *C. elegans*

Manon L. Guillermin, Mayra A. Carrillo, and Elissa A. Hallem

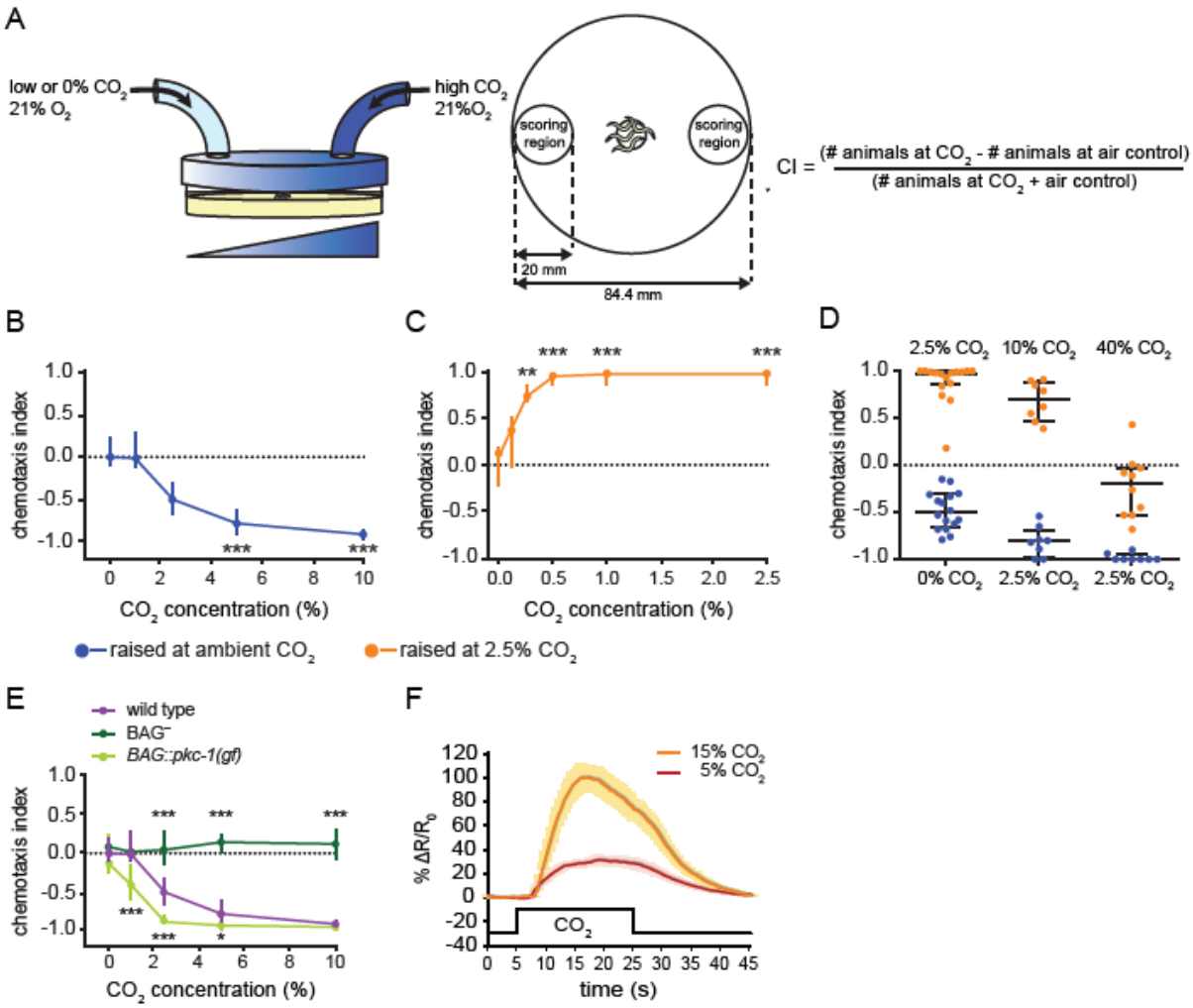

Figure S1. Related to Figure 1. CO_2 response in *C. elegans* is experience-dependent. (A) Schematic of the chemotaxis assay. Animals were placed in the center of a 100-mm agar plate (84.4-mm inside base diameter). A CO_2 gradient was established by delivering gas stimuli through holes on either side of the plate. At the end of the assay, the number of animals in a 20-mm diameter circle centered under each hole was counted and used to determine the chemotaxis index (CI) according to the formula shown above. (B-C) Animals raised at ambient CO_2 avoid CO_2 across concentrations (B), while animals raised at 2.5% CO_2 are attracted to CO_2 across concentrations (C). $^{**}p<0.01$, $^{***}p<0.001$, Kruskal-Wallis test with Dunn's post-test. For each graph, significance was determined relative to the 0% CO_2 condition. n=8-20 trials per condition. (D) Animals raised at either ambient or high (2.5%) CO_2 were tested in 0-2.5% (left), 2.5-10% (middle), or 2.5-40% (right) CO_2 gradients. Animals grown at ambient CO_2 migrate toward the lower CO_2 concentration. Animals grown at high CO_2 are attracted to the higher CO_2 concentration when tested in a 0-2.5% or 2.5-10% CO_2 gradient, but not when tested in a 2.5-40% CO_2 gradient. n=8-16 trials per condition. (E) BAG activity regulates behavioral sensitivity to CO_2. In animals raised at ambient CO_2, genetic ablation of the BAG neurons (BAG^-) eliminates CO_2 avoidance across concentrations. By contrast, animals with more active BAG neurons due to BAG-specific expression of *pkc-1(gf)* show enhanced CO_2 avoidance. $^{*}p<0.05$, $^{***}p<0.001$, two-way ANOVA with Dunnett's post-test. n=8-16 trials per condition. For B-E, graphs depict medians with interquartile ranges. (F) The BAG response to CO_2 is concentration-dependent. Graph shows the calcium responses of BAG neurons to 15% CO_2 (orange) or 5% CO_2 (red), for animals raised at high (2.5%) CO_2, measured using the ratiometric calcium indicator yellow cameleon YC3.60. Solid lines indicate average calcium responses; shading represents SEM. Black line indicates the CO_2 pulse.

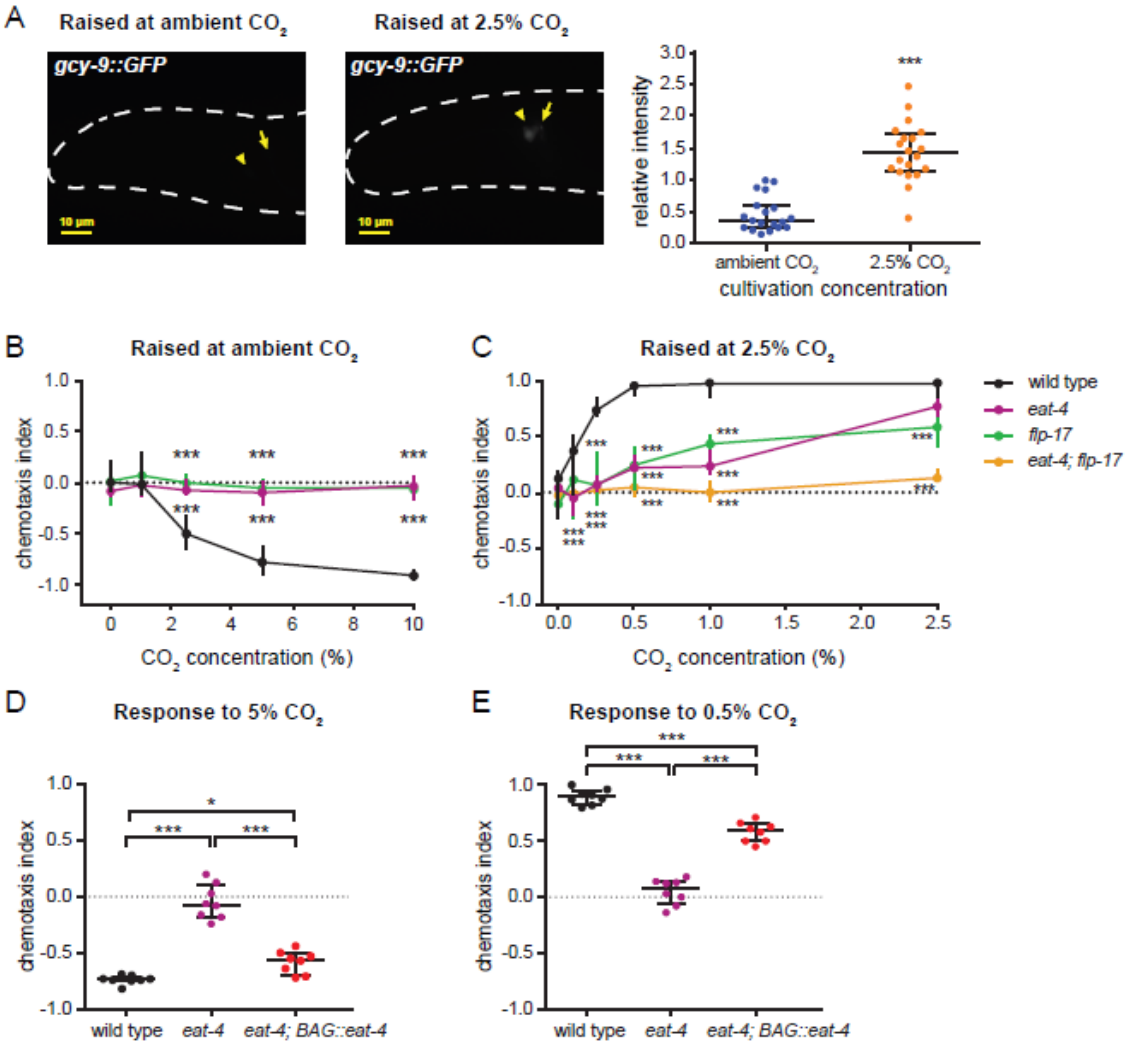

Figure S2. Related to Figure 1. BAG neurons mediate both attractive and aversive CO_2 responses. (A) Epifluorescence images of *gcy-9* expression in the BAG neurons of L4 animals raised at ambient CO_2 (left) or high (2.5%) CO_2 (middle). *gcy-9* expression was measured in animals containing a *gcy-9::GFP* transgene. Arrowheads indicate the location of the BAG neuron cell body; arrows indicate the location of the nerve ring. Anterior is to the left; dorsal is up. GFP expression is faint but detectable in animals raised at ambient CO_2, and brighter in animals raised at high CO_2. Graph (right) shows the relative intensity of expression of the *gcy-9::GFP* transgene in animals raised at ambient vs. high CO_2. ***p<0.001, unpaired t test. n=19-20 animals per condition. (B-C) *eat-4* and *flp-17* are required for normal CO_2 response. (B) Mutation of *eat-4* or *flp-17* abolishes CO_2 avoidance in animals raised at ambient CO_2. ***p<0.001, two-way ANOVA with Dunnett's post-test. n=6-16 trials per genotype and condition. (C) Mutation of either *eat-4* or *flp-17* reduces CO_2 attraction, and mutation of both genes abolishes CO_2 attraction, in animals raised at high (2.5%) CO_2. ***p<0.001, two-way ANOVA with Dunnett's post-test. n=8-26 trials per genotype and condition. (D-E) *eat-4* acts in the BAG neurons to mediate CO_2 avoidance and CO_2 attraction. Restoring *eat-4* expression specifically in the BAG neurons of *eat-4* mutants partially restores CO_2 avoidance (D) and attraction (E). Animals were raised at ambient CO_2 (D) or 2.5% CO_2 (E) and tested for their response to 5% CO_2 or 0.5% CO_2, respectively. *p<0.05, ***p<0.001, one-way ANOVA with Sidak's post-test. n=8 trials per genotype and condition. For A-E, graphs show medians with interquartile ranges.

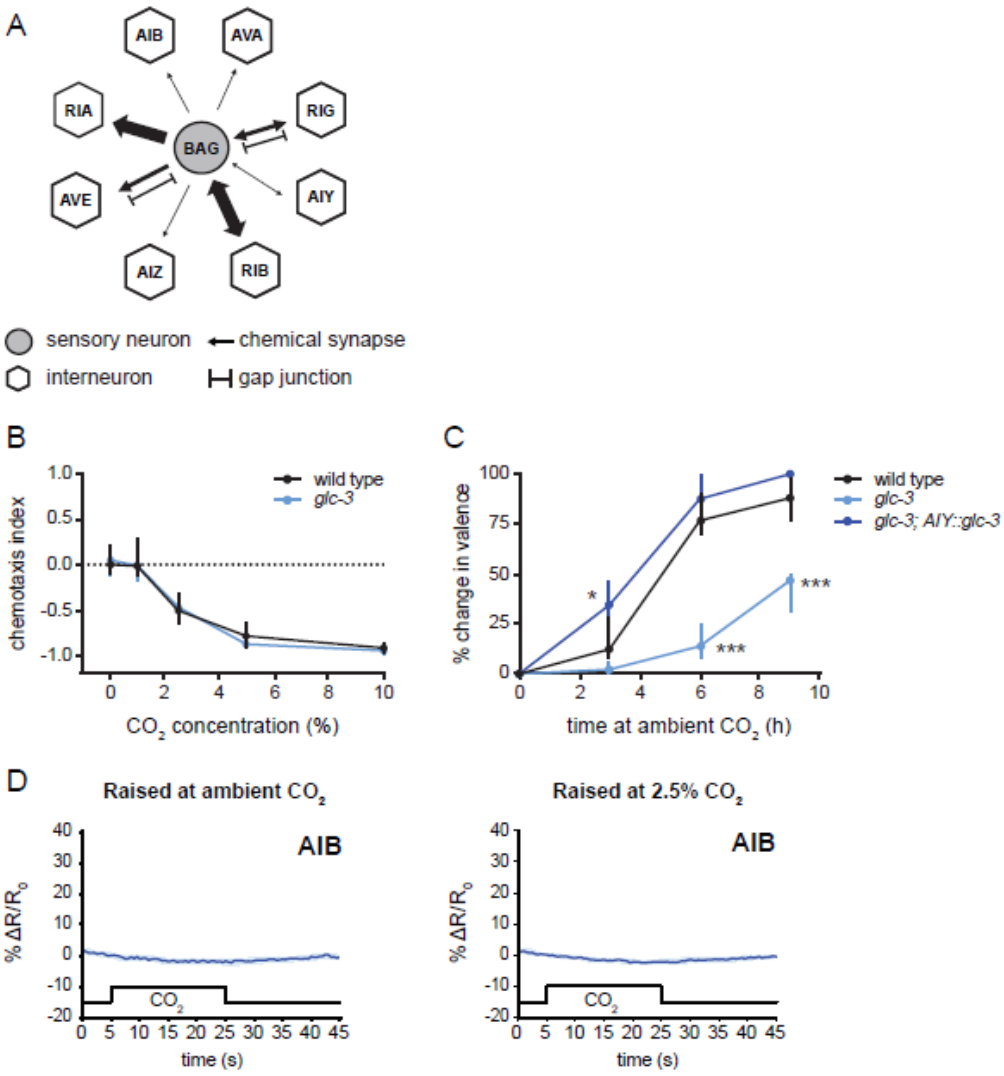

Figure S3. Related to Figure 2, Figure 3 and Figure 4. Distinct interneurons regulate CO_2 avoidance and attraction. (A) Structural connectivity of the CO_2-detecting BAG neurons. Arrow thickness reflects the number of synaptic connections (1-2 synapses, 4-7 synapses, or 10+ synapses) from BAG to the downstream interneurons [S1, S2]. The interneurons shown have documented functions in other chemosensory microcircuits and were therefore investigated in this study. The BAG sensory neurons are also presynaptic to several other interneurons not shown. (B) *glc-3* mutants show normal CO_2 avoidance when raised at ambient CO_2. (C) *glc-3* mutants show a delayed shift from CO_2 attraction to avoidance when raised at high (2.5%) CO_2 and transferred to ambient CO_2. Restoring *glc-3* function specifically to AIY (*AIY::glc-3*) rescues the shift in CO_2 response valence. Animals were tested for their response to 2.5% CO_2. Graph shows the percent change in valence as a function of time (see Methods). *p<0.05, ***p<0.001, two-way ANOVA with Sidak's post-test (B) or two-way ANOVA with Dunnett's post-test (C). n=8-24 trials per genotype and condition. For B-C, graphs show medians with interquartile ranges. (D) AIB is not activated by CO_2 in animals raised at ambient CO_2 or high (2.5%) CO_2. n=8 animals per genotype and condition. Calcium responses were measured using the ratiometric calcium indicator yellow cameleon YC3.60. Graphs show composite calcium responses to a 20-s pulse of 15% CO_2. Solid lines indicate average calcium responses; shading represents SEM.

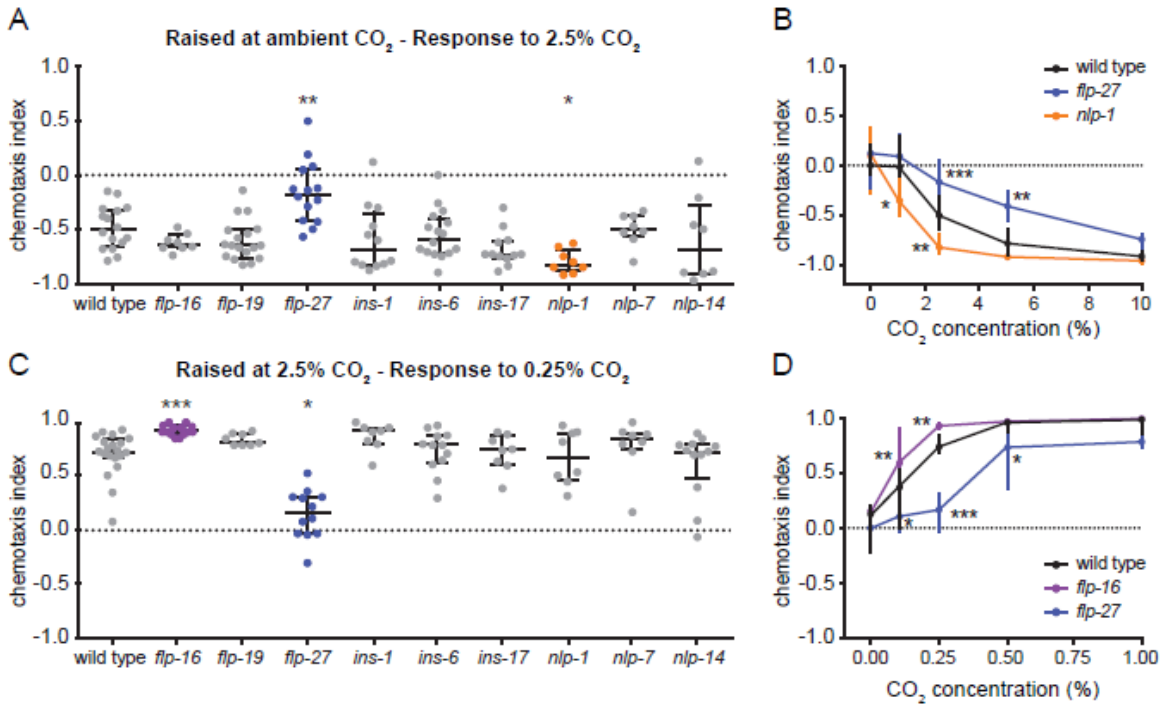

Figure S4. Related to Figure 4. A combinatorial code of neuropeptides regulates CO_2 response valence and sensitivity. (A-B) In animals raised at ambient CO_2, *flp-27* mutants show reduced CO_2 avoidance and *nlp-1* mutants show enhanced CO_2 avoidance. Graphs show responses to 2.5% CO_2 (A) or across CO_2 concentrations (B). *p<0.05, **p<0.01, ***p<0.001, one-way ANOVA with Dunnett's post-test (A) or two-way ANOVA with Dunnett's post-test (B). n=8-18 trials per genotype and condition. (C-D) In animals raised at high (2.5%) CO_2, *flp-16* mutants show enhanced CO_2 attraction and *flp-27* mutants show reduced attraction. Graphs show responses to 0.25% CO_2 (C) or across CO_2 concentrations (D). *p<0.05, **p<0.01, ***p<0.001, Kruskal-Wallis test with Dunn's post-test (C) or two-way ANOVA with Dunnett's post-test (D). n=6-20 trials per genotype and condition. For A-D, graphs show medians and interquartile ranges.

Supplemental References

S1. White, J.G., Southgate, E., Thomson, J.N., and Brenner, S. (1986). The structure of the nervous system of the nematode *Caenorhabditis elegans.* Philos. Trans. R. Soc. Lond. B. Biol. Sci. *314*, 1-340.

S2. Xu, M., Jarrell, T.A., Wang, Y., Cook, S.J., Hall, D.H., and Emmons, S.W. (2013). Computer assisted assembly of connectomes from electron micrographs: application to *Caenorhabditis elegans.* PLoS One *8*, 1-6.

Chapter 4: Conclusions and future work

Tailoring behavioral choice to changing environmental conditions is essential to survival. Behavioral adaptations arise in part from the flexibility of individual neural microcircuits. Over the course of these studies, we have investigated the fundamental mechanisms that drive neural microcircuit reconfiguration, and lead to the generation of context-appropriate functional outputs. For *C. elegans*, we have demonstrated that the CO_2 circuit is dynamically regulated to reflect the complex nature of this chemosensory cue, resulting in many possible behavioral outcomes. In the CO_2 circuit, context and experience are integrated to interpret the ethological significance of CO_2 at any given time, and drive appropriate behavioral choices. We have elucidated a flexible microcircuit that is capable of driving both attraction and avoidance behaviors in response to CO_2. Our circuit model proposes that the same sensory neuron and interneuron connections produce alternative circuit configurations that generate different behavioral outcomes in response to different environmental conditions.

In the microenvironment of fallen rotting fruit, where *C. elegans* is typically found, CO_2 concentrations are highly variable. Although the level of atmospheric CO_2 is only 0.038% (Scott, 2011), in these environments CO_2 levels can rise above 10% (Burg and Burg, 1965). We have found that *C. elegans* retains a memory of the environmental CO_2 levels to which it has been exposed and reacts to CO_2 gradients accordingly. Animals cultivated at ambient CO_2 are repelled by CO_2, while animals cultivated at high CO_2 are attracted to CO_2. CO_2 response valence is flexible and can change over the course of a few hours following a change in cultivation conditions. We have linked these ethologically relevant changes in behavior to a highly flexible microcircuit that drives both attractive and aversive responses to CO_2. In addition, CO_2 cultivation conditions

affect sensitivity to CO_2: animals cultivated at high CO_2 show enhanced sensitivity to CO_2 relative to animals cultivated at ambient CO_2. Furthermore, the change in sensitivity occurs rapidly, as it takes only 3-6 hours for animals transferred from ambient to high CO_2 to display attraction as robust as animals raised at high CO_2. In contrast, many organisms display reduced sensitivity to an olfactory stimulus (Dalton, 2000) or to CO_2 (Dennis et al., 2016; Sachse et al., 2007) following prolonged exposure, likely due to adaptation. *C. elegans* may respond differently to prolonged CO_2 exposure as a result of the high CO_2 environment it inhabits.

A single microcircuit drives CO_2 attraction and repulsion

We analyzed the functional connectivity between BAG and its downstream interneurons to determine how CO_2 is transformed from a chemosensory cue into multiple behaviors. We examined the neural basis of CO_2 response and found that both CO_2 attraction and repulsion are mediated by a microcircuit consisting of the BAG sensory neurons and four postsynaptic interneuron pairs: AIY, AIZ, RIA, and RIG. Our results suggest that the specific behavioral response to CO_2 is determined by the coordinated activity of the four interneuron types, two of which are capable of showing both CO_2-evoked excitation and CO_2-evoked inhibition. CO_2 avoidance results from activation of RIA and RIG, and inhibition of AIY; in contrast, CO_2 attraction results from activation of AIY, inhibition of RIA, and silencing of RIG. The fourth interneuron pair, AIZ, regulates sensitivity regardless of valence. Thus, CO_2 response occurs via an alternative mechanism of valence determination in which the same interneurons contribute to both attractive and aversive responses through modulation of the sensory neuron to interneuron synapse.

An important proof of concept experiment that remains to be performed is the optogenetic activation (using ChR2), and hyperpolarization (using NpHR), of AIY, RIG and RIA to confirm our cooperative model of interneuron interactions (Kocabas et al., 2012; Kuhara et al., 2011). We expect that attraction behavior will be recapitulated with the photostimulated activation of AIY and hyperpolarization of RIA, while avoidance behavior will be recapitulated by the hyperpolarization of AIY and the activation of RIA and RIG. These results will further confirm the validity of our proposed circuit mechanism.

Over course of this study, however, we observed no cases in which ablation or silencing of a single interneuron pair resulted in complete elimination of CO_2 avoidance or attraction behavior. This suggests that, either, all three interneurons: AIY, RIA and RIG, need to be ablated to eliminate CO_2 response, or that other interneurons may act redundantly or in addition to the interneurons we have highlighted here. The highly interconnected nature of the *C. elegans* nervous system suggests that other interneurons may also contribute to experience-dependent changes in CO_2 response valence. To determine the full complement of interneurons involved in the CO_2 circuit, we will ablate or silence multiple interneurons at a time, and look for interneuron combinations that result in complete loss of avoidance or attractive behavior. For example, we will ablate both RIG and RIA to determine if together they can recapitulate the entire CO_2 avoidance behavior.

Several other sensory neuron pairs show CO_2-evoked activity, and have been implicated in CO_2 sensing (Fenk and de Bono, 2015). This is consistent with other sensory modalities, such as oxygen sensing and thermosensation, whose circuits also

implicate multiple sensory neurons (Aoki and Mori, 2015; Chang et al., 2006). The interneurons downstream of these additional sensory neurons could also be investigated to determine if they regulate CO_2 response behaviors in combination with AIY, RIG and RIA.

In addition, the calcium imaging experiments we have presented here were performed using stationary animals. To better understand how *C. elegans* navigates CO_2 gradients, future experiments will attempt to measure the CO_2-evoked activity of interneurons in freely moving worms, crawling across a CO_2 gradient. Observation of real-time interneuron activity, as the animals moves through different CO_2 concentrations, will enhance our understanding of how the circuit dynamically regulates CO_2 response behaviors.

Distinct interneurons in the CO_2 microcircuit regulate valence and sensitivity

The role of the AIZ interneurons in the CO_2 microcircuit is qualitatively different from those of the AIY, RIA, and RIG interneurons. Whereas AIY, RIA, and RIG regulate valence, AIZ regulates behavioral sensitivity regardless of valence. AIZ also differs from AIY, RIA and RIG in that its CO_2-evoked calcium response is only partly dependent on BAG. This suggests that the AIZ interneurons receive input from additional CO_2-sensing neurons. The AIZ interneurons are postsynaptic to the ASE sensory neurons, and are electrically coupled to the ASH sensory neurons through a gap junction. As described above, several sensory neuron pairs other than BAG have been implicated in CO_2 sensing, including ASE, ASH, AFD, ADL, ASJ, ASK, and AWC (Bretscher et al., 2011; Fenk and de Bono, 2015). These neurons sense other stimuli in addition to CO_2,

including salt, temperature, pheromones, light, and noxious chemicals. *C. elegans* must navigate complex sensory landscapes, and the potential activation of AIZ by multiple sensory neurons suggests that AIZ may serve as a point of integration for interpreting CO_2 in the context of other environmental stimuli. Measuring the CO_2-evoked activity of AIZ in ASE- and ASH-ablated animals will determine if the BAG-independent component of AIZ's CO_2 response is due to ASE or ASH signaling. Based on these results, and what we know about the other sensory modalities regulated by these neurons, we will have a better understanding of the stimuli that AIZ integrates to modulate different sensory behaviors.

In addition, the magnitude of the depolarization in AIZ does not differ under ambient vs. high CO_2 conditions, despite BAG activity being significantly different. These results suggest that AIZ activity may be constrained by gain control mechanisms. Similarly, in mammals, a subset of DA neurons projecting to the NAc lateral shell are modified by both attractive and aversive stimuli and have been proposed to regulate salience (Lammel et al., 2011). In addition, dampening sensory responses may result in increased behavioral variability at the population level, leading to greater probabilities of success in shaping appropriate behaviors. Behavioral variability is an important element in determining efficient behavioral strategies and, ultimately, evolutionary success by ensuring that a proportion of the population survives even under straining circumstances. For example, Gordus et al demonstrated that mechanisms generating behavioral variability in response to a single stimulus already exist within the *C. elegans* nervous system (Gordus et al., 2015). They show that probabilistic behaviors arise in *C. elegans* via the integration of sensory input and network states in the interneuron

layer. They found that the reliability of *C. elegans* response to attractive odors sensed by the AWC sensory neuron depends on the alternative network states shaped by the AIB, RIM and AVA interneurons. In their model, internal network states are a source of variability that increases potential behavioral responses to a single stimulus. In our model, decreased sensitivity to CO_2 may result in increased behavioral variability within the population, resulting in a greater likelihood that some members of the population survive. Since CO_2 is an ambiguous cue for *C. elegans*, able to signal both positive stimuli (food, conspecifics) and negative stimuli (predators, pathogens), it follows that increasing response variability in the population, as oppose to a robust, pre-determined and unique response, may better serve the population by ensuring a portion survives in each case. The sensory dampening produced by the AIZ interneurons in the CO_2 circuit may serve as an additional mechanism promoting circuit-level variability. Mechanistically, the AIZ interneurons may achieve this through interference, as has been described in other networks (Gordus et al., 2015). To test this, we can compare calcium imaging trials of CO_2-evoked activity in AIY, RIG and RIA, in N2 vs AIZ-ablated animals, to determine if loss of AIZ leads to more consistent and reliable responses.

The BAG sensory neurons are unique and versatile

In the CO_2-sensing microcircuit we have presented here, both attraction and aversion to a single stimulus are encoded by sensory input from the same sensory neurons. Our data demonstrates the existence of alternative neural mechanisms that couple a single sensory neuron to opposite behaviors. As a result, the BAG neurons are unusual among *C. elegans* chemosensory neurons in the way they mediate both attractive and

repulsive responses. Many of the other chemosensory neurons promote either attraction or repulsion. The AWA and AWC sensory neurons primarily mediate olfactory attraction, while the AWB, ASH, and ADL sensory neurons primarily mediate olfactory avoidance (Bargmann et al., 1993; Chao et al., 2004; Troemel et al., 1997). Interestingly, although known classically as an attraction olfactory neuron, evidence suggests that the AWC^{ON} sensory neuron can also mediate both attraction and avoidance through separate GCY-28/PKC-1 and DGK-1 pathways (Tsunozaki et al., 2008). The downstream circuitry mediating this particular attraction and avoidance has not yet been elucidated, however further investigation may reveal analogous circuit structure to the CO_2 microcircuit we have described here.

Future investigations will determine how the BAG neurons communicate contextual changes to the downstream circuit. Our data suggests that signaling of these changes occurs downstream of the calcium response. Animals grown at ambient CO_2 or high CO_2 both display robust CO_2-evoked depolarization. Activity-dependent regulation of neuropeptide expression has been demonstrated in BAG, where expression of the neuropeptide FLP-19 is greatly reduced in the absence of the CO_2-sensing pathway (Romanos et al., 2017). These results raise the possibility that the BAG neurons may be releasing different combinations of neuropeptides under different CO_2 conditions. Transcriptional profiling of BAG neurons in animals raised at ambient CO_2 has already been performed (Cao et al., 2017; Hallem et al., 2011b). Those results, combined with transcriptional profiling of BAG in animals raised at high CO_2, will reveal the different neuropeptides expressed under each condition and may provide insight into the molecular mechanisms that enable the BAG neurons to drive opposing behaviors.

Similarities and differences in valence-determining circuit motifs across phyla

The mechanisms used to encode CO_2 response valence are distinct from many other chemosensory stimuli, where valence is determined by competition between two separate and opposing pathways involving distinct sensory inputs (Dulac et al., 2014; Li and Liberles, 2015; Semmelhack and Wang, 2009; Wasserman et al., 2013; Yoshida et al., 2012). Valence determination for many chemosensory stimuli is concentration-dependent such that high stimulus concentrations activate an aversive pathway that overrides the low-stimulus-concentration-induced appetitive pathway (Mills et al., 2011; Wragg et al., 2007; Yoshida et al., 2012). *D. melanogaster* is attracted to low concentrations of apple cider vinegar but repelled by high concentrations, a change that is mediated by the recruitment of a low affinity odorant receptor at high concentrations (Semmelhack and Wang, 2009). Attraction to low concentrations of apple cider vinegar in flies is mediated by the Or42b and Or92a olfactory receptors, which innervate the VA2 and DM1 glomeruli, while aversion to high concentrations of apple cider vinegar requires the recruitment of an additional low affinity receptor, Or85a, and the activation of an additional glomerulus, DM5 (Semmelhack and Wang, 2009). This example highlights an important difference between the circuit mechanism we have presented here, and other reported neural mechanisms for valence determination. In contrast to the *D. melanogaster* circuit, where the activation of Or85a and DM5 overrides the activity of VA2 and DM1, leading to avoidance, the AIY, RIA and RIG interneurons exhibit coordinated activity to drive attraction and avoidance behaviors. In addition, the example above describes concentration-dependent changes in apple cider vinegar

response valence, whereas CO_2 response valence in *C. elegans* is consistent across a wide range of concentrations. Furthermore, evidence has shown that projections from individual glomeruli associated with odor attraction and aversion target topographically distinct regions of the lateral horn, suggesting valence is encoded in segregated areas of the nervous system (Li and Liberles, 2015). This contrasts with our study, which describes a circuit mechanism whereby valence is encoded by the coordinated activity of the same set of interneurons.

The activity of the RIA interneurons is similar to the pattern of activity seen in certain mushroom body output neurons in *D. melanogaster* (Owald et al., 2015). Odor detection in *D. melanogaster* is mediated by OSNs found in antennae and maxillary palps, whose axons project to unique glomeruli, and whose activity is relayed to excitatory and inhibitory projection neurons. These projection neurons transmit odor information to neurons in the mushroom body and lateral horn. In the mushroom body, Kenyon cells converge onto downstream output neurons. Similar to ablation of the RIA interneurons, specific inhibition of the glutamatergic mushroom body output neurons M4β/MBON-β2β'2a, M4β'/MBON- β'2mp and M6/MBON-γ5 β'2a transforms avoidance to attraction. In addition, activation of M4β/MBON-β2β'2a, M4β'/MBON- β'2mp and M6/MBON-γ5 β'2a drives avoidance behavior. Furthermore, inhibition of the mushroom body output neurons MB-V2α/MBON-α2sc, MB-V2α'/MBON-α'3, and MB-V3/MBON-α3 has no effect on odor avoidance behavior, suggesting functional specificity of M4β/MBON-β2β'2a, M4β'/MBON- β'2mp and M6/MBON-γ5 β'2a's avoidance-promoting activity. Although specific odor-attraction and odor-avoidance sensory neurons have already been demonstrated in *C. elegans*, the existence of similar avoidance-specific downstream

neurons in *C. elegans* and *D. melanogaster* suggests that valence-deterministic neurons may be conserved across phyla. However, an important distinction between these two circuit motifs must be highlighted. In our study of the *C. elegans* CO_2 circuit, we have been investigating a sensory stimulus with an innate valence, whereas the *D. melanogaster* study looked at a learned association and a conditioned stimulus with an otherwise neutral odor.

Our data reveal a model in which opposing behaviors are generated from a single set of interneurons, and determined by the combined context-dependent activity of these interneurons. This contrasts with examples in which behaviors of opposing valence are mediated by separate circuits. In mammals, evidence has demonstrated that similar neuron subtypes, but distinct neuronal populations in the mammalian nucleus accumbens (NAc) can regulate opposing behaviors (Al-hasani et al., 2015). Activating dynorphin-expressing neurons in the ventral NAc shell results in kappa opioid receptor (KOR)-dependent aversive behaviors, while activating dynorphin-expressing neurons in the dorsal NAc shell results in KOR-dependent reward-seeking behavior. Additionally, attractive and aversive behaviors are both regulated by postsynaptic KORs, which suggests that discrete subpopulations of KOR-expressing cells also mediate opposing valence through topographic and functional specificity. Reports have also revealed distinct subpopulations of dopaminergic (DA) neurons that mediate attractive and aversive behaviors (Matsumoto and Hikosaka, 2009). One study showed selective modification of excitatory synapses in a population of DA neurons projecting to the NAc medial shell by the administration of appetitive stimulus such as cocaine, while an aversive stimulus results in the modification of synapses of DA neurons projecting to the

medial prefrontal cortex, suggesting that distinct population of DA neurons are regulated by opposing stimuli (Lammel et al., 2011). In these examples, similar neuron subtypes, but distinct neuronal populations, regulate opposing behaviors. This differs from our circuit model, in which the same population of interneurons regulates opposing behaviors.

In the CO_2 circuit we have described, the ultimate behavioral outcome is dependent on the interneurons' combined activity states. In other words, the activity state, whether depolarized or hyperpolarized, of each interneuron is critical to specify the appropriate CO_2 response. In mammals and other organisms, it remains to be seen whether behavioral outcomes regulated by the neuronal subpopulations described above are the result of separate or coordinated activity. In *D. melanogaster,* investigation into the neural basis of mate recognition suggests that this mechanism, whereby a net balance of neuronal activity generates specific behavioral outcomes, could be conserved. In male flies, mate recognition and discrimination begins by extending a foreleg and tapping a target fly's abdomen to inspect gustatory pheromones. Subsequent entry into courtship behavior is gated by olfactory and gustatory pheromones which activate excitatory and inhibitory neural pathways and converge onto the male P1 neurons. Initiation of courtship behavior is determined by the resulting net balance between excitatory and inhibitory activity. Female pheromones, which drive courtship, tend to induce net excitation, while male pheromones, which suppress courtship, tend to induce net inhibition. However, the P1 neurons integrate both pathways to discriminate between many varieties of target flies using the olfactory and gustatory spectrums (Clowney et al., 2015). While the mechanism described here, whereby a net balance of

neuronal activity regulates final behavioral outcome, may be similar to the *C. elegans* circuit we present, courtship initiation in *D. melanogaster* is still determined by the convergence two separate excitatory and inhibitory circuits, with input from distinct sensory neurons, while CO_2 response is determined by a unique sensory neuron and a single circuit comprised of neurons that are not exclusively excitatory or inhibitory, but whose individual excitatory and inhibitory activities shape the final behavior.

Context-dependent modulation of CO_2

We have demonstrated that CO_2 response in *C. elegans* is both experience-dependent, based on recently experience CO_2 environments, and context-dependent, based on neuromodulatory state and immediate O_2 environment. Like *C. elegans*, context-dependent modulation of CO_2 responses also occurs in other organisms. CO_2 avoidance by *D. melanogaster* and CO_2 attraction by the mosquito *Aedes aegypti* are reduced in the presence of food odorants through direct inhibition of CO_2-detecting sensory neurons (Turner et al., 2011; Turner and Ray, 2009). In *D. melanogaster*, CO_2 avoidance is attenuated by food odors through a mechanism in which the pathway mediating the response to food odors and the pathway mediating CO_2 response converge in the mushroom body (Bräcker et al., 2013; Lewis et al., 2015). CO_2 response by *C. elegans* can also be modulated by other sensory stimuli, including O_2 and temperature; however, the circuit mechanisms that mediate these effects are not yet clear (Carrillo et al., 2013; Kodama-Namba et al., 2013). Future investigations will have to determine how extensive multisensory integration informs CO_2 response behaviors.

Distinct circuit mechanisms fine-tune representations of CO_2

In *D. melanogaster*, avoidance of low and high concentrations of CO_2 is regulated by two distinct second-order projection neuron (PN) pathways (Lin et al., 2013). Low concentrations of CO_2 activate the PN_v-1 pathway, whereas high concentrations of CO_2 activate the PN_v-2 and PN_v-3 pathways, which are also thought to inhibit PN_v-1 pathway-mediated avoidance. This suggests that olfactory stimuli can be modulated by context, and significance interpreted more accurately by channeling a sensory input into distinct neural pathways. It would be interesting to examine whether this holds true for *C. elegans* as well.

Molecular determinants of CO_2 response valence

Neuropeptides are widely used across phyla to generate rapid, context-dependent changes in behavior (Marder, 2012; Marder et al., 2014). Extensive work has demonstrated the power of neuromodulators and neuropeptides to increase computational power by reconfiguring neural circuits, leading to flexible behaviors (Bucher and Marder, 2013; Chen et al., 2013; Harris et al., 2010; Savigner et al., 2009). Context- and state-dependent patterns of neuromodulator release confer functional flexibility to fixed circuits. The extrasynaptic modulatory network adds a level of complexity to the anatomically defined wiring diagram which expands our understanding of the mechanisms underlying behavioral plasticity. In *C. elegans,* neuromodulation via the NPR-1 receptor can lead to significantly divergent social and pheromone-driven behaviors (Macosko et al., 2009). Neuromodulators can modify neural circuit output in

several ways. They can affect synapse strength and sign through use-dependent changes in synaptic strength (Bucher and Marder, 2013), by altering activity through increasing or decreasing the strength of ionic currents, eliminating or activating specific currents, or changing the voltage- and time- dependence of channel gating (Kaczmarek and Levitan, 1986). They can affect multiple subcellular targets with opposing action (i.e., they can activate both inward and outward currents at the same time), and alter action potential shape and firing rate (Chalasani et al., 2010; Jang et al., 2012; Nadim and Bucher, 2014; Tsunozaki et al., 2008). In addition, depending on the network state, the same neuromodulator can have opposite effects on synapse strength (Cai et al., 2002; Gu and Yan, 2004; Sakurai and Katz, 2009). Neuromodulators can affect multiple different ion channels, and ion channels can be affected by multiple neuromodulators (Bucher and Marder, 2013). The action of different neuromodulators, or a single neuromodulator, on the same ion channel, can result in different signs in different neurons. This has been demonstrated in the crab stomatogastric ganglion (STG) where individual neurons, shaped by sensory activation and the neuromodulatory environment, can change functional roles between the pyloric and gastric rhythms (Weimann and Marder, 1994). In the crab STG, all pyloric neurons have dopamine (DA) receptors. In each neuron, DA modulates a cell-specific combination of ion currents, with the net response reflecting the sum of these effects. This results in inhibition of the PD and VD neurons, and excitation of the AB, PY and LP neurons (Harris-Warrick and Johnson, 2010). In addition, every synapse in the network is affected by DA, with some increased and some decreased in strength. In these circuits, DA changes the synaptic strength and dynamics.

In vertebrates as well as invertebrates, serotonin (5-HT) results in increased excitability. In the sea slug *Aplysia californica*, release of 5-HT facilitates L-glutamate-evoked excitatory currents by activating protein kinase A (PKA)- and protein kinase C (PKC)-induced signaling. This reduces presynaptic potassium current and results in increased tail sensory neuron excitability, with the result that tail sensory neuron to motorneuron transmission is also increased (Glanzman, 2008; Kempsell and Fieber, 2015; Villareal et al., 2009). Similarly, in the crab STG, 5-HT alters the firing properties of several neurons. 5-HT enables the DG neuron to generate plateau potentials triggered by cholinergic depolarization and enhances bursting in the AB/PD neuron group (Katz, 1998). In mammals as well, 5-HT has been shown to increase excitability of motorneurons by increasing inward currents and decreasing outward currents (Perrier et al., 2013). In addition, 5-HT agonists have been shown to significantly increase long-lasting reflexes associated with persistent calcium currents (Murray et al., 2011).

Neuromodulators have also been shown to enhance excitatory postsynaptic potential (EPSPs) by increasing voltage-gated inward currents. In spinal cord injuries, persistent calcium currents are facilitated by the action of norepinephrine on α-adrenergic receptors, leading to increased EPSPs (Rank et al., 2011). In contrast, FMRFamides have been shown to decrease excitability, leading to synaptic depression (Schacher et al., 1990; Sun et al., 1996). Similarly, in the *D. melanogaster* antennal lobe, tachykinins (DTKs) released by local interneurons suppress presynaptic calcium and synaptic transmission in OSNs (Ignell et al., 2009). In addition, both synaptic potentiation and depression have been observed upon activation of dopaminergic neurons in *D. melanogaster* (Cohn et al., 2015).

Neuromodulators can also exert presynaptic modulation: they alter the properties of vesicular release by targeting presynaptic Ca^{2+} influx, proteins in the active zone, and the size of the reserve pool (Higley and Sabatini, 2010; Logsdon et al., 2006; Regehr et al., 2009). Postsynaptically, neuromodulators can modify the expression and properties of transmitter receptors to change postsynaptic responses independent of neurotransmitter release (Feng et al., 2001; Sun et al., 2005).The broadest category of neuromodulation, referred to as 'metamodulation', concerns the modulation of neuromodulators themselves (Mesce, 2002; Ribeiro and Sebastião, 2010). This is exemplified by nitric oxide, which can modify the modulatory actions of glutamate and serotonin (Pinard and Robitaille, 2008).

As described above, neuromodulators affect circuit function in a myriad of ways, and allow small circuits to maximize their adaptive behavioral outcomes. The *C. elegans* genome encodes over 200 neuropeptides (Harris et al., 2010), suggesting that the potential for neuromodulation is considerable. The ability of the CO_2-sensing microcircuit to elicit opposite behaviors suggests that the neuromodulatory environment is a key player in coupling this circuit to divergent behaviors. It is plausible that CO_2-evoked, BAG-specific signals to AIY, AIZ, RIA and RIG are regulated by the neuromodulatory environment, which tunes the CO_2 circuit properties to produce appropriate behavioral responses.

The ability of the BAG neurons to mediate both attractive and repulsive responses could involve changes in the neurotransmitter and/or neuropeptide content secreted by BAG; changes in receptor expression or function in AIY, RIA, and RIG; and/or changes in neuromodulatory input from other regulatory neurons. Our screen of BAG-enriched

neuropeptides revealed a set of functionally diverse neuropeptides that affect CO_2 response valence and sensitivity. Our data demonstrate that BAG mediates both CO_2 avoidance and attraction via neuropeptide and glutamate signaling. In addition, following a shift from high to ambient CO_2 conditions, the inhibitory glutamate-gated chloride channel subunit GLC-3 is required in AIY to promote CO_2 repulsion. However, *glc-3* is not required for CO_2 avoidance in animals maintained at ambient CO_2, suggesting the involvement of other inhibitory receptors in AIY. Transcriptional profiling of AIY in animals raised at ambient CO_2 could identify potential inhibitory receptors that modulate AIY activity at ambient CO_2.

In addition to FLP-17, we identified three BAG-enriched neuropeptides that regulate CO_2 response. The neuropeptide-like protein NLP-1 reduces avoidance, and the FMRFamide-like neuropeptide FLP-16 reduces attraction. Additionally, both attraction and avoidance are enhanced by the FMRFamide-like neuropeptide FLP-27.

We note that NLP-1 is expressed in sensory neurons other than BAG (Chalasani et al., 2010), and the expression patterns of FLP-16 and FLP-27 are poorly characterized (Li and Kim, 2008). The mechanisms by which these neuropeptides act on the CO_2 circuit remain to be elucidated, and their sites of action have not been determined. They may act in a number of ways, including direct action via target neuropeptide receptors, or through modulatory action on the synapses between the BAG sensory neurons and the AIY, AIZ, RIA and RIG interneurons. Although NLP-1, FLP-16 and FLP-27 are enriched in BAG, we cannot exclude the possibility that these neuropeptides modulate valence and sensitivity via neurons other than BAG to generate flexible CO_2-evoked behaviors. Interestingly, our observations regarding neuropeptide action in the CO_2 circuit parallel

the patterns of activity we observe in the interneurons. As observed for first-order interneurons, some neuropeptides regulate CO_2 avoidance, some regulate CO_2 attraction, and some regulate sensitivity regardless of valence. We can determine if NLP-1, FLP-16 and FLP-27 act on the CO_2 circuit via the BAG neurons, by rescuing neuropeptide expression specifically in BAG and testing CO_2 response behaviors.

Although our results raise the possibility that BAG secretes different combinations of neuropeptides in animals raised at ambient vs. high CO_2 to generate context-dependent interneuron responses and CO_2-evoked behaviors, both excitatory and inhibitory glutamatergic signaling has been well-documented in *C. elegans*. For example, in the *C. elegans* olfactory microcircuit, glutamate inhibits AIY via the glutamate-gated chloride channel GLC-3, but excites AIB via the AMPA-type ionotropic glutamate receptor GLR-1 (Piggott et al., 2011). Furthermore, excitatory and inhibitory glutamate signaling has been shown to act on the same neuron to mediate opposing behaviors. In the neural circuit that regulates temperature-seeking behavior in *C. elegans*, opposing behaviors are both regulated by glutamatergic input to AIY: glutamatergic transmission from AFD inhibits AIY through GLC-3, leading to cryophilic movement, while glutamatergic transmission from AWC stimulates AIY, leading to thermophilic movement (Kimata et al., 2012). Therefore, it is possible that expression of glutamate receptors in AIY, as well as RIA, may change under low and high CO_2 conditions, resulting in alternating BAG-induced glutamatergic excitation and inhibition. These differential receptor expression patterns could be the result of neuromodulatory action.

Context-dependent modulation of CO_2 microcircuit function could also be achieved through changes in neuropeptide receptor expression in AIY, RIA and RIG. To

determine the molecular mechanisms that drive this unique circuit, we can transcriptionally profile AIY, RIA and RIG in animals raised at ambient CO_2 and high CO_2. First, the resulting data will allow us to identify changes in receptor expression patterns, which may reveal signaling pathways involved in shaping the different activity profiles of each interneuron under both CO_2 conditions. Second, knowing the identity of the involved receptors in each interneuron under both condition may allow us to identify cognate ligands, including neuromodulators, that may be acting on the circuit. Finally, we might be able to identify neurons expressing these newly identified neuromodulators to find additional neurons acting in the CO_2 circuit. Results from transcriptional profiling experiments may also identify glutamate receptors and indicate how glutamatergic signaling is affecting interneuron activity.

Implications for parasitic nematodes

Studying the behavioral response of *C. elegans* to CO_2 has direct implications for parasitic nematodes. Human-parasitic nematodes infect over a billion people worldwide and cause extensive morbidity, while parasitic nematodes of livestock and crops result in billions of dollars in damages each year (Gang and Hallem, 2016; Jasmer et al., 2003). In contrast, entomopathogenic nematodes (EPNs) are beneficial insect-parasitic nematodes that are used as biocontrol agents for insect pests (Gang and Hallem, 2016). Conservation of sensory neuroanatomy and function across nematode species has allowed studies of *C. elegans* neural circuits to inform studies of parasitic nematode neurobiology (Gang and Hallem, 2016). Thus, the mechanisms we have described that regulate CO_2 response in *C. elegans* may lead to new strategies for combating harmful

nematode infections or increasing the biocontrol efficacy of beneficial nematodes by targeting the CO_2 microcircuit.

Many parasitic nematodes use CO_2 as a host-seeking cue. In EPNs, CO_2 acts in combination with insect odors to act as a host cue (Castelletto et al., 2014; Dillman et al., 2012). The BAG neurons are required for CO_2 response in parasitic nematodes as well as *C. elegans* (Hallem et al., 2011a). In addition, context-dependent changes in CO_2 response valence occur in some parasitic nematodes (Lee et al., 2016). Due to the conserved positional neuroanatomy shared between nematode species, studies of CO_2-sensing in parasitic nematodes are directly informed by understanding the neural basis for CO_2 behavior in *C. elegans*. Evidence has already demonstrated conserved elements of the CO_2-sensing circuit among free-living and parasitic nematode species. In the EPNs *Steinernema carpocapsae* and *Heterorhabditis bacteriophora*, BAG sensory neurons mediate CO_2 chemotaxis, as well as CO_2-evoked jumping in *S. carpocapsae* (Hallem et al., 2011a). Studies examining salt chemotaxis and thermotaxis in mammalian-parasitic nematodes have also demonstrated that sensory neuron function appears to be broadly conserved in free-living and parasitic nematodes species (Gang and Hallem, 2016). Furthermore, the role of RIA in thermotaxis in both *C. elegans* and *H. contortus* suggests that interneuron function could be conserved as well (Gang and Hallem, 2016; Li et al., 2000). Disrupting host-seeking behavior could be a powerful method of preventing devastating infections. The detailed CO_2 circuit we present here can be used as a guide in elucidating and target the CO_2-sensing circuit in parasitic nematodes.

A novel circuit for encoding behavioral flexibility

Our results illuminate a novel circuit mechanism whereby a single set of interneurons is modulated to generate opposite ethologically relevant behavioral responses to a single chemosensory stimulus. We have shown that both attractive and repulsive responses of *C. elegans* to CO_2 are mediated by the same sensory neuron and set of downstream interneurons. The response properties of the attraction- and avoidance-promoting interneurons are flexible and subject to context-dependent modulation. Moreover, the activity states of these interneurons form a combinatorial code from which a spectrum of CO_2-evoked behaviors can emerge. Valence-encoding interneurons also exist in insects and mammals (Gore et al., 2015; Knaden and Hansson, 2014; Li and Liberles, 2015; Root et al., 2014), but how these neurons respond to context-dependent changes in the inherent valence of a chemosensory stimulus remains poorly understood. The finding that valence-encoding interneurons in *C. elegans* can drive opposite responses to the same chemosensory stimulus raises the possibility that similar circuit motifs operate in higher organisms to generate rapid, context-dependent valence changes. Further investigation will have to address the molecular mechanisms that allow context to reconfigure the CO_2 circuit and generate the alternative circuit states we see, and how the CO_2-circuit engages with other sensory circuits to reveal an accurate portrait of the sensory landscape. We have presented a single motif here; however, future work will have to investigate the different types of circuit motifs employed by the nervous system to encode flexibility and adaptability.

References

Al-hasani, R., Mccall, J.G., Shin, G., Gomez, A.M., Gavin, P., Bernardi, J.M., Pyo, C., Park, S. Il, Marcinkiewcz, C.M., Crowley, N.A., Krashes, M.J., Lowell, B.B., Kash, T.L., John, A., Bruchas, M.R., 2015. Distinct Subpopulations of Nucleus Accumbens Dynorphin Neurons Drive Aversion and Reward. *Neuron* 87, 1063–1077.

Anderson, J.F., Ultsch, G.R., 1987. Respiratory gas concentrations in the microhabitats of some florida arthropods. *Comp. Biochem. Physio.* 88, 585–588.

Aoki, I., Mori, I., 2015. Molecular biology of thermosensory transduction in *C . elegans*. *Curr. Opin. Neurobiol.* 34, 117–124.

Bargmann, C.I., 2012. Beyond the connectome: how neuromodulators shape neural circuits. *BioEssays* 34, 458–65.

Bargmann, C.I., Hartwieg, E., Horvitz, H.R., 1993. Odorant-selective genes and neurons mediate olfaction in *C. elegans*. *Cell* 74, 515–527.

Bargmann, C.I., Horvitz, H.R., 1991. Chemosensory neurons with overlapping functions direct chemotaxis to multiple chemicals in *C. elegans*. *Neuron* 7, 729–742.

Barrière, A., Félix, M.A., 2005. High local genetic diversity and low outcrossing rate in *Caenorhabditis elegans* natural populations. *Curr. Biol.* 15, 1176–1184.

Ben Arous, J., Tanizawa, Y., Rabinowitch, I., Chatenay, D., Schafer, W.R., 2010. Automated imaging of neuronal activity in freely behaving *Caenorhabditis elegans*. *J. Neurosci. Methods* 187, 229–234.

Bensafi, M., Iannilli, E., Gerber, J., Hummel, T., 2008. Neural coding of stimulus concentration in the human olfactory and intranasal trigeminal systems. *Neuroscience* 154, 832–838.

Bentley, B., Branicky, R., Barnes, C.L., Bullmore, E.T., Vértes, P.E., Schafer, W.R., 2016. The multilayer connectome of *Caenorhabditis elegans*. *PLoS Comput. Biol.* 1–31. doi: 10.1371/journal.pcbi.1005283

Benton, A.H., Lee, S.Y., 1965. Sensory Reactions of Siphonaptera in Relation to Host-Finding. *Am. Midl. Nat.* 74, 119–125.

Bräcker, L.B., Siju, K.P., Arela, N., So, Y., Hang, M., Hein, I., Vasconcelos, M.L., Grunwald Kadow, I.C., 2013. Essential role of the mushroom body in context-dependent CO_2 avoidance in *Drosophila*. *Curr. Biol.* 23, 1228–1234.

Brandt, J.P., Ringstad, N., 2015. Toll-like Receptor Signaling Promotes Development and Function of Sensory Neurons Required for a *C. elegans* Pathogen-Avoidance Behavior. *Curr. Biol.* 25, 2228–2237.

Bretscher, A.J., Busch, K.E., de Bono, M., 2008. A carbon dioxide avoidance behavior is integrated with responses to ambient oxygen and food in *Caenorhabditis*

elegans. *Proc. Natl. Acad. Sci. U. S. A.* 105, 8044–9.

Bretscher, A.J., Kodama-Namba, E., Busch, K.E., Murphy, R.J., Soltesz, Z., Laurent, P., de Bono, M., 2011. Temperature, oxygen, and salt-sensing neurons in *C. elegans* are carbon dioxide sensors that control avoidance behavior. *Neuron* 69, 1099–1113.

Bucher, D., Marder, E., 2013. SnapShot: Neuromodulation. *Cell* 155, 482–482.

Burg, S.P., Burg, E.A., 1965. Gas Exchange in Fruits. *Physiol. Plant.* 18, 870–884.

Cai, X., Flores-Hernandez, J., Feng, J., Yan, Z., 2002. Activity-dependent bidirectional regulation of $GABA_A$ receptor channels by the $5\text{-}HT_4$ receptor-mediated signalling in rat prefrontal cortical pyramidal neurons. *J. Physiol.* 540, 743–759.

Cao, J., Packer, J.S., Ramani, V., Cusanovich, D.A., Huynh, C., Daza, R., Qiu, X., Lee, C., Furlan, S.N., Steemers, F.J., Adey, A., Waterston, R.H., Trapnell, C., Shendure, J., 2017. Comprehensive single-cell transcriptional profiling of a multicellular organism. *Science.* 357, 661–667.

Carrillo, M.A., Guillermin, M.L., Rengarajan, S., Okubo, R.P., Hallem, E.A., 2013. O_2-sensing neurons control CO_2 response in *C. elegans*. *J. Neurosci.* 33, 9675–83.

Carrillo, M.A., Hallem, E.A., 2015. Gas Sensing in Nematodes. *Mol. Neurobiol.* 51, 919–931.

Castelletto, M.L., Gang, S.S., Okubo, R.P., Tselikova, A.A., Nolan, T.J., Platzer, E.G., Lok, J.B., Hallem, E.A., 2014. Diverse Host-Seeking Behaviors of Skin-Penetrating Nematodes. *PLoS Pathog.* 10. doi: 10.1371/journal.ppat.1004305

Chalasani, S.H., Kato, S., Albrecht, D.R., Nakagawa, T., Abbott, L.F., Bargmann, C.I., 2010. Neuropeptide feedback modifies odor-evoked dynamics in *Caenorhabditis elegans* olfactory neurons. *Nat. Neurosci.* 13, 615–21.

Chang, A.J., Chronis, N., Karow, D.S., Marletta, M.A., Bargmann, C.I., 2006. A distributed chemosensory circuit for oxygen preference in *C. elegans*. *PLoS Biol.* 4, 1588–1602.

Chao, M.Y., Komatsu, H., Fukuto, H.S., Dionne, H.M., Hart, A.C., 2004. Feeding status and serotonin rapidly and reversibly modulate a *Caenorhabditis elegans* chemosensory circuit. *Proc. Natl. Acad. Sci. U. S. A.* 101, 15512–15517.

Chen, Z., Hendricks, M., Cornils, A., Maier, W., Alcedo, J., Zhang, Y., 2013. Two Insulin-like Peptides Antagonistically Regulate Aversive Olfactory Learning in *C. elegans*. *Neuron* 77, 572–585.

Cheung, B.H.H., Cohen, M., Rogers, C., Albayram, O., De Bono, M., 2005. Experience-dependent modulation of *C. elegans* behavior by ambient oxygen. *Curr. Biol.* 15, 905–917.

Chronis, N., Zimmer, M., Bargmann, C.I., 2007. Microfluidics for in vivo imaging of neuronal and behavioral activity in *Caenorhabditis elegans*. *Nat. Methods* 4, 727–

731.

Clowney, E.J., Iguchi, S., Bussell, J.J., Scheer, E., Ruta, V., 2015. Multimodal Chemosensory Circuits Controlling Male Courtship in *Drosophila*. *Neuron* 87, 1036–1049.

Coates, E.L., Ballam, G.O., 1990. Olfactory receptor response to CO_2 in bullfrogs. *Am. J. Physiol.* 258, R1207-1212.

Cohn, R., Morantte, I., Ruta, V., 2015. Coordinated and Compartmentalized Neuromodulation Shapes Sensory Processing in *Drosophila*. *Cell* 163, 1742–1755.

Dalton, P., 2000. Psychophysical and Behavioral Characteristics of Olfactory Adaptation. *Chem. Senses* 25, 487–492.

Dennis, C.E., Adhikari, S., Wright, A.W., Suski, C.D., 2016. Molecular, behavioral, and performance responses of juvenile largemouth bass acclimated to an elevated carbon dioxide environment. *J. Comp. Physiol.* 186, 297–311.

Dillman, A.R., Guillermin, M.L., Ha, J., Kim, B., Sternberg, P.W., Hallem, E.A., 2012. Olfaction shapes host – parasite interactions in parasitic nematodes. *Proc. Natl. Acad. Sci. U. S. A.* 109, E2324–E2333.

Dirnberger, G., Jahanshahi, M., 2013. Executive dysfunction in Parkinson's disease: A review. *J. Neuropsychol.* 7, 193–224.

Dulac, C., O'Connell, L.A., Wu, Z., 2014. Neural control of maternal and paternal behaviors. Science. 345, 765–770.

Eiras, A., Jepson, P., 1991. Host location by *Aedes aegypti* (Diptera: Culicidae): a wind tunnel study of chemical cues. *Bull. Entomol. Res.* 81, 151–160.

Faumont, S., Lindsay, T.H., Lockery, S.R., 2012. Neuronal microcircuits for decision making in *C. elegans*. *Curr. Opin. Neurobiol.* 22, 580–591.

Félix, M.-A., Braendle, C., 2010. The natural history of *Caenorhabditis elegans*. *Curr. Biol.* 20, R965–R969.

Félix, M.-A., Duveau, F., 2012. Population dynamics and habitat sharing of natural populations of *Caenorhabditis elegans* and *C. briggsae*. *BMC Biol.* doi: 10.1186/1741-7007-10-59.

Feng, J., Cai, X., Zhao, J., Yan, Z., 2001. Serotonin receptors modulate $GABA_A$ receptor channels through activation of anchored protein kinase C in prefrontal cortical neurons . *J Neurosci* 21, 6502–6511.

Fenk, L.A., de Bono, M., 2015. Environmental CO_2 inhibits *Caenorhabditis elegans* egg-laying by modulating olfactory neurons and evokes widespread changes in neural activity. *Proc. Natl. Acad. Sci. U. S. A.* 112, E3525-34.

Gang, S.S., Hallem, E.A., 2016. Mechanisms of host seeking by parasitic nematodes. *Mol. Biochem. Parasitol.* 208, 23–32.

Glanzman, D.L., 2008. New Tricks for an Old Slug: The Critical Role of Postsynaptic Mechanisms in Learning and Memory in *Aplysia*. *Prog Brain Res* 169, 277–292.

Gold, J.M., Waltz, J.A., Prentice, K.J., Morris, S.E., Heerey, E.A., 2008. Reward processing in schizophrenia: A deficit in the representation of value. *Schizophr. Bull.* 34, 835–847.

Gordus, A., Pokala, N., Levy, S., Flavell, S.W., Bargmann, C.I., 2015. Feedback from network states generates variability in a probabilistic olfactory circuit. *Cell* 161, 215–227.

Gore, F., Schwartz, E.C., Brangers, B.C., Aladi, S., Stujenske, J.M., Likhtik, E., Russo, M.J., Gordon, J.A., Salzman, C.D., Axel, R., 2015. Neural Representations of Unconditioned Stimuli in Basolateral Amygdala Mediate Innate and Learned Responses. *Cell* 162, 134–145.

Gu, Z., Yan, Z., 2004. Bidirectional Regulation of Ca^{2+} / Calmodulin-Dependent Protein Kinase II Activity by Dopamine D4 Receptors in Prefrontal Cortex. *Mol Pharmacol.* 66, 948–955.

Guillermin, M.L., Carrillo, M.A., Hallem, E.A., 2017. A Single Set of Interneurons Drives Opposite Report A Single Set of Interneurons Drives Opposite Behaviors in *C . elegans*. *Curr. Biol.* 27, 2630–2639.

Guo, D., Zhang, J.J., Huang, X.Y., 2009. Stimulation of guanylyl cyclase-D by bicarbonate. *Biochemistry* 48, 4417–4422.

Hallem, E.A., Dillman, A.R., Hong, A. V., Zhang, Y., Yano, J.M., Demarco, S.F., Sternberg, P.W., 2011a. A sensory code for host seeking in parasitic nematodes. *Curr. Biol.* 21, 377–383.

Hallem, E.A., Spencer, W.C., McWhirter, R.D., Zeller, G., Henz, S.R., Rätsch, G., Miller, D.M., Horvitz, H.R., Sternberg, P.W., Ringstad, N., 2011b. Receptor-type guanylate cyclase is required for carbon dioxide sensation by *Caenorhabditis elegans*. *Proc. Natl. Acad. Sci. U. S. A.* 108, 254–9.

Hallem, E.A., Sternberg, P.W., 2008. Acute carbon dioxide avoidance in *Caenorhabditis elegans*. *Proc. Natl. Acad. Sci. U. S. A.* 105, 8038–43.

Han, J., Luo, M., 2010. Loss of CO_2 sensing by the olfactory system of CNGA3 knockout mice. *Curr. Zool.* 56, 793–799.

Harris-Warrick, R.M., Johnson, B.R., 2010. Checks and balances in neuromodulation. Front. Behav. *Neurosci.* 4, 1–9.

Harris, G., Mills, H., Wragg, R., Hapiak, V., Castelletto, M., Korchnack, A., Komuniecki, R., 2010. The monoaminergic modulation of sensory-mediated aversive responses in *Caenorhabditis elegans* requires glutamatergic/peptidergic cotransmission. *J. Neurosci.* 30, 7889–7899.

Healy, T.P., Copland, M.J., 1995. Activation of *Anopheles gambiae* mosquitoes by carbon dioxide and human breath. *Med. Vet. Entomol.* 9, 331–6.

Hedgecock, E.M., Russell, R.L., 1975. Normal and mutant thermotaxis in the nematode *Caenorhabditis elegans*. *Proc. Natl. Acad. Sci. U. S. A.* 72, 4061–5.

Higley, M., Sabatini, B., 2010. Competitive regulation of synaptic Ca^{2+} influx by D2 dopamine and A2A adenosine receptors. *Nat. Neurosci.* 13, 958–966.

Hobert, O., 2003. Behavioral plasticity in *C. elegans*: Paradigms, circuits, genes. *J. Neurobiol.* 54, 203–223.

Hodgkin, J., Doniach, T., 1997. Natural variation and copulatory plug formation in *Caenorhabditis elegans*. *Genetics* 146, 149–164.

Hu, J., Zhong, C., Ding, C., Chi, Q., Walz, A., Mombaerts, P., Matsunami, H., Luo, M., 2007. Detection of Near-Atmospheric Concentrations of CO_2 by an Olfactory Subsystem in the Mouse. *Science.* 317, 953–957.

Ignell, R., Root, C.M., Birse, R.T., Wang, J.W., Nässel, D.R., Winther, A.M.E., 2009. Presynaptic peptidergic modulation of olfactory receptor neurons in *Drosophila*. *Proc. Natl. Acad. Sci. U. S. A.* 106, 13070–5.

Jang, H., Kim, K., Neal, S.J., Macosko, E., Kim, D., Butcher, R.A., Zeiger, D.M., Bargmann, C.I., Sengupta, P., 2012. Neuromodulatory State and Sex Specify Alternative Behaviors through Antagonistic Synaptic Pathways in *C. elegans*. *Neuron* 75, 585–592.

Jasmer, D.P., Goverse, A., Smant, G., 2003. Parasitic Nematode Interactions with Mammals and Plants. *Annu. Rev. Phytopathol.* 41, 245–270.

Jones, W., 2013. Olfactory carbon dioxide detection by insects and other animals. *Mol. Cells* 35, 87–92.

Jones, W.D., Cayirlioglu, P., Grunwald Kadow, I., Vosshall, L.B., 2007. Two chemosensory receptors together mediate carbon dioxide detection in *Drosophila*. *Nature* 445, 86–90.

Kaczmarek, L.K., Levitan, I.B., 1986. Neuromodulation: The Biochemical Control of Neuronal Excitability, 1st editio. ed. Oxford University Press.

Katz, P.S., 1998. Comparison of extrinsic and intrinsic neuromodulation in two central pattern generator circuits in invertebrates. *Exp. Physiol.* 83, 281–292.

Kempsell, A.T., Fieber, L., 2015. Age-related deficits in synaptic plasticity rescued by activating PKA or PKC in sensory neurons of *Aplysia californica*. *Front. Aging Neurosci.* 7, 1–9.

Kerr, R.A., Schafer, W.R., 2006. Intracellular Ca^{2+} Imaging in *C. elegans*, in: *Methods Mol Biol.* pp. 253–264.

Kim, K., Li, C., 2004. Expression and Regulation of an FMRFamide-Related Neuropeptide Gene Family in *Caenorhabditis elegans*. *J. Comp. Neurol.* 475, 540–550.

Kimata, T., Sasakura, H., Ohnishi, N., Nishio, N., Mori, I., 2012. Thermotaxis of *C.*

elegans as a model for temperature perception, neural information processing and neural plasticity. *Worm* 1, 31–41.

Kiontke, K.C., Félix, M.-A., Ailion, M., Rockman, M. V, Braendle, C., Pénigault, J.-B., Fitch, D.H., 2011. A phylogeny and molecular barcodes for *Caenorhabditis*, with numerous new species from rotting fruits. *BMC Evol. Biol.* doi: 10.1186/1471-2148-11-339.

Knaden, M., Hansson, B.S., 2014. Mapping odor valence in the brain of flies and mice. Curr. Opin. *Neurobiol.* 24, 34–38.

Kocabas, A., Shen, C.H., Guo, Z.C. V, Ramanathan, S., 2012. Controlling interneuron activity in *Caenorhabditis elegans* to evoke chemotactic behaviour. *Nature* 490, 273–277.

Kodama-Namba, E., Fenk, L.A., Bretscher, A.J., Gross, E., Busch, K.E., de Bono, M., 2013. Cross-Modulation of Homeostatic Responses to Temperature, Oxygen and Carbon Dioxide in *C. elegans*. *PLoS Genet.* 9. doi: 10.1371/journal.pgen.1004011

Kuhara, A., Ohnishi, N., Shimowada, T., Mori, I., 2011. Neural coding in a single sensory neuron controlling opposite seeking behaviours in *Caenorhabditis elegans*. *Nat. Commun.* doi: 10.1038/ncomms1352.

Kuhara, A., Okumura, M., Kimata, T., Tanizawa, Y., Takano, R., Kimura, K.D., Inada, H., Matsumoto, K., Ikue Mori. 2008. Temperature Sensing by an Olfactory Neuron in a Circuit Controlling Behavior of *C. elegans*. *Science* 320, 803–808.

Kunitomo, H., Sato, H., Iwata, R., Satoh, Y., Ohno, H., Yamada, K., Iino, Y., 2013. Concentration memory-dependent synaptic plasticity of a taste circuit regulates salt concentration chemotaxis in *Caenorhabditis elegans*. *Nat. Commun.* 4, 2210.

Kwon, J.Y., Dahanukar, A., Weiss, L.A., Carlson, J.R., 2007. The molecular basis of CO_2 reception in *Drosophila*. *Proc. Natl. Acad. Sci. U. S. A.* 104, 3574–8.

Lahiri, S., Forster, R.E., 2003. CO_2/H^+ sensing: Peripheral and central chemoreception. *Int. J. Biochem. Cell Biol.* 35, 1413–1435.

Lammel, S., Ion, D.I., Roeper, J., Malenka, R.C., 2011. Projection-Specific Modulation of Dopamine Neuron Synapses by Aversive and Rewarding Stimuli. *Neuron* 70, 855–862.

Laurent, P., Soltesz, Z., Nelson, G.M., Chen, C., Arellano-carbajal, F., Levy, E., Bono, M. De, 2015. Decoding a neural circuit controlling global animal state in *C . elegans*. *Elife 1*–32. doi: 10.7554/eLife.04241

Lee, D.L., Atkinson, H.J., 1977. The physiology of nematodes. Columbia Univ Pr, London.

Lee, J.H., Dillman, A.R., Hallem, E.A., 2016. Temperature-dependent changes in the host-seeking behaviors of parasitic nematodes. *BMC Biol.* 14, 36. doi: 10.1186/s12915-016-0259-0

Leifer, A.M., Fang-Yen, C., Gershow, M., Alkema, M.J., Samuel, A.D.T., 2011. Optogenetic manipulation of neural activity in freely moving *Caenorhabditis elegans*. *Nat. Methods* 8, 147–52.

Lewis, L.P.C., Siju, K.P., Aso, Y., Friedrich, A.B., Bulteel, A.J.B., Rubin, G.M., Grunwald Kadow, I.C., 2015. A Higher Brain Circuit for Immediate Integration of Conflicting Sensory Information in *Drosophila*. *Curr. Biol.* 25, 2203–2214.

Li, C., Kim, K., 2008. Neuropeptides. WormBook. http://www.wormbook.org

Li, J., Zhu, X., Boston, R., Ashton, F.T., Gamble, H.R., Schad, G.A., 2000. Thermotaxis and thermosensory neurons in infective larvae of *Haemonchus contortus*, a passively ingested nematode parasite. *J. Comp. Neurol.* 424, 58–73.

Li, Q., Liberles, S.D., 2015. Aversion and attraction through olfaction. *Curr. Biol.* 25, R120–R129.

Lin, H.-H., Chu, L.-A., Fu, T.-F., Dickson, B.J., Chiang, A.-S., 2013. Parallel neural pathways mediate CO_2 avoidance responses in *Drosophila*. *Science* 340, 1338–41.

Logsdon, S., Johnstone, A.F., Viele, K., Cooper, R.L., 2006. Regulation of synaptic vesicles pools within motor nerve terminals during short-term facilitation and neuromodulation. *J. Appl. Physiol.* 100, 662–671.

Luo, M., 2008. The necklace olfactory system in mammals. *J. Neurogenet.* 22, 229–38.

Ma, D.K., Ringstad, N., 2012. The neurobiology of sensing respiratory gases for the control of animal behavior. *Front. Biol.* 7, 246–253.

Macosko, E.Z., Pokala, N., Feinberg, E.H., Chalasani, S.H., Butcher, R.A., Clardy, J., Bargmann, C.I., 2009. A hub-and-spoke circuit drives pheromone attraction and social behaviour in *C. elegans*. *Nature* 458, 1171–5.

Marder, E., 2012. Neuromodulation of Neuronal Circuits: Back to the Future. *Neuron* 76, 1–11.

Marder, E., Leary, T.O., Shruti, S., 2014. Neuromodulation of Circuits with Variable Parameters : Single Neurons and Small Circuits Reveal Principles of State-Dependent and Robust Neuromodulation. *Annu. Rev. Neurosci.* 37, 329–46.

Marella, S., Fischler, W., Kong, P., Asgarian, S., Rueckert, E., Scott, K., 2006. Imaging taste responses in the fly brain reveals a functional map of taste category and behavior. *Neuron* 49, 285–295.

Matsumoto, M., Hikosaka, O., 2009. Two types of dopamine neuron distinctly convey positive and negative motivational signals. *Nature* 459, 837–841.

Mesce, K.A., 2002. Metamodulation of the biogenic amines: Second-order modulation by steroid hormones and amine cocktails. *Brain. Behav. Evol.* 60, 339–349.

Mills, H., Wragg, R., Hapiak, V., Castelletto, M., Zahratka, J., Harris, G., Summers, P., Korchnak, A., Law, W., Bamber, B., Komuniecki, R., 2011. Monoamines and neuropeptides interact to inhibit aversive behaviour in *Caenorhabditis elegans*.

EMBO J. 31, 667–678.

Milo, R., Shen-Orr, S., Itzkovitz, S., Kashtan, N., Chklovskii, D., Alon, U., 2002. Network motifs: simple building blocks of complex networks. *Science* 298, 824–827.

Mohri, A., Kodama, E., Kimura, K.D., Koike, M., Mizuno, T., Mori, I., 2005. Genetic control of temperature preference in the nematode *Caenorhabditis elegans*. *Genetics* 169, 1437–1450.

Monchi, O., Petrides, M., Doyon, J., Postuma, R.B., Worsley, K., Dagher, A., 2004. Neural Bases of Set-Shifting Deficits in Parkinson' s Disease. *J. Neurosci.* 24, 702–710.

Mori, I., Ohshima, Y., 1995. Neural regulation of thermotaxis in *Caenorhabditis elegans*. *Nature* 376, 344-8

Mueller, K.L., Hoon, M.A., Erlenbach, I., Chandrashekar, J., Zuker, C.S., Ryba, N.J.P., 2005. The receptors and coding logic for bitter taste. *Nature* 434, 225–229.

Murray, K.C., Stephens, M.J., Ballou, E.W., Heckman, C.J., Bennett, D.J., 2011. Motoneuron Excitability and Muscle Spasms Are Regulated by 5-HT2B and 5-HT2C Receptor Activity. *J. Neurophysiol.* 105, 731–748.

Nadim, F., Bucher, D., 2014. Neuromodulation of neurons and synapses. *Curr. Opin. Neurobiol.* 29, 48–56.

Nagel, G., Brauner, M., Liewald, J.F., Adeishvili, N., Bamberg, E., Gottschalk, A., 2005. Light activation of Channelrhodopsin-2 in excitable cells of *Caenorhabditis elegans* triggers rapid behavioral responses. *Curr. Biol.* 15, 2279–2284.

Nguyen, J.P., Shipley, F.B., Linder, A.N., Plummer, G.S., Liu, M., Setru, S.U., Shaevitz, J.W., Leifer, A.M., 2015. Whole-brain calcium imaging with cellular resolution in freely behaving *Caenorhabditis elegans*. *Proc. Natl. Acad. Sci. U. S. A.* 113, E1074-E1081.

Owald, D., Felsenberg, J., Talbot, C.B., Das, G., Perisse, E., Huetteroth, W., Waddell, S., 2015. Activity of defined mushroom body output neurons underlies learned olfactory behavior in *Drosophila*. *Neuron* 86, 417–427.

Pantelis, C., Barber, F.Z., Barnes, T.R.E., Nelson, H.E., Owen, A.M., Robbins, T.W., 1999. Comparison of set-shifting ability in patients with chronic schizophrenia and frontal lobe damage. *Schizophr. Res.* 37, 251–270.

Perrier, J.-F., Rasmussen, H.B., Christensen, R.K., Petersen, A.V., 2013. Modulation of the intrinsic properties of motoneurons by serotonin. *Curr. Pharm. Des.* 19, 4371–4384.

Piggott, B.J., Liu, J., Feng, Z., Wescott, S. a, Xu, X.Z.S., 2011. The neural circuits and synaptic mechanisms underlying motor initiation in *C. elegans*. *Cell* 147, 922–33.

Pinard, A., Robitaille, R., 2008. Nitric oxide dependence of glutamate-mediated modulation at a vertebrate neuromuscular junction. *Eur. J. Neurosci.* 28, 577–587.

Pinto, M.C., Campbell-Lendrum, D.H., Lozovei, A.L., Teodoro, U., Davies, C.R., 2001. Phlebotomine sandfly responses to carbon dioxide and human odour in the field. *Med. Vet. Entomol.* 15, 132–139.

Pleil, J.D., Lindstrom, A.B., 1995. Measurement of volatile organic compounds in exhaled breath as collected in evacuated electropolished canisters. *J. Chromatogr. B Biomed. Sci. Appl.* 665, 271–279.

Pokala, N., Liu, Q., Gordus, A., Bargmann, C.I., 2014. Inducible and titratable silencing of *Caenorhabditis elegans* neurons in vivo with histamine-gated chloride channels. *Proc. Natl. Acad. Sci. U. S. A.* 111, 2770–2775.

Qi, Y.B., Garren, E.J., Shu, X., Tsien, R.Y., Jin, Y., 2012. Photo-inducible cell ablation in *Caenorhabditis elegans* using the genetically encoded singlet oxygen generating protein miniSOG. *Proc. Natl. Acad. Sci. U. S. A.* 109, 7499–504.

Quaegebeur, A., Carmeliet, P., 2010. Oxygen Sensing: A Common Crossroad in Cancer and Neurodegeneration. *Curr. Top. Microbiol. Immunol.* 345, 71–103.

Rank, M.M., Murray, K.C., Stephens, M.J., D'Amico, J., Gorassini, M. a, Bennett, D.J., 2011. Adrenergic receptors modulate motoneuron excitability, sensory synaptic transmission and muscle spasms after chronic spinal cord injury. *J. Neurophysiol.* 105, 410–422.

Regehr, W.G., Carey, M.R., Best, A.R., 2009. Activity-Dependent Regulation of Synapses by Retrograde Messengers. *Neuron* 63, 154–170.

Rengarajan, S., Hallem, E.A., 2016. Olfactory circuits and behaviors of nematodes. *Curr. Opin. Neurobiol.* 41, 136–148.

Ribeiro, J.A., Sebastião, A.M., 2010. Modulation and metamodulation of synapses by adenosine. *Acta Physiol.* 199, 161–169.

Romanos, T.R., Petersen, J.G., Pocock, R., 2017. Control of Neuropeptide Expression by Parallel Activity-dependent Pathways in *Caenorhabditis elegans*. *Sci. Rep.* 7, 1–11.

Root, C.M., Denny, C.A., Hen, R., Axel, R., 2014. The participation of cortical amygdala in innate, odour-driven behaviour. *Nature* 515, 269–273.

Sachse, S., Rueckert, E., Keller, A., Okada, R., Tanaka, N.K., Ito, K., Vosshall, L.B., 2007. Activity-Dependent Plasticity in an Olfactory Circuit. *Neuron* 56, 838–850.

Saeki, S., Yamamoto, M., Iino, Y., 2001. Plasticity of chemotaxis revealed by paired presentation of a chemoattractant and starvation in the nematode *Caenorhabditis elegans*. *J. Exp. Biol.* 204, 1757–64.

Sakurai, A., Katz, P.S., 2009. State-, timing-, and pattern-dependent neuromodulation of synaptic strength by a serotonergic interneuron. *J. Neurosci.* 29, 268–279.

Savigner, A., Duchamp-Viret, P., Grosmaitre, X., Chaput, M., Garcia, S., Ma, M., Palouzier-Paulignan, B., 2009. Modulation of spontaneous and odorant-evoked

activity of rat olfactory sensory neurons by two anorectic peptides, insulin and leptin. *J. Neurophysiol.* 101, 2898–2906.

Schacher, S., Montarolo, P., Kandel, E.R., 1990. Selective short- and long-term effects of serotonin, small cardioactive peptide, and tetanic stimulation on sensorimotor synapses of *Aplysia* in culture. *J. Neurosci.* 10, 3286–94.

Schiavo, G., Benfenati, F., Poulain, B., Rossetto, O., Polverino de Laureto, P., DasGupta, B.R., Montecucco, C., 1992. Tetanus and botulinum-B neurotoxins block neurotransmitter release by proteolytic cleavage of synaptobrevin. *Nature* 359, 832–835.

Schrödel, T., Prevedel, R., Aumayr, K., Zimmer, M., Vaziri, A., 2013. Brain-wide 3D imaging of neuronal activity in *Caenorhabditis elegans* with sculpted light. *Nat. Methods* 10, 1013–1020.

Scott, K., 2011. Out of thin air: sensory detection of oxygen and carbon dioxide. *Neuron* 69, 194–202.

Seeley, T.D., 1974. Atmospheric carbon dioxide regulation in honey-bee (*Apis mellifera*) colonies. *J. Insect Physiol.* 20, 2301–2305.

Semenza, G.L., Kappler, M., Taubert, H., Eckert, A.W., 2011. Oxygen sensing, homeostasis, and disease. *N. Engl. J. Med.* 365, 1845-6.

Semmelhack, J.L., Wang, J.W., 2009. Select *Drosophila* glomeruli mediate innate olfactory attraction and aversion. *Nature* 459, 218–223.

Sengupta, P., Chou, J.H., Bargmann, C.I., 1996. *odr-10* Encodes a seven transmembrane domain olfactory receptor required for responses to the odorant diacetyl. *Cell* 84, 899–909.

Shusterman, D., Avila, P.C., 2003. Real-time monitoring of nasal mucosal pH during carbon dioxide stimulation: Implications for stimulus dynamics. *Chem. Senses* 28, 595–601.

Smith, E.S.J., Martinez-Velazquez, L., Ringstad, N., 2013. A chemoreceptor that detects molecular carbon dioxide. *J. Biol. Chem.* 288, 37071–37081.

Song, S., Sjöström, P.J., Reigl, M., Nelson, S., Chklovskii, D.B., 2005. Highly nonrandom features of synaptic connectivity in local cortical circuits. *PLoS Biol.* 3, 0507–0519.

Steullet, P., Guerin, P.M., 1992. Perception of breath components by the tropical bont tick, *Amblyomma variegatum*. *J. Comp. Physiol.* 170, 677–685.

Stirman, J.N., Crane, M.M., Husson, S.J., Wabnig, S., Schultheis, C., Gottschalk, A., Lu, H., 2011. Real-time multimodal optical control of neurons and muscles in freely behaving *Caenorhabditis elegans*. *Nat. Methods* 8, 153–8.

Strauss, G.P., Robinson, B.M., Waltz, J.A., Frank, M.J., Kasanova, Z., Herbener, E.S., Gold, J.M., 2011. Patients with schizophrenia demonstrate inconsistent preference

judgments for affective and nonaffective stimuli. *Schizophr. Bull.* 37, 1295–1304.

Suh, G.S.B., Wong, A.M., Hergarden, A.C., Wang, J.W., Simon, A.F., Benzer, S., Axel, R., Anderson, D.J., 2004. A single population of olfactory sensory neurons mediates an innate avoidance behaviour in *Drosophila*. *Nature* 431, 854–859.

Sun, L., Wang, H., Hu, J., Han, J., Matsunami, H., Luo, M., 2009. Guanylyl cyclase-D in the olfactory CO_2 neurons is activated by bicarbonate. *Proc. Natl. Acad. Sci. U. S. A.* 106, 2041–2046.

Sun, X., Zhao, Y., Wolf, M.E., 2005. Dopamine Receptor Stimulation Modulates AMPA Receptor Synaptic Insertion in Prefrontal Cortex Neurons. *J. Neurosci.* 25, 7342–7351.

Sun, Z.Y., Kauderer, B., Schacher, S., 1996. Differential distribution of functional receptors for neuromodulators evoking short-term heterosynaptic plasticity in *Aplysia* sensory neurons. *J. Neurosci.* 16, 7540–7549.

Tobin, D.M., Madsen, D.M., Kahn-Kirby, A., Peckol, E.L., Moulder, G., Barstead, R., Maricq, A. V., Bargmann, C.I., 2002. Combinatorial expression of TRPV channel proteins defines their sensory functions and subcellular localization in *C. elegans* neurons. *Neuron* 35, 307–318.

Torrents, D., Suyama, M., Zdobnov, E., Bork, P., 2003. A genome-wide survey of human pseudogenes. *Genome Res.* 13, 2559–2567.

Troemel, E.R., Kimmel, B.E., Bargmann, C.I., 1997. Reprogramming chemotaxis responses: Sensory neurons define olfactory preferences in *C. elegans*. *Cell* 91, 161–169.

Tsunozaki, M., Chalasani, S.H., Bargmann, C.I., 2008. A Behavioral Switch: cGMP and PKC Signaling in Olfactory Neurons Reverses Odor Preference in *C. elegans*. *Neuron* 59, 959–971.

Turner, S.L., Li, N., Guda, T., Githure, J., Cardé, R.T., Ray, A., 2011. Ultra-prolonged activation of CO_2-sensing neurons disorients mosquitoes. *Nature* 474, 87–91.

Turner, S.L., Ray, A., 2009. Modification of CO_2 avoidance behaviour in *Drosophila* by inhibitory odorants. *Nature* 461, 277–282.

Varshney, L.R., Chen, B.L., Paniagua, E., Hall, D.H., Chklovskii, D.B., 2011. Structural properties of the *Caenorhabditis elegans* neuronal network. *PLoS Comput. Biol.* 7. doi: 10.1371/journal.pcbi.1001066.

Villareal, G., Li, Q., Cai, D., Fink, A.E., Lim, T., Bougie, J., Sossin, W.S., Glanzman, D.L., 2009. Role of protein kinase C in the induction and maintenance of serotonin-dependent enhanement of the glutamate response in isolated siphon motor neurons of *Aplysia*. *J. Neurosci.* 29, 5100–5107.

Voskamp, K.E., Everaarts, E., Den Otter, C.J., 1999. Olfactory responses to attractants and repellents in tsetse. *Med. Vet. Entomol.* 13, 386–392.

Walz, A., Feinstein, P., Khan, M., Mombaerts, P., 2007. Axonal wiring of guanylate cyclase-D-expressing olfactory neurons is dependent on neuropilin 2 and semaphorin 3F. *Development* 134, 4063–4072.

Wasserman, S., Salomon, A., Frye, M.A., 2013. *Drosophila* tracks carbon dioxide in flight. *Curr. Biol.* 23, 301–6.

Weimann, J.M., Marder, E., 1994. Switching neurons are integral members of multiple oscillatory networks. *Curr. Biol.* 4, 896–902.

White, J.G., Southgate, E., Thomson, J.N., Brenner, S., 1986. The Structure of The Nervous System of the Nematode *Caenorhabditis elegans*. *Philos. Trans. R. Soc. Lond. B. Biol. Sci.* 314, 1–340.

Wragg, R.T., Hapiak, V., Miller, S.B., Harris, G.P., Gray, J., Komuniecki, P.R., Komuniecki, R.W., 2007. Tyramine and octopamine independently inhibit serotonin-stimulated aversive behaviors in *Caenorhabditis elegans* through two novel amine receptors. *J. Neurosci.* 27, 13402–13412.

Xu, M., Jarrell, T.A., Wang, Y., Cook, S.J., Hall, D.H., Emmons, S.W., 2013. Computer Assisted Assembly of Connectomes from Electron Micrographs: Application to *Caenorhabditis elegans*. *PLoS One* 8, 1–6.

Yarmolinsky, D.A., Zuker, C.S., Ryba, N.J.P., 2009. Common Sense about Taste: From Mammals to Insects. *Cell* 139, 234–244.

Yoshida, K., Hirotsu, T., Tagawa, T., Oda, S., Wakabayashi, T., Iino, Y., Ishihara, T., 2012. Odour concentration-dependent olfactory preference change in *C. elegans*. *Nat. Commun.* doi: 10.1038/ncomms1750.

Young, J.M., Waters, H., Dong, C., Fülle, H.J., Liman, E.R., 2007. Degeneration of the olfactory guanylyl cyclase D gene during primate evolution. *PLoS One* 2, 1–8.

Youngentob, S.L., Hornung, D.E., Mozell, M.M., 1991. Determination of carbon dioxide detection thresholds in trained rats. *Physiol. Behav.* 49, 21–26.

Zhang, M., Chung, S.H., Fang-Yen, C., Craig, C., Kerr, R.A., Suzuki, H., Samuel, A.D.T., Mazur, E., Schafer, W.R., 2008. A Self-Regulating Feed-Forward Circuit Controlling *C. elegans* Egg-Laying Behavior. *Curr. Biol.* 18, 1445–1455.

Zhao, G.Q., Zhang, Y., Hoon, M.A., Chandrashekar, J., Erlenbach, I., Ryba, N.J.P., Zuker, C.S., 2003. The Receptors for Mammalian Sweet and Umami Taste. *Cell* 115, 255–266.

Zheng, M., Cao, P., Yang, J., Xu, X.Z.S., Feng, Z., 2012. Calcium imaging of multiple neurons in freely behaving *C. elegans*. *J. Neurosci. Methods* 206, 78–82.

Ziemann, A.E., Allen, J.E., Dahdaleh, N.S., Drebot, I.I., Coryell, M.W., Wunsch, A.M., Lynch, C.M., Faraci, F.M., Howard, M.A., Welsh, M.J., Wemmie, J.A., 2009. The Amygdala Is a Chemosensor that Detects Carbon Dioxide and Acidosis to Elicit Fear Behavior. *Cell* 139, 1012–1021.

Ziesmann, J., 1996. The physiology of an olfactory sensillum of the termite *Schedorhinotermes lamanianus*: Carbon dioxide as a modulator of olfactory sensitivity. *J. Comp. Physiol.* 179, 123–133.